EPRI

Cavitation-Induced Excess Heat in Deuterated Metals

WARNING:
Please read the Export Control Agreement on the back cover.

Technical Report

Cavitation-Induced Excess Heat in Deuterated Metals

TR-108474

Final Report, March 1998

Prepared by
E-Quest Sciences
2166 Old Middlefield Way
Mountain View, California 94041

Principal Investigators
R. S. Stringham
D. R. George

SRI International
333 Ravenswood Avenue
Menlo Park, California 94025

Principal Investigators
F. L. Tanzella
M. Williams

Prepared for
Electric Power Research Institute
3412 Hillview Avenue
Palo Alto, California 94304

EPRI Project Manager
T. O. Passell
Advanced Nuclear Technology Target

Energy Conversion Division

DISCLAIMER OF WARRANTIES AND LIMITATION OF LIABILITIES

ORGANIZATION(S) THAT PREPARED THIS REPORT

E-QUEST SCIENCES

ORDERING INFORMATION

Requests for copies of this report should be directed to the EPRI Distribution Center, 207 Coggins Drive, P.O. Box 23205, Pleasant Hill, CA 94523, (510) 934-4212.

REPORT SUMMARY

Intense cavitation at a palladium interface with heavy water apparently generates excess heat. The heat appears to be far too large to be a chemical or metallurgical transformation. By inference, a nuclear reaction is the likely heat source because helium of a unique isotopic character has frequently been observed in the gas phase. This report summarizes selected examples of energy output, including excess energy and measurement of ^{4}He via mass spectrometry.

Background
Since first announced in 1989 by Fleischmann, Pons, and Hawkins, "old fusion" has been the subject of widespread interest and intense controversy. Palladium (Pd) cathodes electrochemically charged with deuterium (D) to unusually high D/Pd ratios exhibited episodes of heat in excess of measured electrical inputs. This work explored a non-electrochemical method of adding heavy hydrogen (D) to metals, that is, via intense cavitation driven by ultrasound.

Objectives
To measure, optimize, and control the excess heat produced in deuterated Pd and other metals; to measure any signatures of possible nuclear reactions associated with the production of the excess heat.

Approach
Investigators developed small heat-transferring flow loops to measure total energy calorimetrically for comparison with baseline measurements of acoustic and electric (joule heater) inputs. The total acoustical inputs combined with electrical inputs ranged from 10-100 W over a typical experimental duration of 24 h. Investigators designed the experiments, as a whole, to produce intense cavitation bubbles at the surface of a metal foil (primarily Pd) submerged in heavy water. (They did not explicitly vary Pd purity, using whatever Pd was available from the few suppliers.) To control the cavitation process, they used argon cover gas at various pressures. Based on observations of volumetric expansion and subsequent crinkling of the foils, D input clearly occurred; however, investigators made no attempt to quantify the level of D loading. They surmised that D entered from free D gaseous molecules or atoms from the decomposed heavy water in the collapsing cavitation bubble. It is a well known fact that such cavitation can provide cleaning action at surfaces, even to the point of destroying metal integrity. Hence, it was not surprising to find similar heat effects to those in electrochemical cell experiments.

Results

Investigators observed and measured excess power levels of ~20-100% to an accuracy of ~5-10%. These excess power levels integrated to a total of about 1-10 MJ for ~3 g (1/35 mol) Pd foil. The excess heat generated ranged from 35-350 MJ/mol Pd, assuming uniformity across the foil. These excess heats, appearing in such a small mass of metal foil, were well above the largest known heats of chemical or metallurgical transformations.

^{4}He was observed well above the background levels seen in near zero excess heat experiments (about one-third of the 65 tests failed to show excess heat). However, the helium observed in the argon cover gas was only a fraction of that expected from hypothetical exothermic nuclear reactions that produce ^{4}He.

This work confirms the claims of Fleischmann, Pons, and Hawkins concerning the production of excess heat in D-loaded Pd. The success rate (2 of 3 tests) appears to be greater using the ultrasonic cavitation technique than relying on the cathodes of electrochemical cells.

EPRI Perspective

It is a reasonable assumption that the majority of the excess heat observed in these cavitation experiments comes from a new class of nuclear reactions among the isotopes of light elements within the palladium metal lattice. Among the possible "ashes" of hypothesized nuclear reactions, investigators have observed ^{4}He, tritium (in only very small amounts), localized melting of the metal foils, and possible alteration of the isotopic ratios of the Pd metal itself. These effects support, but do not yet prove, the hypothesis that D-containing Pd and titanium targets are the locale of excess heat production.

Further work on this subject remains to demonstrate which nuclear reactions, if any, are generating the excess heat. The only way to achieve this is to observe in generally quantitative fashion the nuclear reaction products, or "ashes." At this time, investigators believe that the most likely ashes to be found will be ^{4}He observable in the vapor phase. This study provides information that will be valuable for long-term utility planning concerning potential heat sources that might become available several decades into the future. However, the specific reaction(s) producing the heat and helium must be determined to allow maximization of the phenomena for practical uses in the power industry. Other EPRI reports address nuclear processes in deuterated metals (TR-104195) and include Proceedings: Fourth International Conference on Cold Fusion (TR-104188, Vols. 1-4).

TR-108474

Interest Category: Advanced nuclear technology

Keywords: Cavitation, Palladium, Heavy water, Deuterium, Cold fusion, Heat source

ABSTRACT

Intense cavitation at a palladium interface with heavy water apparently generates excess heat. The heat appears to be far too large to be a chemical or metallurgical transformation. By inference, a nuclear reaction is the likely heat source because helium of a unique isotopic character has frequently been observed in the gas phase. This report summarizes selected examples of energy ouput, including excess energy and measurement of ^{4}He via mass spectrometry. Overall, this work confirms the claims of Fleischmann, Pons, and Hawkins concerning the production of excess heat in D-loaded Pd. The success rate (about two-thirds of the 65 tests performed showed excess heat) appears to be greater using the ultrasonic cavitation technique than relying on the cathodes of electrochemical cells.

Table of Contents

Table of Figures

1. Introduction

This demonstration project was undertaken between the period of May 1995 and January 1996 with modest funding and support from the Electric Power research Institute (EPRI), E-Quest Sciences and SRI International (SRI). The goal was to repeat (within the limit of funding available) experiments similar to those conducted by E-Quest Sciences in its own laboratories and on two separate occasions at the Los Alamos National Laboratory (October 1992 and April 1993 the latter included the support of EPRI and Rockwell International). These experiments repeatedly demonstrated large excess heat effects and the production of ^{4}He of a unique isotopic character. This previous work has been reported by E-Quest Sciences at scientific conferences in 1993 ICCF-4, Maui, 1994 ICCF-5, Monaco, and 1995 ACS, Anaheim. The principal experiments in this project were conducted using an E-Quest Mark II (patent pending) apparatus located in SRI laboratories in Menlo Park, CA. The experiments were designed to produce intense cavitation within a small stainless steel reactor vessel filled with circulating heavy water and upon a metal (generally palladium) target lattice (5cm x 5cm x 0.1-0.25mm) contained within the reactor vessel.

It has been a central tenet in "cold fusion" experiments that if there is evidence of nuclear heat effects in an experiment there must be significant quantities of nuclear by-products. The experiments were designed to primarily accommodate the measurement of ^{4}He from the reactor assembly and to measure energy calorimetrically from experiments including the use of active cells, blanks, and joule heater calibrations. This report summarizes selected examples of energy output, including excess energy and measurement of ^{4}He via mass spectroscopy. Additional preliminary data from dynamic and time of flight SIMS analysis to determine isotopic ratios are also included.

In the E-Quest cavitation experiments no radiative emissions have been measured emanating from the apparatus during operation in spite of observations made with various forms of sensitive emissions detection hardware. The detectors included large LN_2 cooled germanium gamma spectrometers, ^{3}He neutron counters, BF_3 neutron detectors, Geiger-Mueller detectors, neutron bubble dosimeters, portable germanium x-ray spectrometers, TLD type dosimeters, and x-ray sensitive films. No radiative emissions studies were judged necessary nor were any conducted during the SRI experiments save for TLD dosimeter type devices placed on and around the instrument. SRI personnel routinely wear dosimeter badges while working in the laboratory containing the equipment and reported no exposures.

Approximately 65 experiments were performed during the period June 1 through Jan. 31, 1996. Experiments were designed to last for approximately 24 hours though frequent electronic and mechanical failures resulted in a number of the experiments being of much shorter duration.

The E-Quest Mark II research device (see figure 1 below) was developed in 1989 as an extension of technology used in the practice of sonochemistry experiments by E-Quest scientists prior to 1989. It has undergone continuing modification to accommodate new parts and improved material handling and data gathering. The device consists of three principal components: an ultrasonic amplifier, the reactor assembly, and a large (15 liter) uninsulated sealed heat exchanger. The amplifier is a Misonixs device which delivers an adjustable power 20 khz signal up to ~ 550 watts coupled to a piezo electric converter attached to a tuned titanium horn. The reactor assembly consists of a "sonicator" assembly that contains the acoustic horn, a reactor vessel that contains the foil target, and a pressurized circulation system for two separate fluid coolant / operating fluid systems. The single heat exchanger receives the heat from the operation of the reactor/sonicator assembly through two separate metal cooling lines through which heated fluids from the reactor/sonicator components circulate and exchange heat with the large mass of water in the heat exchanger.

Figure 1 The E-Quest Mark II Research Reactor at SRI

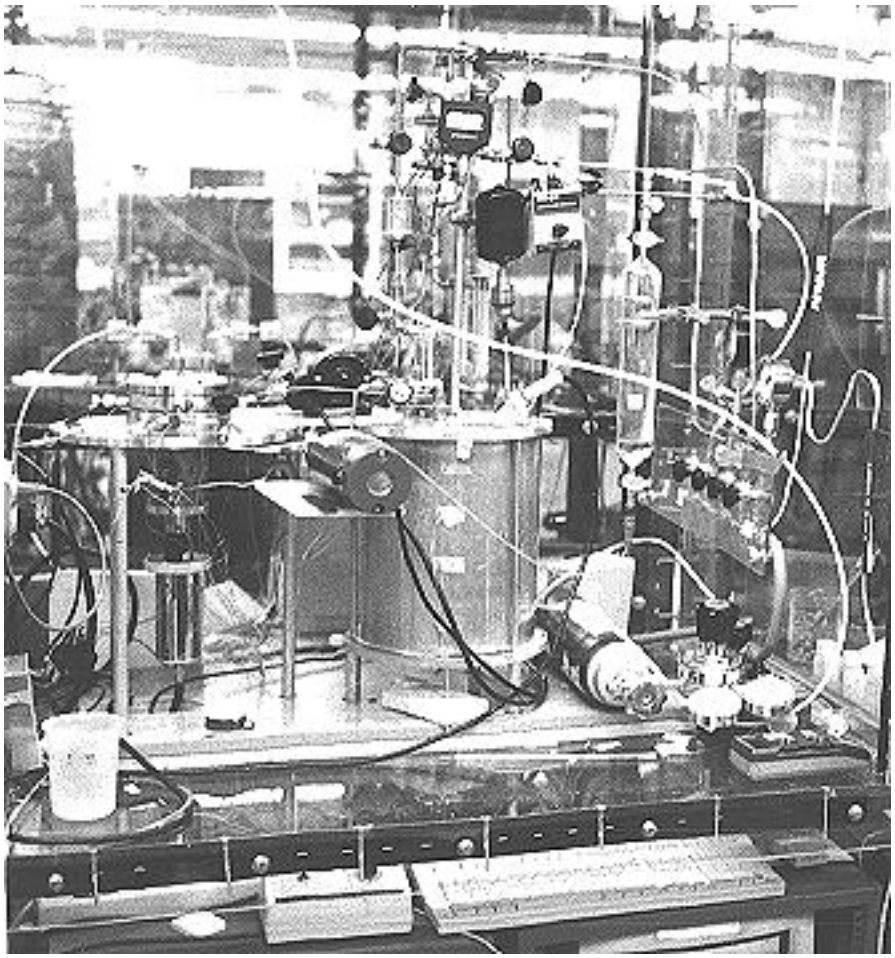

[1] Photograph of the Mark II (patent pending) situated at SRI International in Menlo Park, CA. 1995

Figure 2 Schematic of E-Quest Mark II Research Reactor at SRI

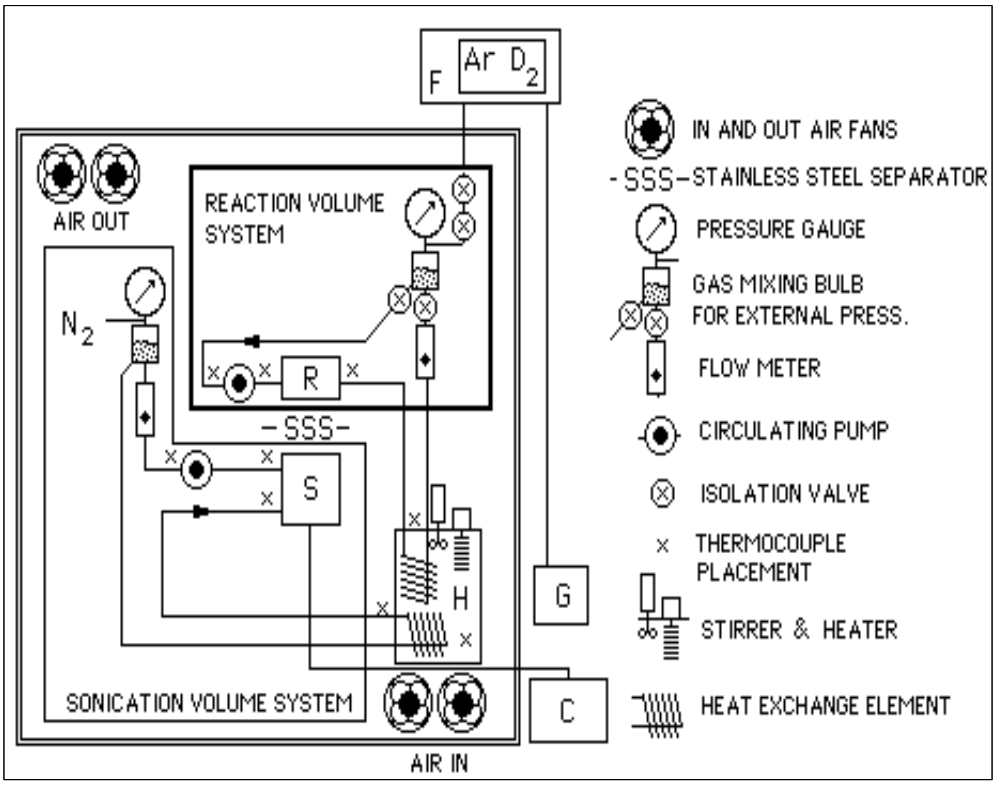

[2] The figure is a schematic of the Mark II. The upper case letters, [C], [F], [G], [H], [R], & [S] show the major components of the system. Those components that either produce and dissipate heat are: the reaction volume [R]; the sonication volume [S]; the heat exchanger for the reaction and for the sonication volume systems [H]. The other support components do not directly contribute to the heat. The gas mixing reservoir and flow meter for [R] and [S] are [RR] and [SR] and include some of the associated tubing for [R] and [S]. The two displacement pumps contribute very little, in the range of a watt, to the heat input. The power supply that supplies energy to the acoustic driver is [C], the vacuum manifold for the measurement and management of gases is [F]; and the vacuum pump is [G] these support but do not directly contribute to the heat input Q_{in}. As indicated, [R] and [S] are separated by a l mm (40mil) stainless steel disk [SSS]. The sonication volume system [S] is isolated in the figure by the dark line, and the reaction volume system [R] is isolated by the light line. The icons at the right represent the important parts of the system including the stainless steel separator [SSS]. Their locations are roughly indicated on the block diagram.

In operation the acoustic signal is delivered to the heavy water reactor vessel via a water coupled link between the titanium horn and a stainless steel separator plate SSS. Ordinary water is circulated to remove heat from the horn/sonicator containment S of the system via a pumped flow (~ 0.5 liter) in a stainless steel coil immersed in the heat exchanger. Simultaneously hot "heavy" water (~ 0.1 liter), which comprises the operating fluid for the reactor R of the reactor assembly, is circulated by the pump via stainless steel lines and coil and similarly gives up heat within the same heat exchanger volume as does the sonicator flow system. Nitrogen pressure is applied to the sonicator flow at its gas mixing bulb to suppress cavitation within the sonicator assembly and a pressure of gas either argon or deuterium is maintained on the reactor flow system at its gas mixing bulb to provide optimum cavitation conditions within the reactor vessel. A target lattice, typically a foil of palladium metal (99.9% Aithica or higher purity Johnson Matthey) and 5cm x 5cm x 0.1-0.25mm, is located in the reactor assembly directly above SSS.

Figure 3 Exploded Schematic of the Mark II Reactor Assembly

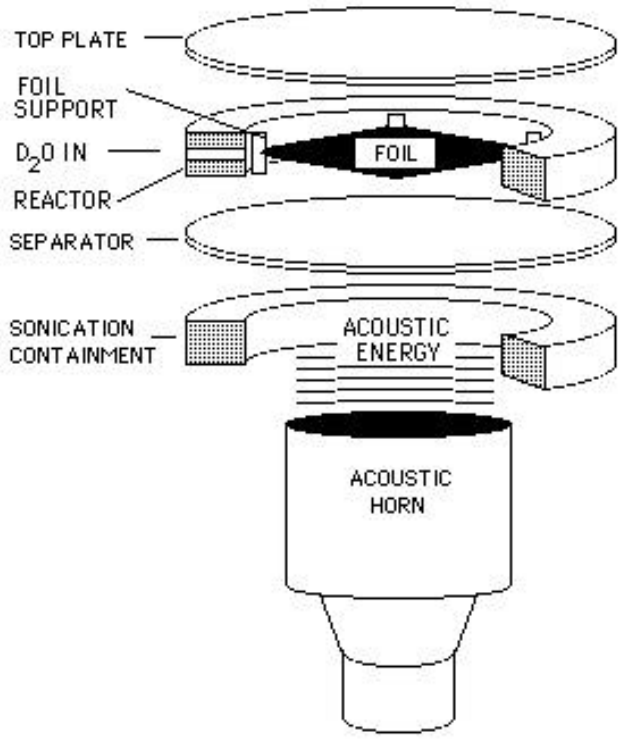

[3] The E-Quest MKII reactor consists of a stainless steel "doughnut" sandwiched between two stainless steel separator plates. The target foil is placed inside this reactor chamber that is filled with circulating D_2O or H_2O. Beneath the reactor chamber a titanium acoustic horn acts as a piston operating at 20khz.

2. Calorimetric Studies Of The Experiments Performed At SRI International

Calorimetry for this project was accomplished via the instrumentation with a strategic array of thermocouples within the fluid system and upon radiative surfaces. Heater current, heater voltage, sonicator pressure, reactor pressure, and in some experiments a voltage nominally proportional to sonicator power was measured. All of the signals were multiplexed using a Keithley model 706 scanner, employing Keithley models 7057A thermocouple and 7056 general purpose scanner cards to a Keithley model 195A digital multi-meter(DMM). A Macintosh IIsi computer with an IOTech SCSI 488 interface is used to control the multiplexer and collect data from the DMM. The data is collected at 5 minute intervals. The results are stored and displayed. Other data (flow rates, ultrasonic oscillator settings, etc.) were noted and logged into a project notebook.

The measurement of the heat balance in these experiments demands some explanation. While the method may at first appear complicated it is in fact quite simple and is based on the measure of total watts in and total heat out. We have developed over the past 7 years a “cooling curve” calorimetry method which relies on a steady state heat balance and a determination of heat loss from the component surfaces.

Under this steady state condition power variables in the system are the power in from the electrical wall plug and heat out to the environment seen as heat. Heat input to the system is delivered from two sources, the acoustic source (sonicator) and a Joule heater. The heat distribution through the components of the system is accomplished via circulating water through the nearly all metal apparatus. Heat is lost from the system solely via convective and radiative loss from metal surfaces to the experiment booth which is maintained at a constant temperature ≅ 2ºC. The one never changing factor in the system is the mass and surface area of the metal components which make up the “radiator” for apparatus. With calibration using a Joule immersion heater and through measurement of the rate of cooling of each component surface from a number of steady state temperatures we determine the precise convective and radiative rate of heat loss for each component at its steady state temperature. Collectively thermal watts out to the air must equal the electrical heat into the system via the sum of the Joule heater, the acoustic source heat, and heat from any “unusual” reaction (eg. micro-fusion). Indeed the calibration of the apparatus with the Joule heater shows that this method is highly accurate (~2%) at measuring the heat into the system as a function of heat loss. (A more thorough description of the calorimetric method is provided in the Appendix C.)

Once calibrated (and this was done repeatedly throughout the project) energy loss from the system is readily determined using a mathematical model constructed in a spreadsheet program. The case for anomalous energy reactions is made when heat in and heat out is not in balance. If more energy is measured as being lost from the system than going in then that excess energy must be coming from some exothermic source within the device. If more energy is going in than

is observed going out some endothermic reaction must be occurring in the system. The latter case is not observed, save in one experiment for which no problematic explanations could be found. Calibration of the system is complicated by the fact that the electrical input component is in the form of acoustic energy and is inherently inefficient at being converted to heat in the system when compared to the Joule heater. A variety of experiments are used to determine the efficiency of the acoustic source at adding heat to the system. These were repeatedly performed throughout the course of the project and an efficiency factor of **0.45** emerged as the thermal efficiency of the acoustic input. This efficiency factor is in good agreement with projected acoustic efficiency determined through electrical circuit efficiency expectations. In this series of experiments the acoustic source is rated at a maximum of 550 watts (having repeatedly overloaded the system) we are very confident of this number being an effective maximum. The actual electrical input varied from experiment to experiment and was much less than this maximum. In addition to the acoustic source, in many experiments a Joule immersion heater was used to raise the operating temperature. We have observed that a higher operating temperature provides a benefit to the rate of the excess heat producing reactions.

Figure 4 Mark II Watts In Heat Out Diagram

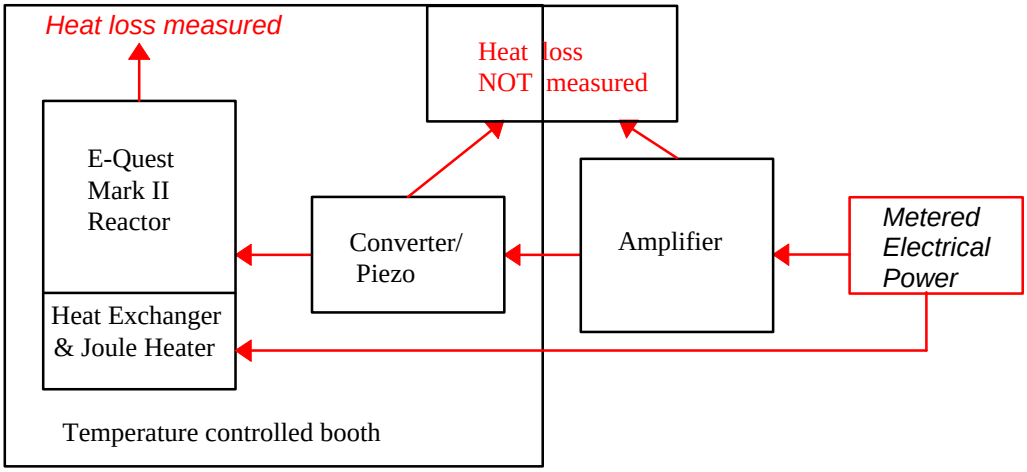

[4] This simple diagram shows the heat in and heat out paths. The measurement of electrical power in is performed via a watt meter measurement of heat out is a measure of heat loss from various components using the steady state cooling curve method which accounts for all heat out of the system with the important exceptions of heat loss from the amplifier and minor loss from the converter/piezo transducer. Energy lost from the Amplifier/Converter components are estimated to be in the neighborhood of 200+ watts and is accounted for in the energy balance for the reactions via the determination of the sonicator efficiency factor.

Thermal Efficiency of Acoustic Circuit

The Mark II apparatus is a three part system made up of the electro-acoustic signal generator, the reactor assembly, and the heat transfer/calorimetry system. The largest signal the experiments produce is an apparent large excess heat anomaly. Since we are primarily concerned with thermal effects in the operation of the device our primary method for measuring the electro-acoustic input is via calorimetric measurements. It is well known in the ultrasound industry that an acoustic signal can be nearly 100% captured by sinking it into a volume of water (19,20,21,22). Indeed

this method is commonly used in the industry to determine the efficiency of transducer components. The Mark II with it's two chambers of water is, by design, a nearly ideal acoustic sink. Measurement of electro-acoustic transducer efficiency is readily performed using calorimetry. In day to day operation these measurements are performed, as are all experiments, in the context of use of a known standard heat source - the essentially 100% efficient Joule (electrical resistance) heater. However to provide additional confidence regarding the calorimetric measurement of the electro-acoustic input one can approach the system efficiency from an electric circuit design point of view.

The electro-acoustic components of the system are composed of the amplifier/signal generator, the cable, and the converter/transducer. The signal that is delivered to the reactor is a 20khz signal of between 1000-1500 volts which is derived via electronic components from the 110volt 60hz wall power. The operating signal production is known to be a lossy system and the cumulative losses are easily accounted for in the following signal path. In the signal path the power from the wall is first converted from AC to DC, next it is converted to a sine wave, followed by passage through a capacitive coaxial cable, and finally into the converter/transducer where the signal leaves the transducer horn as a mechanically driven pressure wave . In each of these steps one encounters losses between the input power and output wave. In the demonstration experiments described in this report the measure of power into the system was made at the electrical outlet supplying the electro-acoustic system. This is performed using a watt meter and by measuring the current and voltage which comes from a stabilized input source.

The power measured from the wall outlet is reduced as follows as each parts losses comes into play in the sequence described. The loss figures are estimated and are in accordance with standard electrical expectations.

AC to DC conversion loss	~2 % loss	~98 % efficient
Oscillator to sine wave	~32 % loss	~68 % efficient
Cable capacitance	~1 % loss	~99 % efficient
Transducer/converter	~25 % loss	~75 % efficient

In a typical Mark II run for example a 300 watt draw of wall power is reduced according to the loss expectations to ~148 watts or 49%. Without fine tuning of these estimated loss factors this is in very good agreement with the 45% figure for efficiency determined using the purely calorimetric method.

To better correlate the results obtained at SRI with experiments using a similar Mark II device at the E-Quest laboratory, parallel experiments were run at both laboratories under the same conditions. The reactors were without a foil, the flow rates through the reactor R and the sonicator containment S were the same, the pressures of argon and nitrogen were the same, and the % of power from the sonicator power supply was the same.

The focus of the experiments conducted in this series was deemed to be best targeted to obtain high concentration ^{4}He measurements, as had been seen over a number of years in E-Quest labs and in one series of experiments at Los Alamos National Laboratory (1994). Since there was also

a difficult learning curve for the SRI scientific team it was decided to limit the calorimetry effort during the start up cycle. However we are able to report here on the experiments conducted which indeed show that we can both obtain a solid zero effect, where heat out = heat in, as well as a substantial positive effect.

List of symbols used in the calorimetric calculations.

α_i =The exponential temperature decay constant= $h_i(\sum A_j)_i)/(\sum M_j C_j)_i$
$(\sum A_j)_i$ =The sum of the surface area of the j elements of component i
A_j =Area of the jth element of component i
"(A)" =The air losses
c = The partition factor for split of Q(H) between H and R&S
C = The partition factor for W defining the acoustic heating inputs into R and S.
C_i = Heat capacity of component i
CC = The cooling curve
$(\sum M_j C_j)_i$ = The sum of masses x their heat capacities of the j elements of component i
Conv. = Heat loss due to convection = $k\sum(h_i(\sum A_j)_i)(T_{iss}-T_r))$
E1 = The efficiency of XL 2020 at SRI (.60)
E2 = The efficiency of XL 2010 at EQ (.45)
E = The efficiency factor of the acoustic generator
D = The differential temperature between R and S exit temperatures
DT R = The differential temperature between R input and exit temperatures
DT S = The differential temperature between S input and exit temperatures
DT_i = The delta T at steady state of component i
H = The heat exchange component
h_i = The convection heat transfer coefficient for component i
k = The steady state correlation constant [Qout/Qin = 1.00] (from heater run)
K = The partition factor for Q(x)
k = The Stefan-Boltzman constant
MF = Mass flow calorimetry
MFR = The flow rate through R in ml/sec
MF S = The flow rate through S in ml/sec
Q(i) = The heat input to each component.
Q(x) = The excess heat from run at steady state conditions = TW-(W+Q(H))
Q'H = The disbursed heat at steady state for the component H
Q'R = The disbursed heat at steady state for the component R
Q'S = The distributed heat at steady state for the component S
Q(H) = The heat production at steady state in component H
Q(R) = The heat production at steady state in component R
Q(S) = The heat production at steady state in component S
q(R) = The partitioned Q(x) at steady state in component R
q(S) = The partitioned Q(x) at steady state in component S
Q(P) = The wattmeter % of power from the acoustic power supply
Qin = The acoustic and heater input = [W+Q(H)] = TW-Q(x)

Qout = TW The total watts lost to air at steady state
R = The reactor or reaction volume component
r = The partition factor for c - the split of heat from H going to R
Rad. = The radiative heat loss $e\,\mathbf{k}[T_{iss}^4-T_r^4]A_i$
S = The sonicator containment or sonication volume.
s = The partition factor for c - the split of heat from H going to S
SSS = The 40 mil stainless steel separating disk.
t = Time in seconds
Tr = The ambient temperature
Tss = The steady state temperature of the surface of component i
Tiss = The CC steady state temperature of the surface of component i at t=0 (CC.)
[Tiss-Tr]= The DT temperature at steady state of component i at t=0 (CC.)
TW = Qout The total watts lost to air at steady state
W = E*Q(P) The acoustic heat generated in R and S
"(w)" = The power input

The plot of data from these experiments reveal a clearly anomalous heat effect of substantial magnitude and good reproducibility. The results from the calorimetry analysis of this data is that the total heat input, Q_{in}=W +Q(H), and the total heat output, Q_{out}=TW, of the system at steady state temperature has clearly demonstrated many runs with excess heat with some over 100 watts. The difference between the values Q_{out} and Q_{in} ,TW-(W+Q(H)) is the excess heat Q(x).
See figure - 5

Figure 5 Scatter Plot showing Excess Heat Demonstrated by the Experiments

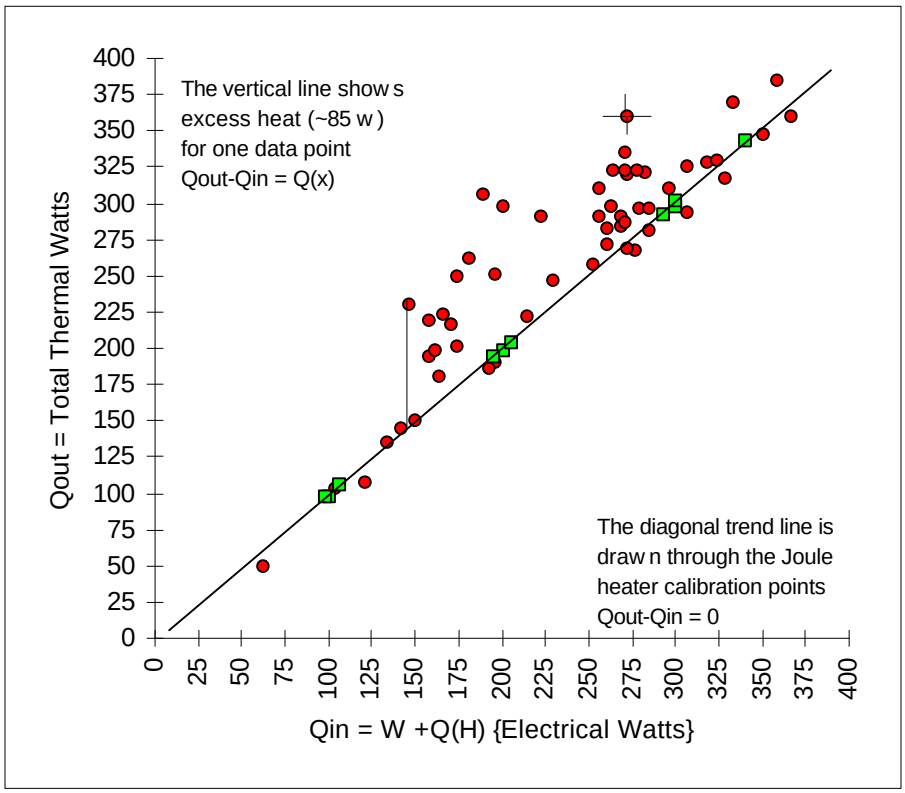

[5] The over all plot of the data. The total output watts, Q_{out}, vs. the total input watts, Q_{in}. The diagonal line represents $Q_{out}=Q_{in}$ of the calibration runs, where the excess heat, Q(x), equals zero (see the outlined squares that represent the heater runs, H, and argon runs, Ar with an error of +- 2watts). All the other points are Pd foil runs except for two titanium runs, +, and two stainless steel runs, x. In this plot the distance from the calibration line to the point along the parallel to the Q_{out} axis, is the Q(x) for that run. This plot shows the error is about ± 10 watts for the foil runs represented as circles. Some runs generated Q(x) in excess of 100 watts for periods of a day.

The upward diagonal line indicates the calibration for input power at steady state where power in must equal power out and the heater calibration points are on this line. Those points that fall below this calibration line were from runs where the system did not achieve steady state. Of those runs that did achieve steady state, the points lying above the diagonal Joule heater calibration line represent excess heat Q(x). In this representation of the data one can see many data points are well clear of the input and represent large excess heats for ~18-30 hours. The calibration, heater and stainless steel runs fall on or near the calibration line. See spread sheet in appendix showing data from all runs.

The following plot, figure - 6, shows the data of excess heat Q(x) versus acoustic heating W. It shows that as W increases Q(x) increases at an increasing rate.

Figure 6 Measured Excess Heat versus Measured Acoustic Heat

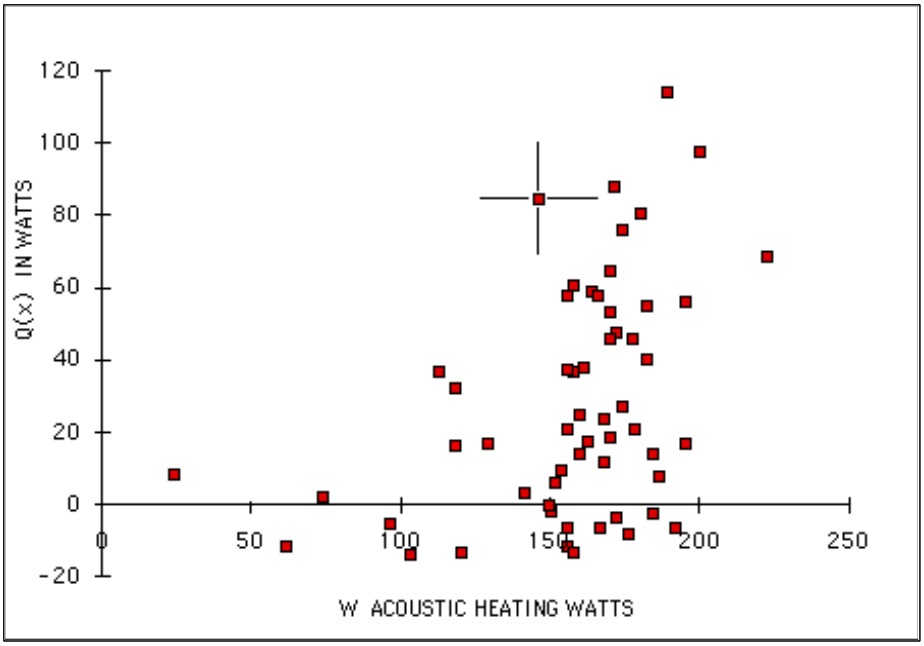

[6] The Q(x) vs. W for all the steady state runs except the calibration runs with the Joule heater, empty cell runs, stainless steel foil runs and the argon run. the Q(x) error is ± 15 watts.

The following plot, figure - 7, shows the data as represented in delta "T" at steady state (ss) in the heat exchanger at steady state.

Figure 7 Delta T vs. Input Watts

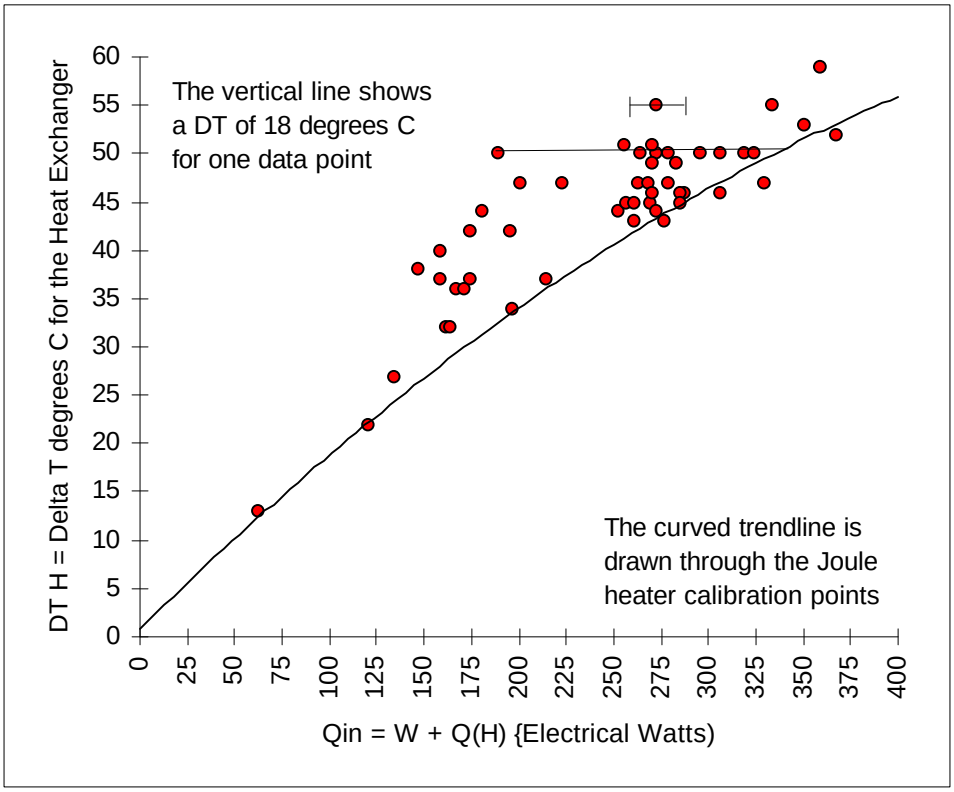

[7] The plot of the data to determine the relation between DT H and input watts. The curved line is the best fit of the temperature runs, and the scatter of the cavitation runs with input of W+Q(H) show the expected output of watts. If there were no excess heat Q(x) all data would fall on the curved heater calibration line. Those points that fall below the line were not at steady state. The input watts from any source should fall on this line if Q(x)=0. The straight line connecting one data point to the calibration line shows that point would require a joule heater input of nearly 350 watts but was instead produced with a an acoustic input of about 190 watts there-by revealing an excess heat of approximately 160 watts. The measurements in this figure have an error of no more than ± 10 watts.

The line is the best fit for the Joule heater calibration data of the heat exchanger. The data points for the delta temperature of the heat exchanger are located on or above the line, and are determined through the thermocouple measurement of the stirred heat exchanger water at steady state temperature. The excess heat produced, Q(x), can be determined by the distance to the point from the calibration line measured parallel to the Q_{in} axis. For example run Pd 8D the value for DT H is 51°C and the value for Q_{in} is 189 watts. The delta temperature 51°C requires an input to the Mark II system of 325 watts according to the calibration curve. Therefore 26 watts input to the system must come from a heat source Q(x). 114 watts must be added to Q_{in} to reach the calibration line.

The following plot, figure - 8, shows the data as the ratio of the Q_{out}/Q_{in} for run Pd 17E. The plot is from data taken on 5 minute intervals. The ratio would be equal to 1.00 if $Q_{out} = Q_{in,}$ but the system is at steady state so to make the ratio to 1.00 we add the amount of Q(x) to Q_{in} [W+Q(H)+Q(x)] and now heat in equals heat out the true steady state requirement. The plot of the power ratio shows a sharp peak at about 12 hours which was caused by a partial power failure to the Joule heater which reduced its load from 100 watts to 58 watts. Since the plot shows a ratio of measured electrical power in vs. measured thermal power out the Joule heater anomaly is seen as an excess heat burst. It is useful as a separate calibration for the run.

Figure 8 Run Pd17E Showing Steady State Excess Heat

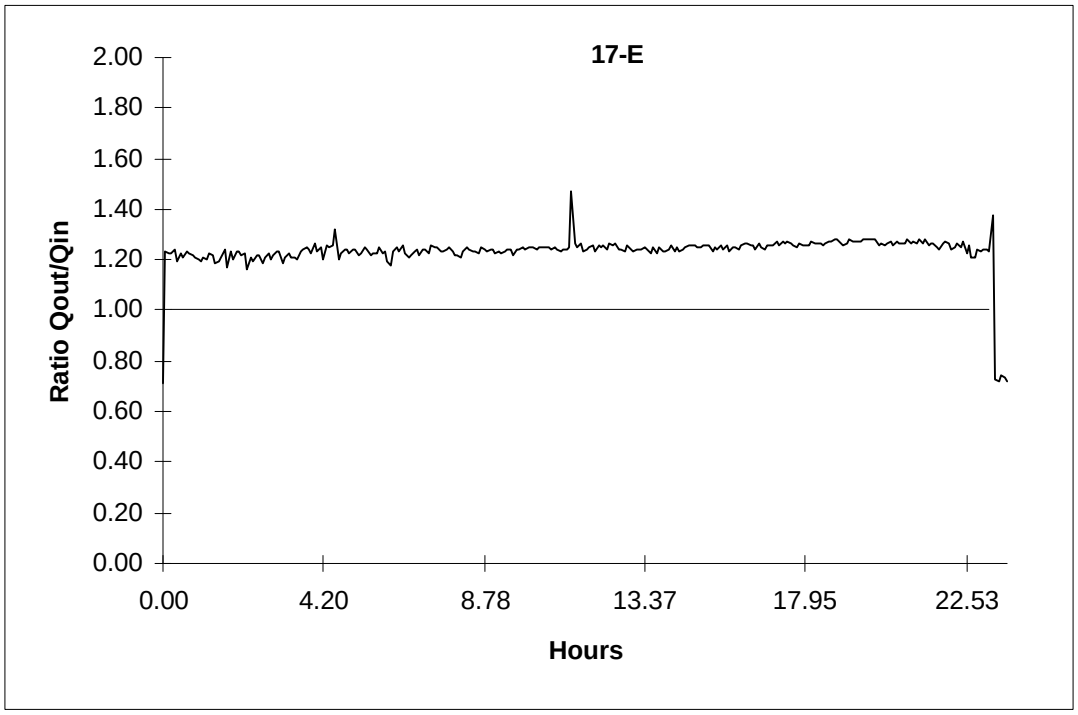

[8] The run 17-E, with a 250µ Pd foil 50x50 mm from Johnson Matthey, and its plot of the ratio of Q_{out}/Q_{in} vs time in hours of the run. The ratio exceeded 1.00 with an average value of about 1.25. The amount over Q_{in} is Q(x) (Q_{out}-Q_{in}=Q(x)) which is 0.25 in this case. Q_{in} = 170 watts from the sonicator and 100 watts from the heater for total of 270 watts for Q_{in}. The value for Q(x) is .25xQ_{in} = 67 watts. The result from run 17-E is the production of 67 watts of excess heat for 23 hours with the input of 170 sonication watts a fraction of which go to the reactor. The ratio of Q(x)/[sonicator power in] is 67/170=0.40. The run was terminated to measure the ^{4}He evolved. The sharp peak seen at about 12 hours is the result of the internal Joule heater suffering a partial power failure which resulted in the heater dropping from 100 watts to 58 watts. The peak shows this 42 watt Joule heater anomaly and is useful as a calibration.

The following plot, figure - 9, shows the data as a ratio of Q_{out}/Q_{in} for the calibration heater run 17 HEATER. The DC Joule immersion heater was set at three different levels to obtain the steady state data for calibration purposes. The plot shows the rise to steady state temperature of all the components using the CC calorimetry with the heat exchanger being the slowest, because its large mass. The constant k that forces Q_{out} to equal Q_{in}, when there is no Q(x), varies with the total heat TW. The k is unique for the Mark II device and normalizes all runs. There is more information on the determination of k in Appendix C.

Figure 9 Joule Heater Calibration for run 17 Heater

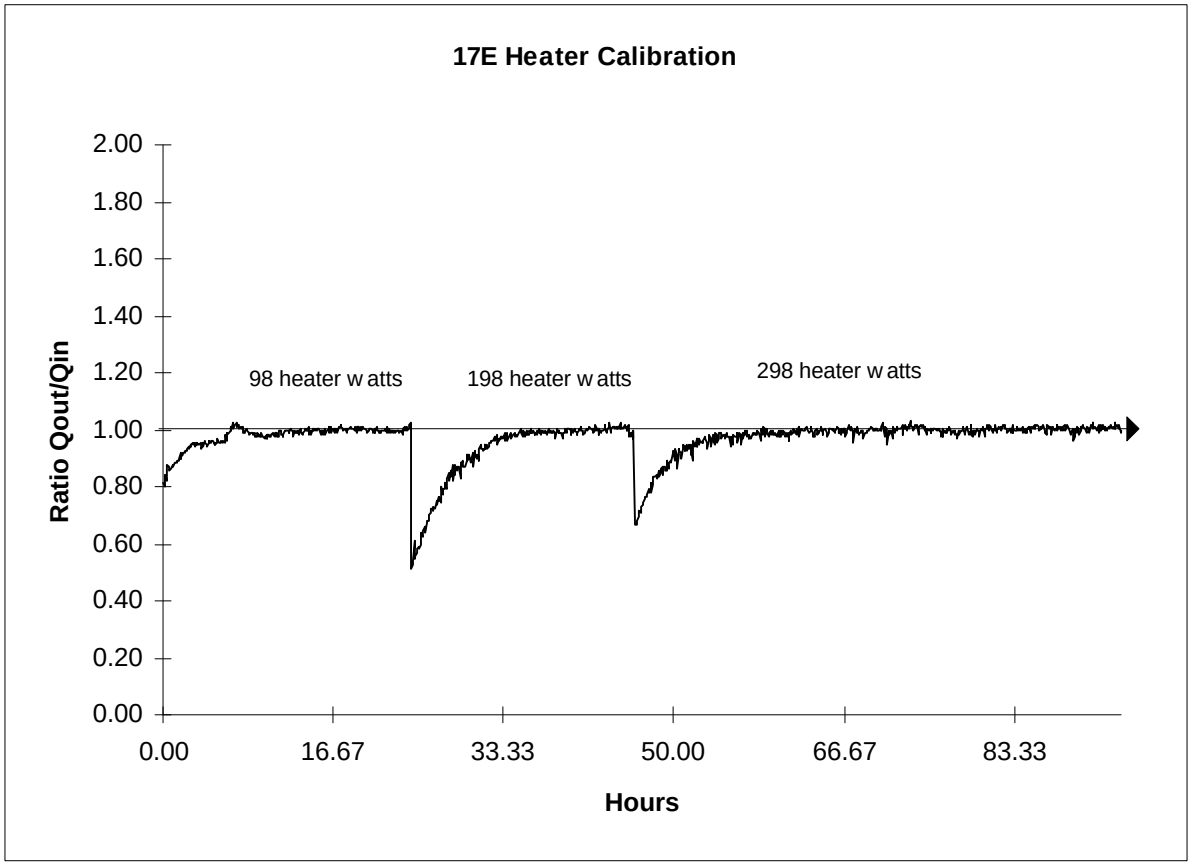

[9] The run 17-Heater, with a 250µ Pd foil 50x50 mm from Johnson Matthey, and its plot of the ratio of Q_{out}/Q_{in} vs time in hours of the run. Data is recorded on five minute intervals. The run replicated a foil run in every way except there was no sonication input. This run is a calibration run using a joule heater input at several values of Q_{in} (98, 198 and 298 watts). A constant was found for the 17-Heater run that forces Q_{out} to equal Q_{in} for the entire system and for all runs. With the appropriate constant found, the ratio for all Q_{out}/Q_{in} equals 1.00. The result from run 17-Heater is the determination of the constant k that is used in the calculations of all the runs.

The following plot, figure - 10, shows the excess heat Q(x) versus the heat produced in R and S which is Q(R)+Q(S). This plot will be very similar to the plot of Q(x) versus the steady state temperature of the run because of the relation of watts to temperature in the Mark II system. The result is the increase of Q(x) as the heat production or input is increased.

Figure 10 Summary Plot showing excess heat increase as power and/or temperature increase

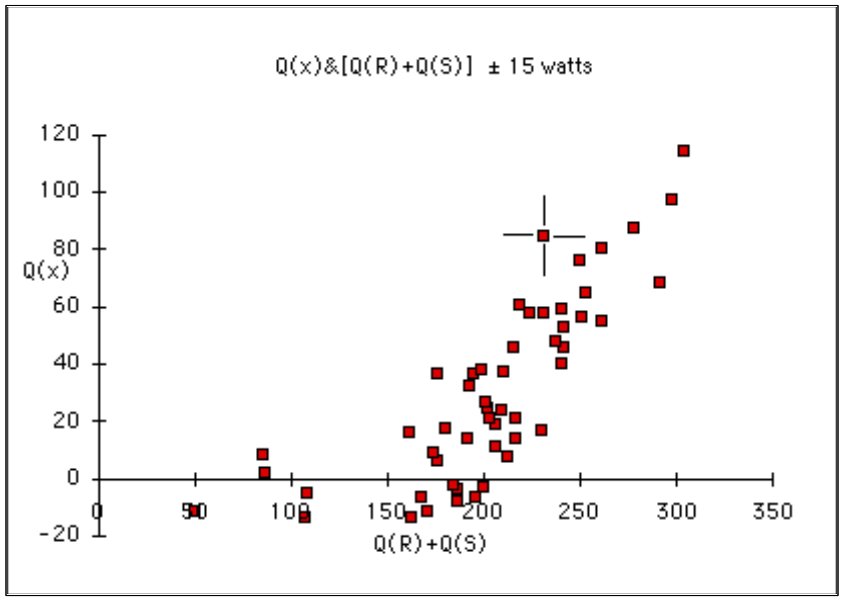

[10] All the run data, except for four runs 2B, 13C, 2F, 3A and 8B that were not at steady state and the calibration runs, are in this plot. The excess heat Q(x) produced increases as the heat input increases which means the steady state temperature increases. Q(R) and Q(S) represents the heat generated by the sonicator, heater and the generated excess heat Q(x).

3. Helium Studies

The E-Quest Mark II apparatus used in these demonstration experiments is designed to provide a simple means to obtain reactor gas samples for helium analysis. The system is largely stainless steel (save for some small cross linked Teflon (TFE) thermocouple wells, tubing, and ceramic pump parts) and is regularly checked to insure it is vacuum tight and without leaks. Observation of low ^{4}He concentration inside the apparatus as operated in the air is consistent with no leakage of ^{4}He into the system). In operation the reactor side of the system is pressurized with high purity argon or deuterium gas to between 2 and 3 atmospheres any leakage is apparent as a pressure drop observed in the data monitoring of the system. Gases are removed after a run via an evacuated 50cc metal sample flask and analyzed via an Extrel C-50 (QMS) optimized for measuring ^{4}He in the presence of D_2. See figure 11

Total ^{4}He is quantified using PVT gas equations to calculate the number of ^{4}He atoms. The information required for this calculation is the final pressure, the free gas volume in the gas manifold, and the gas pressure and volumes after expansion into the evacuated sample volume. After expansion the sample volume is closed and removed for analysis in an adjacent laboratory. Analysis can be within about 10 minutes after taking the sample. The Argon gas for the system is provided via a cylinder from Air Products Corp. and contained a measured background of ^{4}He in the amount of 0.09 ppm, the D_2 used in several runs contained 0.7 ppm ^{4}He. These introduce ~10^{13} atoms of ^{4}He into the apparatus as gases are added into the reaction volume providing the external gas pressure required for proper operation.

The ^{4}He analyses were performed at SRI using an Extrel Corporation QMS with a National Instruments NB-MIO-16 analog / digital interface coupled to a Macintosh IIcx. Using a program developed for this purpose, mass spectra are collected over a three or nine minute period, measuring the contents of the spectrometer chamber. A calibration standard is run both before and after the "test" sample. The data is stored to the computer's disk. Using Microsoft Excel, the average area under the two calibration spectra are averaged and compared to the area of the sample spectra. The concentration of ^{4}He in the sample is calculated using a simple linear concentration vs. area relation traversing the origin. The peak height of all three samples is also calculated automatically and the concentration of He in the sample is calculated as a simple proportion. The concentrations calculated by height and area are reported automatically and stored to disk.

The sample input is equipped with a carbon cold trap to remove D_2 based on a design used by the US Bureau of Mines Helium Field Laboratory, see figure 12. It consists of a short "U" tube filled with activated charcoal suspended in a dewer of liquid nitrogen. This traps almost all of the D_2 and other gases except He and Ne allowing for very well resolved ^{4}He masses without interference of the nearby D_2 masses. The instrument can measure 30ppb ^{4}He in a pure D2 sample. The absolute sensitivity is 5 x 10^{10} atoms ^{4}He with mass resolution of ~0.001 AMU. The resolution between the two masses ^{4}He and D_2 is about 1.5 half widths of the ^{4}He peak (see Fig 11). The MS analyses of the samples were checked before and after analyses with analyses of a calibrated gas mixture of 5ppm ^{4}He in Argon. Calibration checks have shown that a sample

which showed 1.8ppm in the instrument showed 2.0ppm upon analysis by the U.S. Bureau of Mines Helium Lab in Amarillo, TX. A list of the results of these ^{4}He analyses and total ^{4}He atoms found is presented on the table in Appendix . D

Figure 11 Sample Spectra from Extrel MS used in the experiments

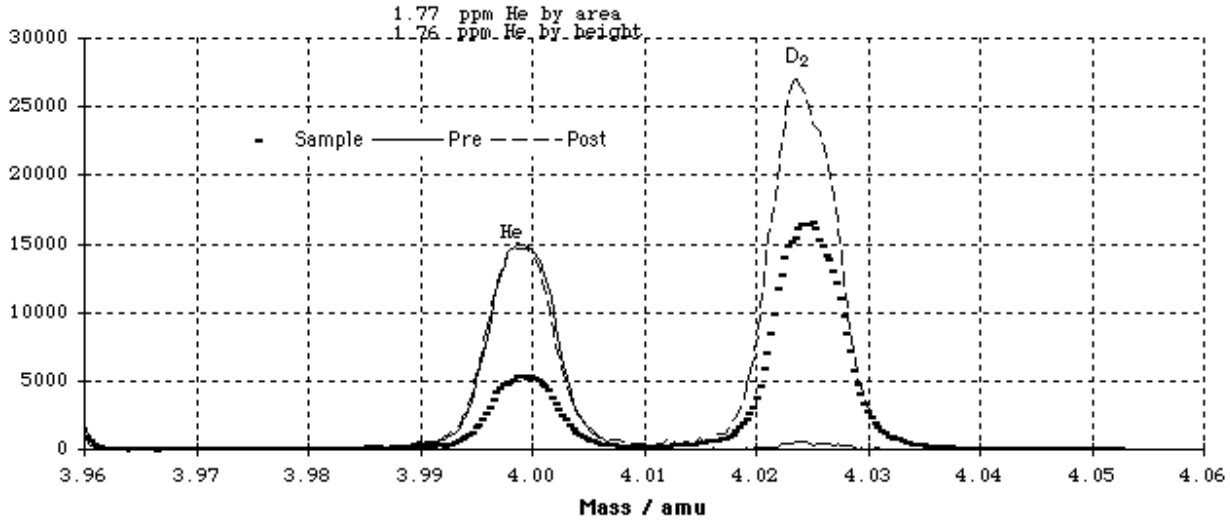

Figure 12 Illustration of the Mass Spec input manifold

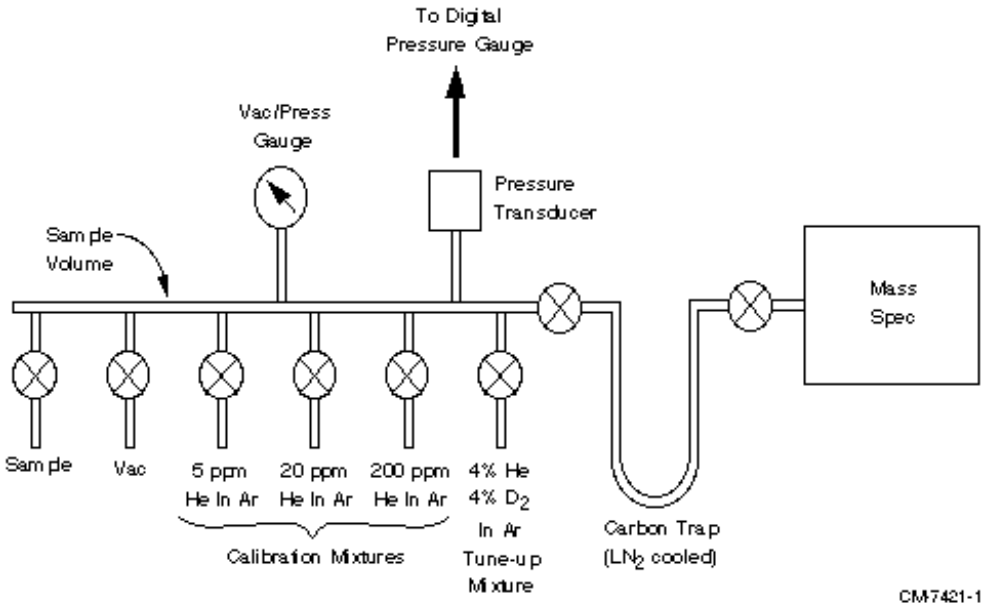

The following 5 plots of helium data collected during this project show some interesting results which we interpret as a trend toward increasing ^4He in the experiments associated with several parameters. The data also shows a stable background as seen in some experiments which we interpret as a good instrument background data. The background in the plots is represented by an arrow. The background is determined by run 17 ARGON where the conditions were the same as the run conditions, except the sonicator was turned off and replaced with a heater input of 300 watts. After 24 hours the gas over the circulating D_2O was removed and was found to contain 0.13 ppm ^4He (the cylinder gas measured 0.09 ppm). This number was, using the PVT relation, converted to atoms ^4He produced and had a value of $6.0x10^{14}$ ^4He atoms. Some runs where ^4He was measured were not included as they were runs that used D_2 instead of argon as the pressurizing gas. the D2 had higher levels of ^4He contamination. The ^4He conservatively has an error of ± 3% in its measurement.

The following plot, figure - 13, displays the data for all the ^{4}He run data that used argon as the pressurizing gas. The total ^{4}He atoms measured are plotted against the excess heat Q(x) in watts. There appears to be a trend in the data indicating a correlation with increasing ^{4}He as the excess heat Q(x) increases. The background (^{4}He atoms in the argon gas after circulating D_2O at running conditions) was measured at a level $6x10^{14}$ atoms after 24 hours. Also of interest are the two runs using Ti foil.

Figure 13 Summary of Helium Data

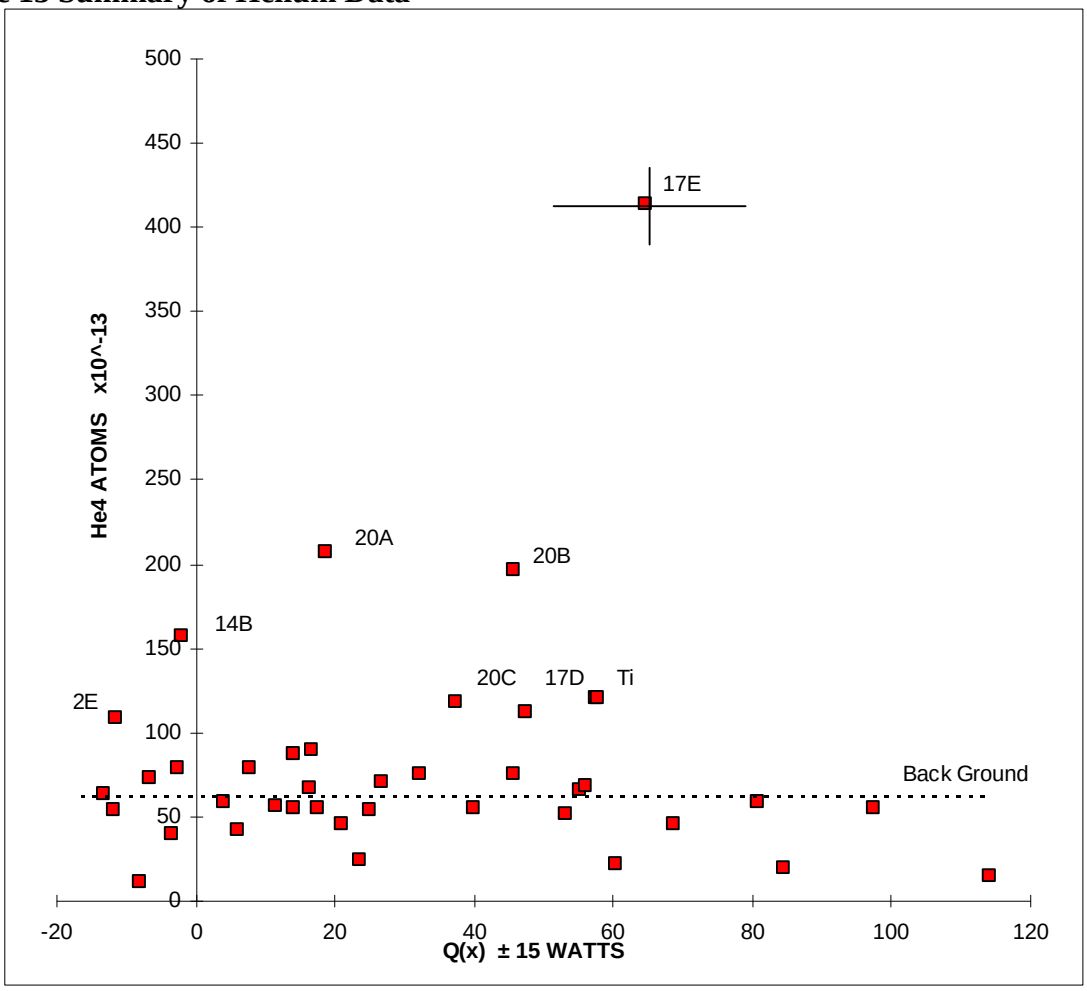

[13] The total ^{4}He atoms measured are plotted against the excess heat Q(x) in watts. There appears to be a trend in the data indicating increases in ^{4}He in runs with 250µ Pd foils. Also of interest are the two runs using the Ti foil.

The following plot, figure - 14, shows the data from all the ^{4}He runs that used argon as the pressurizing gas and not using the few runs that used the deuterium that had a higher level of contamination of ^{4}He. The rate at which ^{4}He atoms are produced per hour is plotted against the excess heat Q(x) in watts. The runs Pd 4A, 9A, 14A and 14B were short runs with extensive foil damage and produced ^{4}He at a higher rate is possibly linked to the foil damage. The rate of ^{4}He production of runs Pd 14A and B leads to a value of 10 watts and an ^{4}He production at about $6x10^{14}$ atoms which equates to a Q(x) from ^{4}He at 24mev per atom of about .4 watts/day. The Q(x) value 10±15 watts may correlate with heat production from the formation of ^{4}He atoms at a rate of .4 watts/day assuming 24mev per atom.

Figure 14 Rate of ^{4}He production plotted on Excess Heat

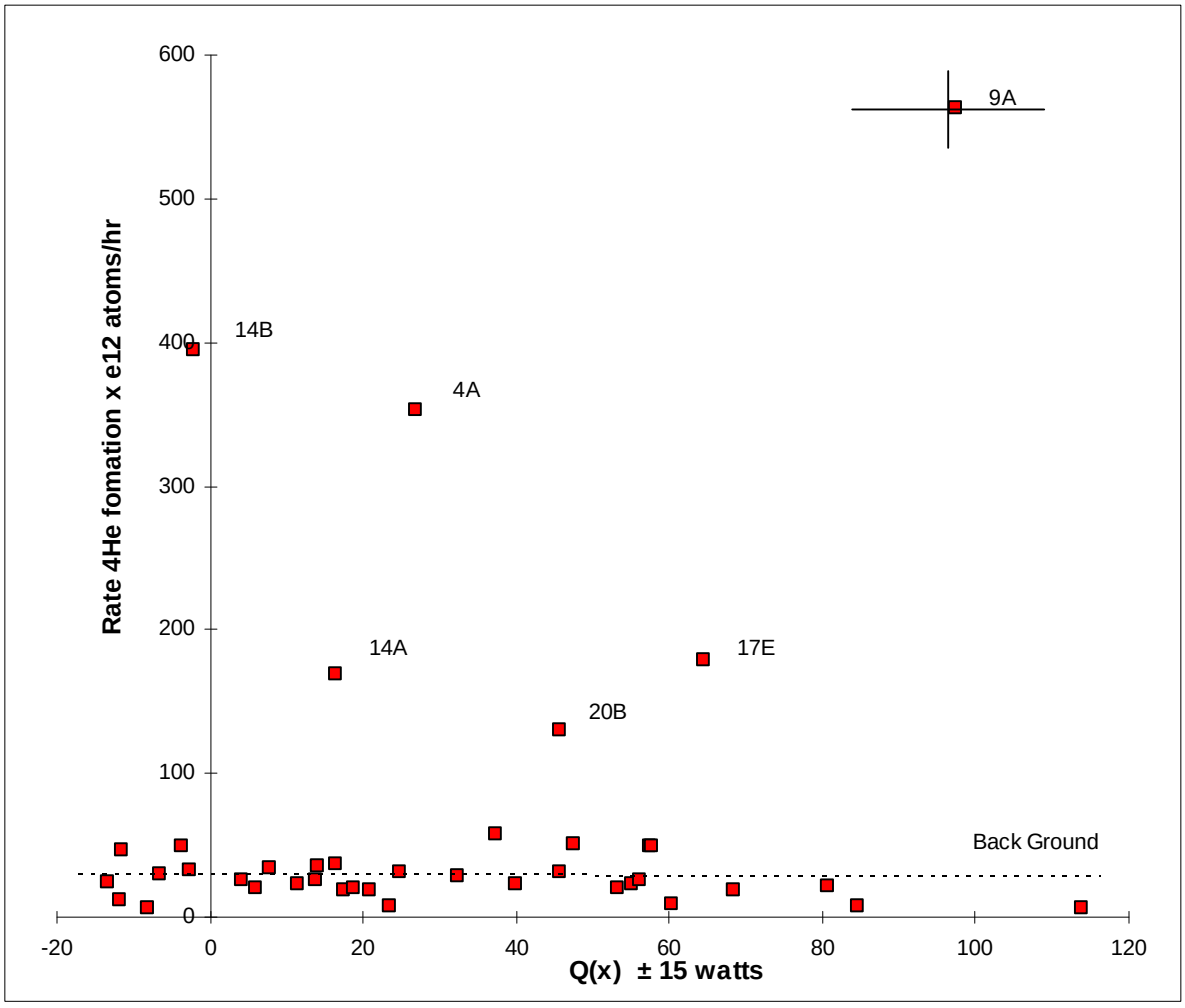

[14] The data here represents all the ^{4}He run data that used argon as the pressurizing gas. The rate at which ^{4}He atoms are produced plotted against the excess heat Q(x) in watts. The runs Pd 4A, 9A, 14A, and 14B were short runs with extensive foil damage.

The following plot, figure - 15, displays the data showing the quantity of ^{4}He versus the excess heat for all of the runs. This is the rate at which ^{4}He atoms are produced when plotted against the heat input to both components Q(R)+Q(S) with short runs with extensive foil damage. The Q(R)+Q(S) are the inputs in R and S and is equal to W+cQ(H)+Q(x).

Figure 15 Helium Data from Argon Runs

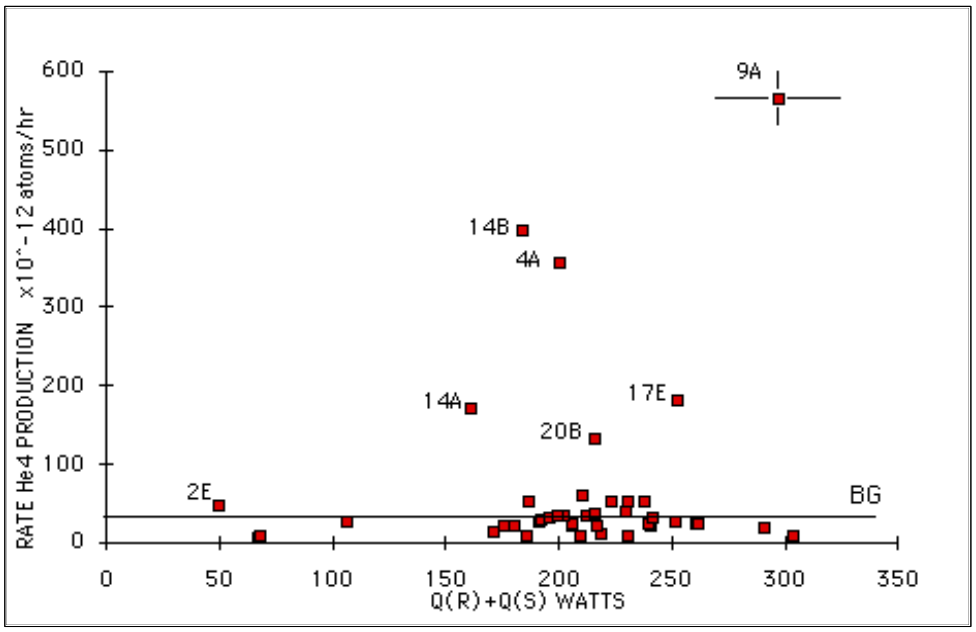

[15] The data here represents all the He4 run data that used argon as the pressurizing gas. The rate at which He4 atoms are produced are plotted against the heat input to both components Q(R)+Q(S). This sum is input to R and S with the source being mostly the sonicator heating and the excess heat produced in the reactor.

The following plot, figure - 16, displays the data showing the quantity of ^{4}He for the runs using Pd foils #17, #18 and #20 including the 17 argon run which defines the background ^{4}He in the argon. These foils are 250μ thick from Johnson Matthey and exhibited the typical foil damage after several runs. The trend in the data indicates at least in runs with these 250μ thick foils that there is some correlation between ^{4}He atoms produced in 24 hours and Q(x). The correlation between heat from the formation of ^{4}He and the Q(x) watts is .25/100. Only 0.25% of the Q(x) comes from the formation of ^{4}He assuming a 23mev per atom reaction, hence the remaining heat must result from other reaction paths.

Figure 16 ^{4}He runs for the Pd foils #17, #18 and #20

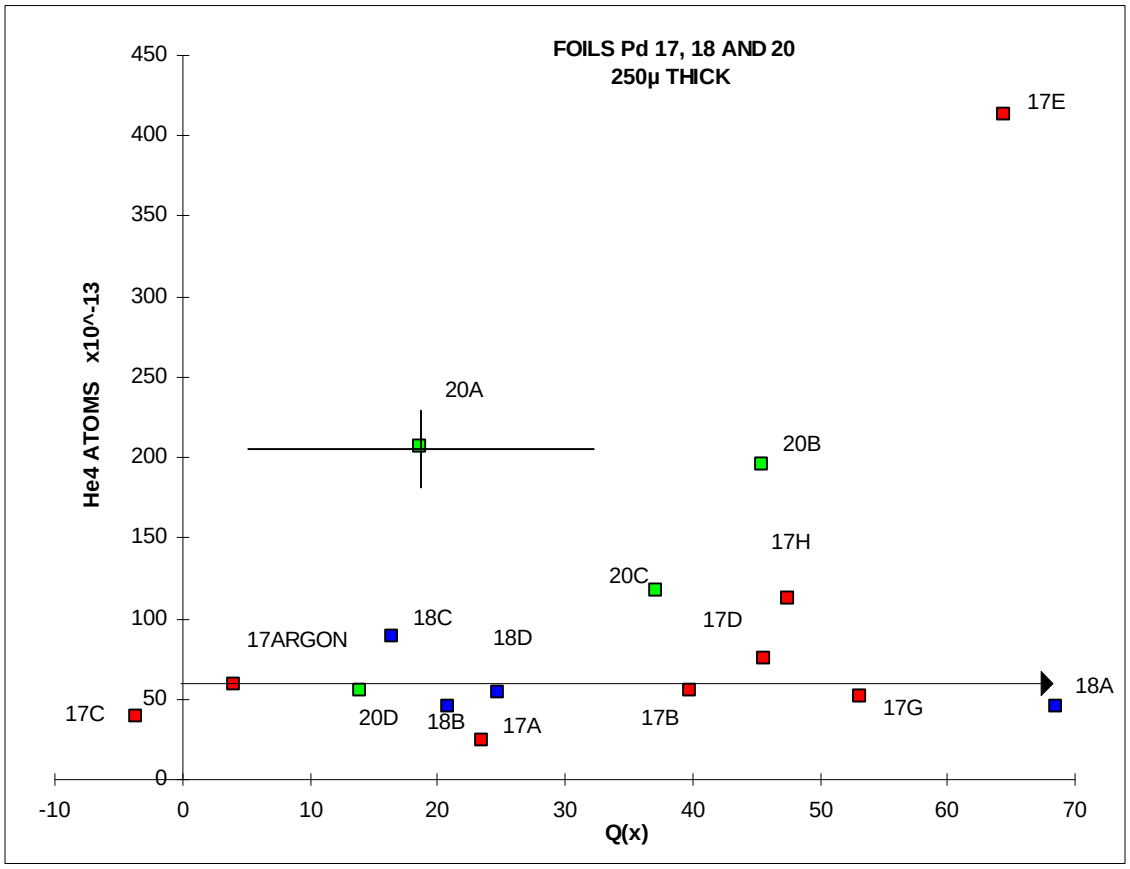

[16] The data here represents all the ^{4}He runs for the foils Pd 17, 18 and 20 including the 17 argon run. The ^{4}He atoms measured from foils are plotted against their excess heat Q(x) in watts. These foils are 250µ thick from Johnson Matthey and exhibited the typical foil damage after several runs. There appears to be a trend in the data indicating a correlation between ^{4}He atoms and Q(x) watts of about 1% based on assumption of a 24mev ^{4}He Rx.

The method of cooling curve calorimetry (discussed later in this document), which was used on this project, requires that a steady thermal state be attained before confidence in the calorimetry is obtained. Experiments sometimes did not achieve steady state for a variety of reasons, not infrequently due to gross melting of the Palladium target as evidenced externally by a great deal of debris seen in the fluid flow or by a sudden changes in the Mark II data. It is difficult to see a clear trends in this representation of the data, but there appear to be some under lying correlation's between atoms of ^{4}He and Q(x) watts as shown in fig. 10 and 14. There is also a correlation trend in the rate of production of ^{4}He atoms and Q(x) and again in the rate of production of ^{4}He atoms and Q(R)+Q(S). The total heat input to the R the reactor and S the sonicator is Q(R)+Q(S).

4. Secondary Ion Mass Spectroscopy - SIMS analysis

Beginning in 1995 E-Quest has performed a limited amount of SIMS analysis using both dynamic and time of flight SIMS techniques at Lawrence Berkeley National Laboratory, Charles Evans and Associates, Phillips Laboratories, and in association with French scientists at the University of Marseilles. The SIMS analytical technique makes use of an energetic ion beam which is used to bombard a very small target on the surface of a foil (ion spot size 2μ-30μ in diameter) inside a vacuum chamber. The metal material ablated by the ion beam is drawn into a high resolution mass spectrometer. The resolution of some of the SIMS instruments used in this work has been in excess of 1/10,000 AMU providing a definitive means to determine with precision the species present at each peak. A mass resolution of ~ 1/8500 is sufficient to determine the presence of single proton interference's on a peak. Further comparison of the spectra with species both up and down the mass spectrum provides a second means to determine possible interfering ions. In general the isotope ratios for a given element can be determined to an accuracy of better than 1% and this level of accuracy has been often observed in our SIMS analysis.

Both dynamic and time of flight SIMS techniques are ideal tools in the search for nuclear shifts in isotopes of the elements present in the targets. One advantage is the amount of material analyzed is very small thus minimizing the background signal. With the amount of energy observed in the experiments a large concentration of isotopically shifted material is not expected and the small signal expected would be easily lost in the background signal inevitable in bulk analytical techniques. The SIMS technique is ideally suited since the dramatic melted appearance of the targets provides predictive morphology assisting in locating the beam on a "melted" zone which we presume to be near the site of the energy releasing nuclear reactions.

Analysis was performed targeting the SIMS beam on an outermost corner of a palladium target foil which we observe is apparently unaffected by any obvious heating effects. The isotope ratio of all isotopes present are determined. Next a site in a "hot" melted zone of the target is selected for the SIMS beam and again the isotope ratios determined.

Upon examining the spectra of isotope ratios of the palladium and silver present one can see that dramatic shifts are observed (see Fig 17). The measured isotope ratios of the "Pd target corner" are quite close to the predicted book values. In the "melt" zone sample the Pd isotopes are observed to have a large anomaly, immediately obvious as an increased ratio of ^{104}Pd relative to the other Pd isotopes. Whether this is an increasing amount of ^{104}Pd relative to the other isotopes of Pd or a decrease of all the isotopes except ^{104}Pd has not yet been determined. (It is curious that ^{104}Pd is known to have a very low neutron cross section.) Examining the silver isotopes we see they are in good agreement with the book values in the target corner analysis but reveal a substantial anomaly in the "hot" zone analysis.

Isotope ratio anomalies have been observed not only in the Pd and Ag but also in lower mass trace elements as well. In some observations of the trace constituent of Ti found in Pd samples revealed a dramatic shift in Ti isotopes. ^{48}Ti normally the most abundant isotope (73.5%) has been observed to be reduced to about 7% while ^{47}Ti originally at 7.9% increases to ~70%. We believe this evidence suggests loss of a neutron from ^{48}Ti to produce the observed ratio shifts. Additional isotope ratio anomalies in elements approximately 1/2 the mass of Pd are observed and are the subject of intensive ongoing studies. Finally SIMS analysis has also been used to examine the targets for isotope anomalies in low mass species such as hydrogen and helium isotopes in the targets. Large increases of deuterium are seen in the "melt" zone samples on the order of 50X that found in the "cool" target corners. Helium has also been observed in the lattice using SIMS which is particularly interesting since in the SIMS instrument is not sensitive to He.

Further studies of the substantial inventory of targets from a these experiments as well as other E-Quest experiments is certainly warranted. Such studies provide a promising means to identify the nuclear reactions which are present in the experiments by finding the reaction products. This will undoubtedly throw substantial light on the reaction mechanism.

Figure 17 TOF SIMS spectra of palladium as described (reproduced from peak height data).

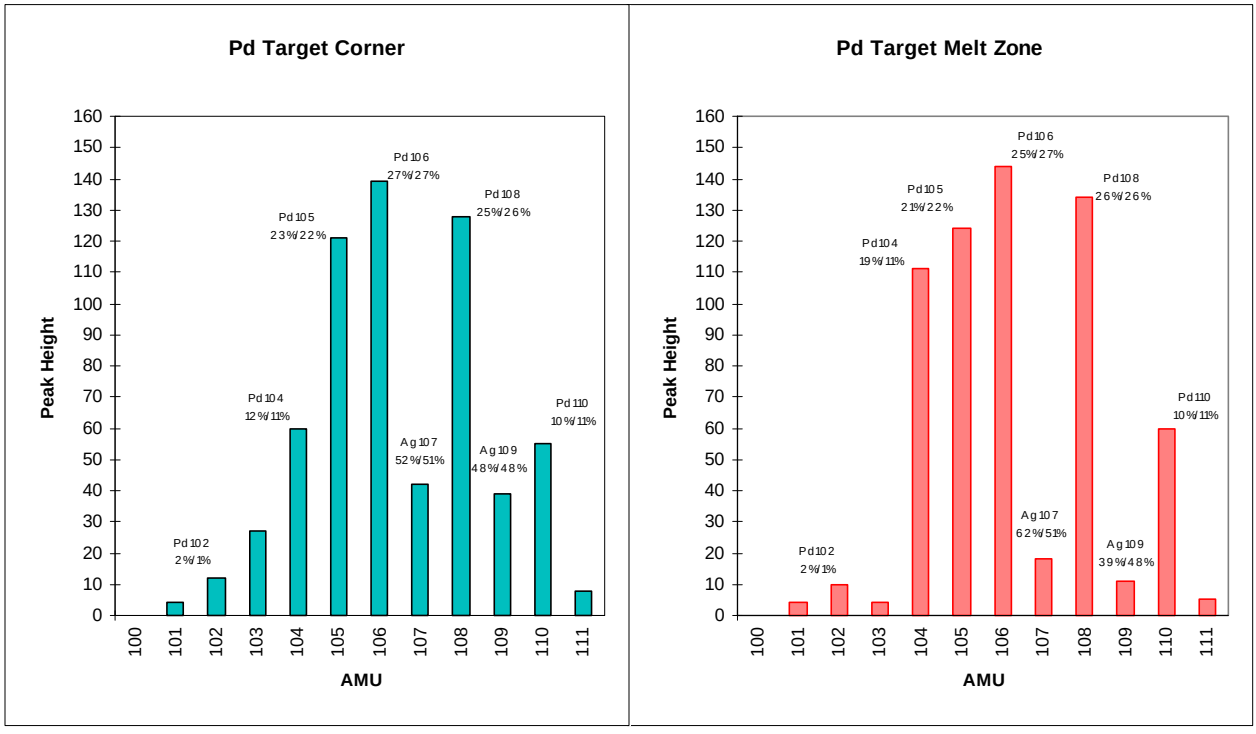

[17] These spectra show the isotopic anomaly found in palladium targets consistent with a nuclear process. The spectra show anomalies in both Pd and Ag groups. The spectra on the left is from the corner of the target (a relatively inactive region) while the spectra on the right is from a "melt" zone. The resolution of the instrument allows us to rule out all but a very small (< 1%-2%) effect of ion interference, the fact that both Pd and Ag groups are in close agreement with established ratios in the inactive region strongly suggests that such interference's can be minimized. SIMS spectra Tranh van Duc Lyon France.

5. Discussion

The previous sections of this report provide details on the experimental apparatus, methods, and the quantitative information ascertained during the course of this project. Inevitably in any pioneering experimental field there is additional evidence that is of a less quantitative and more observational nature. This data is important to understanding the experiments and is presented in this discussion section.

Source of the Excess Heat

It is our assumption that the majority of excess heat comes from a new class of nuclear reactions within the "reactor" segment of the apparatus. An accurate partitioning of the excess energy production has not been within the scope of this project however it merits some discussion. Our observations of allied reaction effects from the heavy water reactor system which include production of ^{4}He, T, melting of the metal targets, and isotopic ratio anomalies in the target metals has allowed us to hypothesize that deuterium containing metal (Pd and Ti) target systems are a key location for the production of excess energy. There are however three other possible locations for the portions of the excess heat. In many experiments of a gas or electrochemical nature (eg. hydrogen isotope loading of metals) excess energy is reported from ordinary water experiments with various metals (see ICCF conference reports 89-95). The Mark II does have an ordinary water titanium / aluminum / stainless steel portion where intense acoustic energy is first introduced to the apparatus. It is possible that some part of the excess energy in the system is sourced in this "sonicator" part of the system. Other researchers (notably Lawrence Livermore National Laboratory - LLNL) have proposed and are currently engaged in research focused on the potential of ultrasound induced cavitation to produce nuclear fusion reactions within the collapsing bubble unassociated with a metal target (15, 16, 18) While the reports from LLNL have stated that no reactions have yet been observed (based on neutron emission data only) they persist on their several year course of experimentation to produce such events. Similar conditions to those in the LLNL experiments occur as a matter of course in the E-Quest Mark II apparatus. Finally researchers at the Cavendish laboratory in the UK have recently published papers suggesting a fourth potential energy source from cavitation effects common in the Mark II apparatus. The Cavendish paper based on somewhat on a hypothesis of the late Julian Schwinger who suggested Casimir and vacuum energy field effects may result during bubble collapse and produce anomalous energy [25]. While these four potential partitionable energy effects exist in the Mark II apparatus we have concerned ourselves for this report to one for which the most evidence exists, the D Pd system.

Target Foils

A number of target foils were used in the experiments, most of which were used in an as-received state. Some foils were annealed before use while others were observed to have differing characteristics. The examination of data pertaining to the target foils leads to some interesting possibilities. It appears foil ductility and thickness plays a roll in the durability of the foil. For example the runs that used 100µ Pd foil from Aithica were damaged at a high rate. The foil was damaged to the extent that its exposed surface area was a small fraction of the original. This damage occurred in 1 to 4 hours. Cavitation extending for longer periods at times hinders production of ideal calorimetric data as foils may be substantially destroyed before the system can reach steady state. A factor that may influence this rapid destruction may be the relative grain size of the foils. The Aithica foils are more ductile and have a larger grain size. Foil 7A was annealed for 3 hours at 850°C and subjected to cavitation for about one hour resulting in the about a 50% destruction of the foil with a large hole in the center. On the other extreme the foils 10A&B, which used the Pd with 2.5% boron foil (provided by the Naval Research Laboratory) which was quite hard and had a very fine grain structure, experienced very little damage during the runs. It was demonstrated in runs 19A&B, which used #316 stainless steel foils with a thickness of 75µ also a fine grain material, shows little if any damage. Also the runs produced very little measurable Q(x) as did runs 10A&B. These were all fine grain foils.

We believe that thicker Pd foils are not necessarily more durable than thin foils. More likely when palladium foils from Aithica and JM are compared, it is the grain size that dictates the durability. The 100µ JM foil used in runs 2A-F is about as durable as the 250µ JM foils used in many runs. These foils show little damage after running in experiments lasting several days. The 100µ foil from JM lasted for six runs (~ 24 hrs each) and was less ductile than the same thickness Aithica foils. Grain size appears to be responsible for the durability in the palladium foils. Both 100µ Aithica and JM foils produce ^{4}He and Q(x).

In terms of excess heat production from several different foils some results are worth mentioning. The Pd foils produce excess heat, Q(x), in about 80% of the runs. The two titanium foil runs also produced a measurable amount of Q(x). The runs using the PdB foil from NRL did not produce a measurable amount of Q(x) nor did the stainless steel foil runs. When the foil was removed from the reactor and run with no foil under the same operating conditions, except flow rates, there was no Q(x) produced. The series of foils used in the experiments at SRI are shown in figure 18.

Figure 18 Photos of foils used in the demonstration experiments

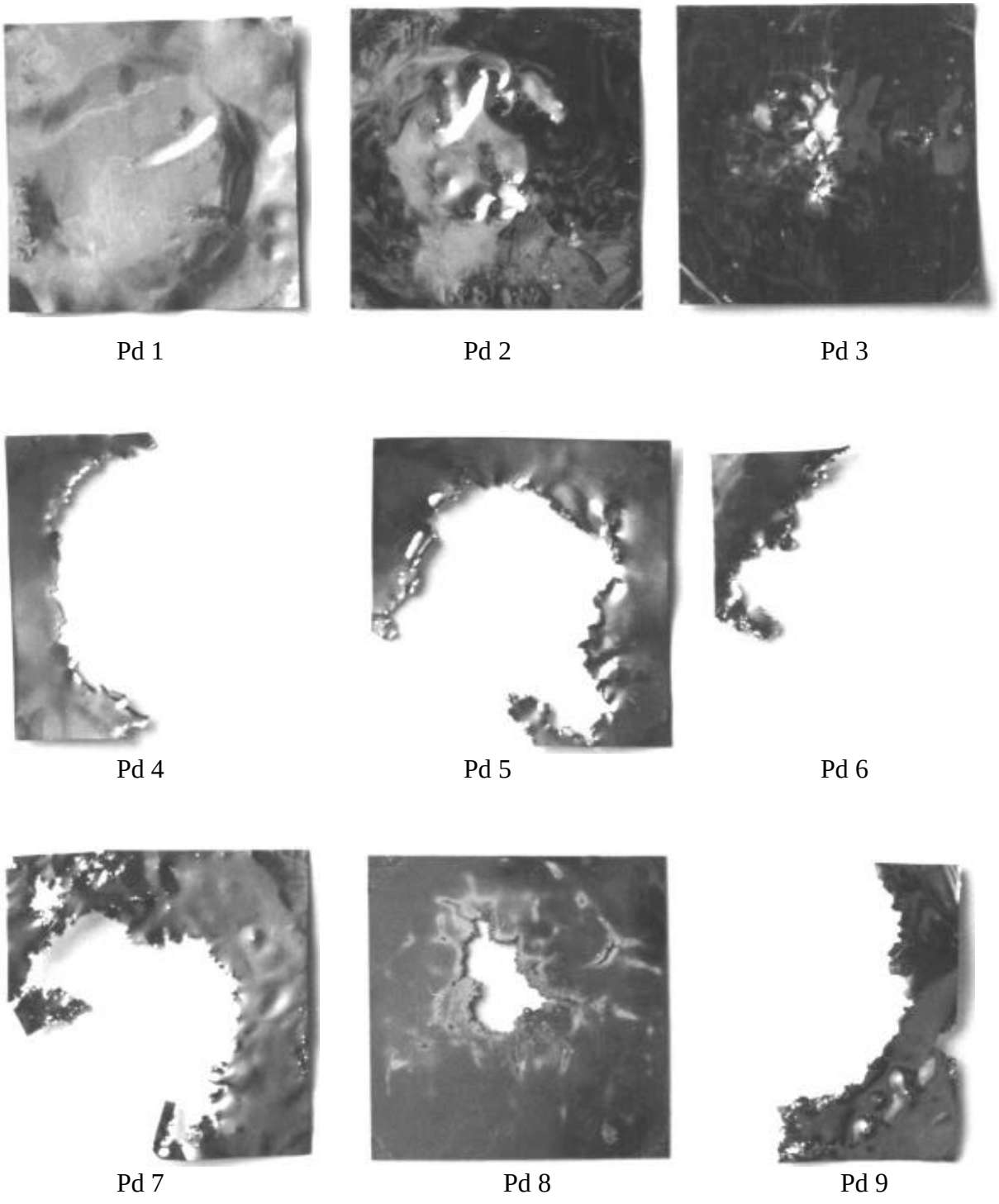

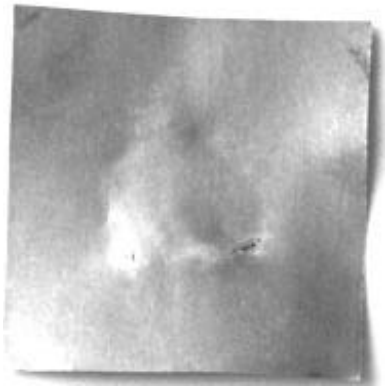

Pd 10

Pd 11

Pd 12

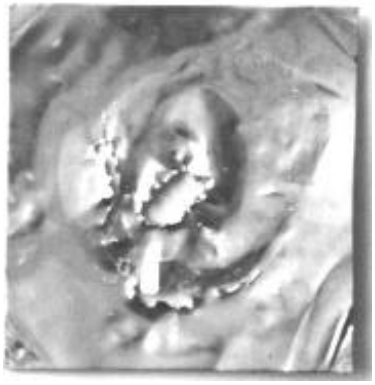

Pd 13

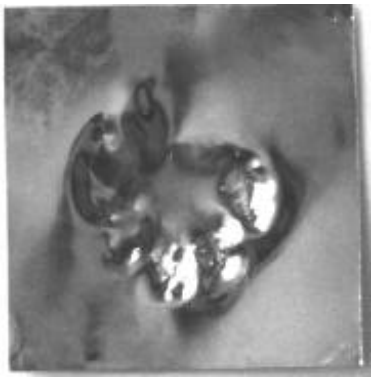

Pd 14

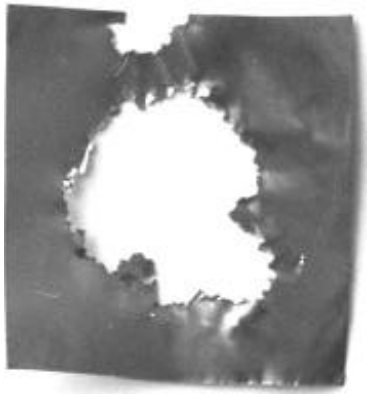

Pd 15

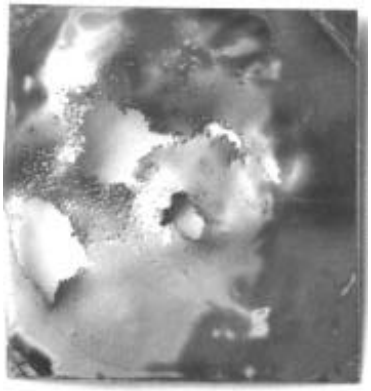

Pd 16

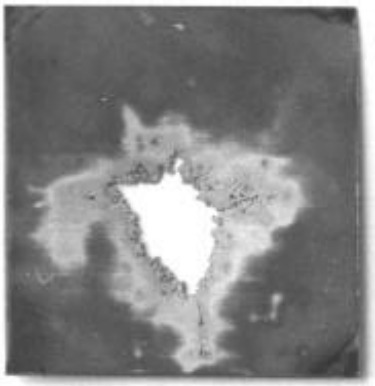

Pd 17

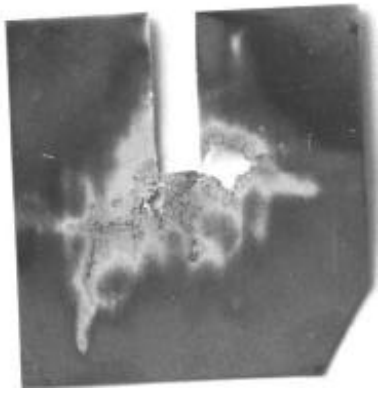

Pd 18

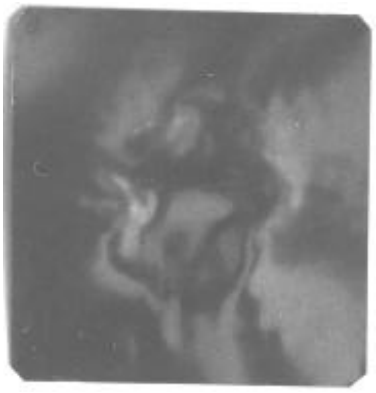

SS 19

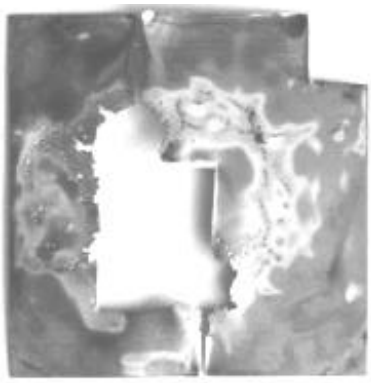

Pd 20

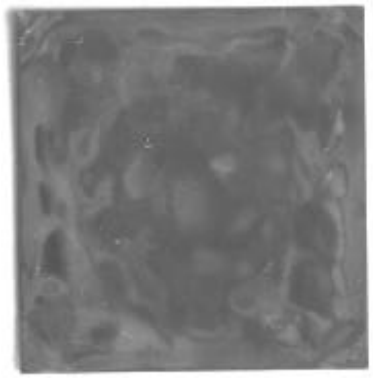

Ti 21

The physical effects of heat production in the foil can be seen in discoloration, holes, debris and regions appearing to have an obvious melted appearance. From x-ray diffraction, bulk mass spectroscopy, and SIMS studies we know there is D and ^{4}He present in the lattice with the assumption that the D is implanted by the bubble action. Other atoms in sizable concentrations and thus with an implantation potential are O and Ar. ^{4}He in the metal has been shown, using quantitative and non-quantitative techniques, to increase in the foils producing heat when compared to virgin samples of the same material. Since helium is virtually immobile in metals there could be a significant portion of the ^{4}He produced by the nuclear processes still residing in the foil awaiting measurement.

Examining the runs with the Aithica foils, some of which lasted 24 hours, presents the possibility that runs characterized by rapid destruction of the foil may be producing a lower reaction rate at the end of the run as the foil is destroyed. Presumably if the majority of the foil was destroyed early in the run then the collected data should show runs with diminished activity levels. The two runs that fall into this category are 5A and 6A, however in looking at the data, these two runs were productive in Q(x). The explanation probably rests in that the metal debris produced, which remains as potentially usefully large pieces, contributes to Q(x). These runs are indicative of some advantageous conditions that would promote activity with small bits of foil. In the short runs, which lasted only a few hours were short because of the relatively rapid destruction of the foil where the rate of ^{4}He production was high. The runs that fall into this category are 4A, 7A, 9A, 14A&B and 15A with no ^{4}He measurement in 7A and 15A. The ^{4}He was perhaps produced at higher rates apparently at the expense of the foils.

D_2O Tritium Analysis

Samples of the D_2O used in the experiments were routinely checked for tritium content before and after the experimental runs using liquid scintillation analysis. One cc samples are distilled to dryness and the distillate measured using a well established liquid scintillation method. No significant changes in tritium content of the heavy water were observed.

Distribution of Acoustic Energy Relative to the Target Foils

Acoustically etched patterns observed on some of the foils (particularly the apparently inactive stainless steel foils) is a useful indicator of the acoustic energy distribution within the reactor. From the visual, unaided eye and microscope, examination of the foils a consistent process can be detected in the reactor R. The acoustic energy as it passes from S to R is best described as a forced resonance at 20 Khz in a clamped circular plate. A standing wave is produced in the reactor side of reactor separator plates. The etched pattern on reactor separator plates indicates concentric rings of a standing wave with nodes at 1.1 and 2.7 cm from the center of reactor separator plates. The diameter of the .1 cm thick plate was 7.6 cm. The acoustic energy from reactor separator plates is coupled to the partially clamped foil forcing it to resonate in a unique pattern depending on the thickness and composition of the foil (see Fig 19). For example for the 100μ thick palladium foil the acoustic pattern is a checkerboard with 0.22 cm squares etched in the surface and for the 250μ thick foil the squares are 0.75cm on a side. The effect of the acoustic energy as it is absorbed into the lattice is to stretch and compress it. The total acoustic energy in the lattice has components of forced resonance waves and chaotic waves. This will add to the probability of high energy density existing for an instant in regions of the lattice.

Figure 19 Titanium foil showing acoustic node pattern

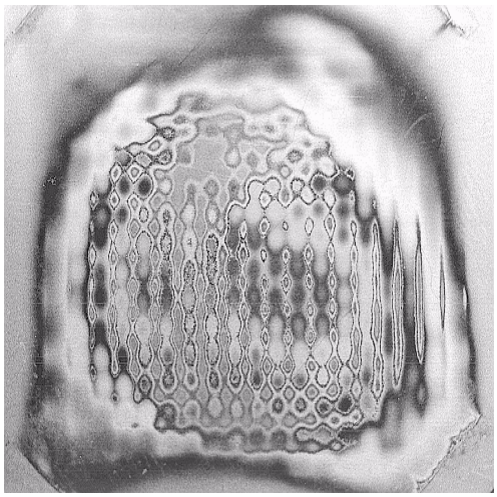

[19] The above image (1.5X larger than life-size) shows a Ti foil from an E-Quest experiment demonstrating acousticnodes which indicate acoustic energy is distributed over a fairly large portion of the target.

Particulate matter produced in the reactor during a run will collect at the nodes of the forced resonance in the reactor. These particles will scour the surface in their neighborhood keeping it clean. Also being at the nodes these particles will be subjected to intense acoustic energies. These particles are collected on a filter and may hold much information when analyzed.

Nuclear Ash

There appears to be a trend in the data suggesting increasing ^{4}He with increasing heat output, W+Q(H)+Q(x). The same trend exists for W the acoustic heat input to R and S and for Q(x) the excess heat. An interesting possibility is that if based on the excess heat observed in the system factored by a hypothetical ~20Mev per reaction there is evidence for 10^{19} reactions. The 10^{15} atoms of ^{4}He observed would be consistent with an incidental spallation yield of alphas of one part in 10^{4} events which is in keeping with established spallation yields from other nuclear processes (such as tritium yield in ^{235}U fission).

$$\mathbf{N+D \rightarrow [transition] \begin{matrix} \nearrow [N+1] \\ \searrow [N-1] + \propto \end{matrix}}$$

The ^{4}He and the Q(x) heat factor; One might for example assumes the heat that evolved from a D+D fusion reaction with 24 Mev liberated as heat during the formation of one mole of ^{4}He. The level of 10^{16} atoms of ^{4}He produced (measured) in a 24 hour run by this above reactions yields heat equivalent to about 0.4 watts/day far less than observed.

The heat production, Q(x), is not explained by a reaction such as D+D → ^{4}He. Evidence is mounting of a nuclear ash with a variety of constituents thus the nuclear heat arises from many obscure paths of a nuclear nature of which only a few of many have been identified.

Heat data in the reactor and sonicator

The following describes the collection and treatment of data for the determination of Q(x) from R and S. The Q(x) was assumed to come from R only by assigning the value of 1.00 to the constant K (K being the partition factor for Q(x)). In fact there may have been some of Q(x) generated in S. Whether some of the Q(x) came from S and the light (ordinary) water and titanium system or R and the heavy water and palladium system is not as important as the production of Q(x). The sorting out of the value of K will take more effort.

6. Path Forward

This report describes a series of demonstration experiments that generated a vast amount of data which has not been completely considered at the time of writing this "final report." A large amount of useful and perhaps very revealing data is still being given consideration in an ongoing more thorough analysis in conjunction with 7 years of experimental data in hand. For example examination of the target materials and the remnant materials to study isotopic ratio anomalies and thermal effect is expected to provide important and perhaps profound understanding of the experiments. In parallel experiments conducted in a sister device during this same time frame, in association with French scientists, follow-up analysis (in France) of target materials using time of flight SIMS to determine isotope ratios has revealed dramatic isotope shifts which give rise to a proposal of several essentially simultaneous nuclear processes. Additional work on this project would usefully include study of surface and bulk effects using scanning electron microscopy (SEM), secondary ion mass spectroscopy (SIMS), thermal neutron capture prompt gamma analysis, and various other analytical techniques to examine isotope ratios and possible anomalies which might point to particular nuclear reactions taking place in the materials.

Modification of the experimental apparatus to improve performance with regard to heat production and nuclear measurements are also warranted. In parallel to these experiments the E-Quest team operates a sister Mark II device and newer generation of Mark III devices, and is constructing Mark IV and Mark V devices in our labs in Mountain View, CA. The compilation and analysis of the experiments using all these devices is an ongoing process but preliminary results from Mark II and III series devices are in good accordance with the operation of the Mark II at SRI. Earlier experiments performed since 1989 using Mark I and Mark II apparatus by E-Quest scientists are also in good agreement with the work presented here.

Experiments as part of an ongoing collaboration between E-Quest and SRI are continuing. the SRI efforts focus on the science involved in determining the possible products and mechanisms of the nuclear processes while at E-Quest’s own labs the emphasis is now being placed on the optimization of the demonstration protocols to produce larger excess heat by application of a number of engineered improvements to the system as well and the use of improved materials. Through these improvements we expect to achieve sustained energy input to output ratios of up to 5x or larger which are currently observed for some experiments at E-Quest using a newer generation of research apparatus.

The search for unusual nuclear "ash" by measurement of isotopic ratios in the reaction materials will continue with an emphasis on both helium and higher Z nuclei. Helium analysis ought to best include determination of the ratio of ^{4}He to ^{3}He and ^{22}Ne to provide a clear evidence that the helium produced is not due to contamination. Already background controls show the helium levels to be above the experiment ambients. In earlier experiments performed both at E-Quest and Los Alamos National Labs large amounts of helium produced was shown to be in a unique isotopic ratio with regard to both ^{3}He and ^{22}Ne and hence could not be sourced from contamination. High Z isotopic anomalies have been previously confirmed using SIMS analysis on equipment at Lawrence Berkeley National Labs and very recently in laboratories in France and the US. The nature and quantitative measurement of these isotopic anomalies must be further confirmed by repeated determination but shows great promise toward providing a basic understanding of the new nuclear reactions produced by the E-Quest experimental devices and protocols.

E-Quest is now engaged in active arrangements with major research organizations around the world to continue with and establish new collaborative research projects in respected national nuclear laboratories in India, China, Japan, France, and the United States. The task of unraveling the mysteries of this new field of nuclear energy technology has just begun. With a reliable test bed reactor as demonstrated in the E-Quest MK II reactor further studies to determine the nature of the “micro-fusion” reactions is now possible and indeed relatively inexpensive in comparison to previous nuclear fusion research methods and technologies.

In addition to on-going work on scientific fronts to understand the mechanisms engaged in the nuclear processes E-Quest is working to engineer practical applications involving the use of this apparent new energy source. While it is difficult to predict when such product engineering will deliver large numbers of consumer level devices certainly some useful technology will be ready for sale within a few years.

7. Appendix A A Primer On The Behavior Of Cavitation In The "Micro-Fusion" Context

The behavior of cavitating (collapsing) bubbles have been studied since the turn of the century. One of the most noted study was by Lord Rayleigh (1) in his early work on cavitation damage to ship propellers for the British Navy. More recently the study of stable cavitating bubbles (SCB) as generated by an ultrasonic acoustic wave in water has drawn considerable attention for the characteristic light emission generally referred to as sonoluminesence (2,3,4,5,6). Research at E-Quest Sciences has focused on another unexpected behavior of ultrasound generated transient cavitating bubbles (TCB) in water upon metallic foils. The work described here is new but some portions have been previously reported in scientific conferences (7,8,9). The work of the authors bears a number of similarities and common elements with the more thoroughly published studies of stable cavitating bubble / sonoluminesence systems. It is therefore important to understand the similarities and differences of the two regimes.

In both the sonoluminesence experiments and the E-Quest micro-fusion experiments an ultrasound source of approximately 20khz is directed into a small volume of water, either ordinary or heavy (D_2O) water. The acoustic wave passing through the water causes small non-conformities in the water, nucleation sites, to produce bubbles which grow and collapse during the wave cycle(s). The bubble contents are a mixture of gases dissolved in the water and water/liquid vapor. The physics of this bubble growth and collapse is well described in scientific literature as a result of both experimental observation and theoretical modeling. Of particular note Flynn, Apfel, Laterburn, Prossperitti, Crum, Putterman, and others have used the differential equations developed by Rayleigh and Plesset to model and describe the cavitating bubble. Recently speculations in the scientific literature about energy concentration within a cavitating bubble have led to discussions of very high energy density of the final phase of adiabatic collapse of the bubble where shock waves add to the overall energy in the bubble system (3,4,10).

The cycle of bubble growth and collapse and the mathematical treatment of the bubble is very similar in both TCB and SCB systems to within the final picoseconds at the end of the first wave cycle. The primary difference between the two systems is that in the stable cavitating bubble system the bubble shrinks to a tiny size but is regenerated and endures through successive wave cycles lasting for many generations of growth and collapse. In the transient cavitating bubble system the bubble collapses to destruction in a single wave cycle.

Figure 20 Stable Cavitation Bubble Diagram

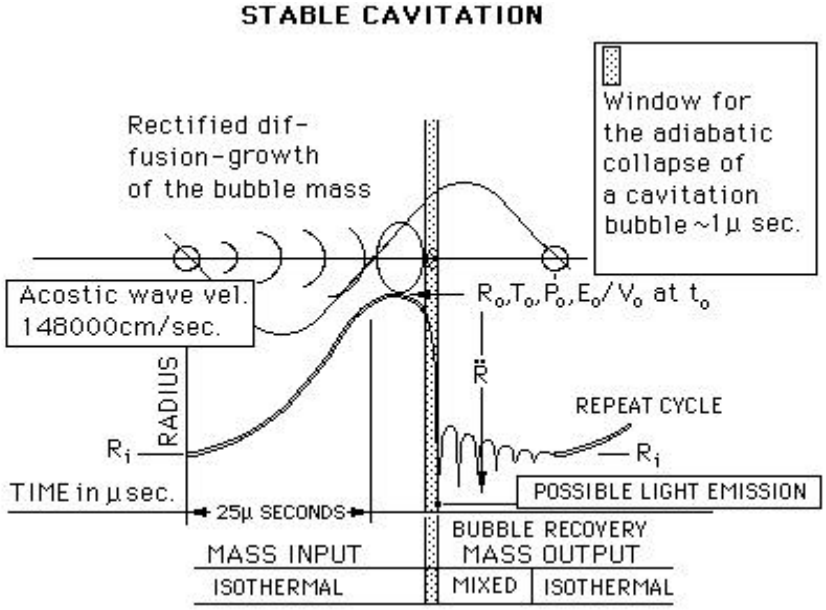

Figure 21 Transient Cavitation Bubble Diagram

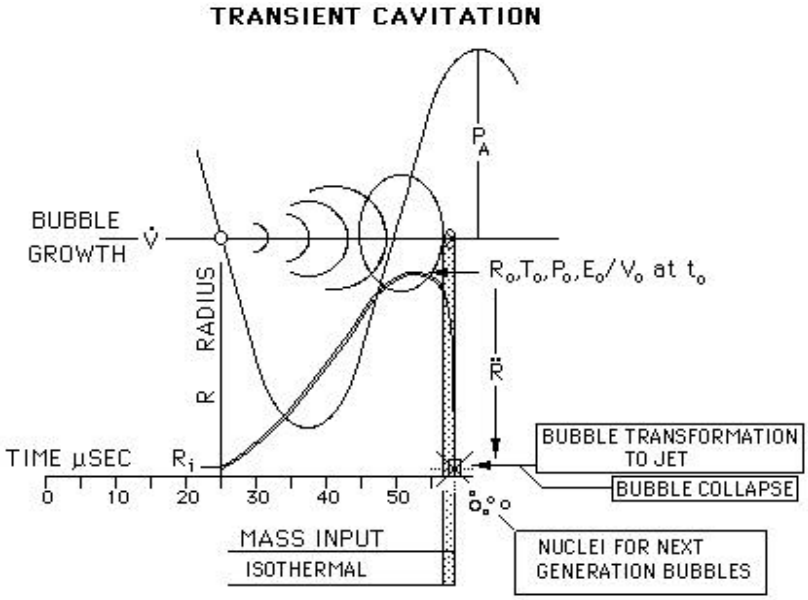

Figures 20 & 21 depict some of the complexities in bubble growth and collapse in an acoustic field for both stable and transient cavitation bubbles (SCB and TCB). The velocity of the acoustic wave depends on the media it passes through, in this case D_2O. The frequency depends on a mechanical driver which generates the waves at a particular amplitude. Bubble growth starts during the negative portion of the acoustic wave with a bubble radius R_i and continues to grow into the positive portion of the pressure wave until the momentum is lost at R_o and the collapse begins.

During the growth phase the mass of the bubble also increases via a process described as rectified diffusion (11,12,13,14). In the SCB system the bubble is a cyclic steady state process lasting many cycles. In the TCB system the collapse is a one cycle event. The rectified diffusion process for both is isothermal and for a 20khz frequency will last for about 30µ seconds.

At a point where the radius has reached its maximum, R_o at t_o, the forces acting on the bubble initiate an adiabatic collapse with a duration of less than a µ second. The parameters R_o, T_o, P_o, to and E_o/V_o (is the same as E_o/cR_o^3) represent the state of the bubble at the start of its adiabatic collapse commencing at time T_o. R_o is the maximum radius of the bubble, T_o is the temperature of the D_2O in the liquid phase, P_o is the internal pressure in the bubble and E_o/cR_o^3 is the energy density in the bubble all at R_o. During the collapse the bubble shell is accelerating towards the center of the bubble at a rate that permits little communication kinetically with the surrounding liquid. If the shell collapse velocity is high the collapse system will create shock waves [3,4,10]. The collapse of a SCB reaches a minimum R and rebounds with additional oscillations losing mass in the process and finally stabilizing at R_i to start the cycle again. Just before the initial rebound the sonoluminesence light flash occurs. The TCB collapses violently with formation of a jet that is formed in the final stages and which appears to generate a vortex of the contents of the bubble. The destructive collapse causes the generation of small bubbles that will act as nucleation sites to start new bubbles in the next acoustic cycle.

Figure 22 Bubble Jet Formation
Velocity vectors depicting the movement of the bubble contents during adiabatic collapse.

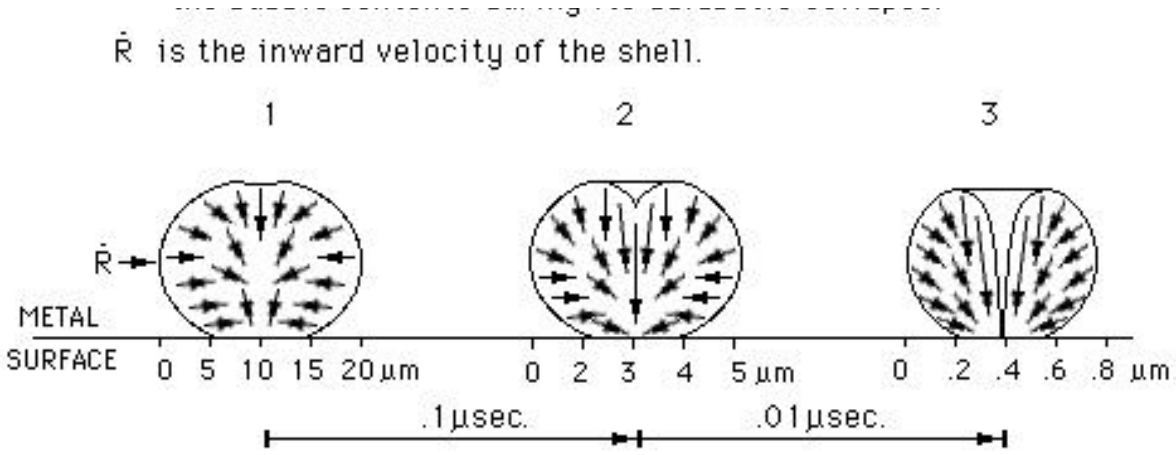

[22] The illustration shows the velocity vectors of the mass movement during transient bubble collapse. The speed of the collapse provides indication of the likelihood of shock wave generation. In the time frame of the final collapse the kinetic communication between particles is lost but the electromagnetic communication still exists in the high density collapsing bubble system.

The studies of the picosecond synchronous light emissions from a single stable cavitating bubble oscillating in an acoustic field have suggested that the synchronous light emissions are less than 50 picoseconds (6,15) and may be on the order of 14-15 picoseconds (16). Reports have been recently published in both scientific and popular press about the surmised potential of SCB systems to produce energies needed to initiate classical "hot" fusion of hydrogen isotopes contained within the bubble (10,15,17,18). Such reactions would be readily observed by the characteristic emission of energetic neutrons. The reports refer to experiments producing sonoluminesence bubbles in D_2O which have been made by researchers at Lawrence Livermore National Laboratory where neutron detectors have been used to search for evidence of hot fusion. As of fall 1995 results of experiments began in the spring of 1994 had not yet revealed any neutrons that could be attributed to a source other than normal background (16).

In the E-Quest transient bubble cavitating system the destructive transient collapse is brought on by greater amplitude in the acoustic wave. Sonoluminesence is not a typical characteristic of the TCB system. If the transient bubble is located on a surface, the energy of the wave is distributed unevenly with respect to the bubble and the bubble undergoes asymmetric transient collapse with the contents directed toward the surface as a "jet" (see bubble jet image fig 23 and bubble vector illustration fig 22). In the typical experiments conducted at E-Quest and powerful acoustic horn produces the asymmetric transient bubble collapse on a metal target lattice.

Figure 23 Illustration of a Bubble and "Jet" on a Metal Lattice

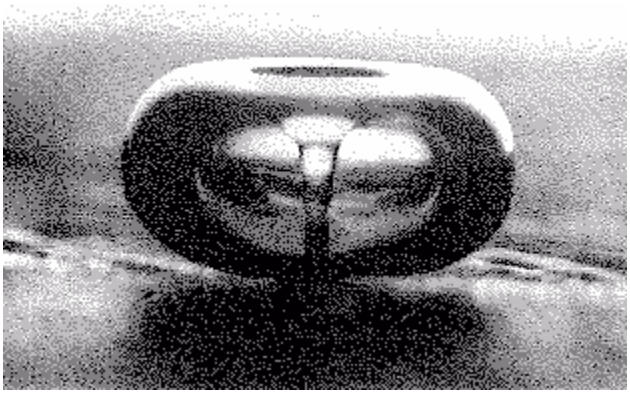

[23] This photomicrograph shows an asymmetrical transient cavitation bubble collapsing on a metal surface. The bubble reveals the characteristic tornadic jet directing toward the surface. (The image is squashed due to the scanning process and ought to appear more spherical.) Photo courtesy Prof. Larry Crum Univ. of Seattle.

8. Appendix B Melting of Pd Target Foils and Ejecta Events as Evidence of Nuclear Heating

Melting of the target metal during the course of the E-Quest "micro-fusion" experiments is a common occurrence (see photo of melted Pd target foil fig 24). It is, however, not a necessary effect as experiments may be operated in a fashion which produce heat with little lattice damage. In considering the experiments that produce this melting phenomenon a comment is often heard that such damage is consistent with cavitation damage. However, this is not the case. Damage due to cavitation alone as has been studied in systems such as pumps, ship propellers, and directed ultrasound on thin foils is much different in character than the cavitation damage produced in the E-Quest experiments. Typically "normal" cavitation damage is similar to erosion and presents itself as removal of material grain by grain from the surface inward. Indeed some "normal" cavitation damage does appear on the targets in the E-Quest experiments but the major cavitation damage observed is thermal damage and involves a much different process.

Figure 24 Photo of Melting Effect on Palladium Foil

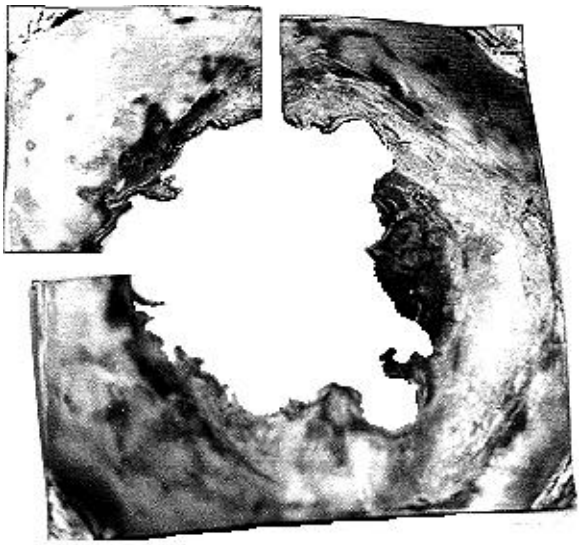

[24] This photograph shows a palladium Target (50mm x 50mm x 0.1mm) with a large melted central portion. Debris from melt includes ~1 micron sputtered Pd beads. Exposure time in the reactor <24hr.

In the micro-fusion experiments of E-Quest the target foils often reveal a dramatically melted appearance. This characteristic melting is composed of numerous thermal ejecta events. These are revealed under scanning electron microscopy as small volcano like craters which remain following an eruption of molten or gaseous metal from a heated reservoir within the lattice. The ejecta event starts as a vaporous sphere of lattice atoms which rapidly transfers heat to other lattice atoms. The vaporous sphere of atoms will either transport its heat to the surrounding lattice until the lattice atoms re-solidify or the vaporous sphere of atoms will break the surface of

the lattice and spring out as vaporous or molten ejecta. These events are captured in the following SEM photos (fig 25 & 26). Such ejecta are readily identified by their cone and fan shaped craters radiating out from a cylindrical vent. The ejecta cone or fan is often littered with tiny ~1 micron fused spheres of metal which have the appearance of sputtered metal and/or glassy smooth cones or fans where the metal was ejected at a very high temperature. This is a common occurrence in palladium targets but also occurs with other metals.

Figure 25 High Temperature Ejecta Crater

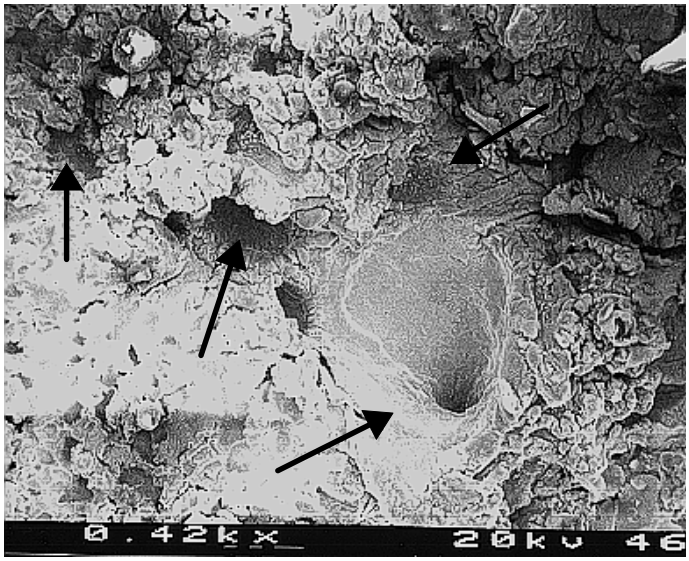

[25] SEM 1 shows an SEM Image (420X) of a Pd target showing "vent -like" holes where hot metal has been ejected from deep within the material. Photo J. Dash and R. George.

Figure 26 Lower Temperature Ejecta Vent

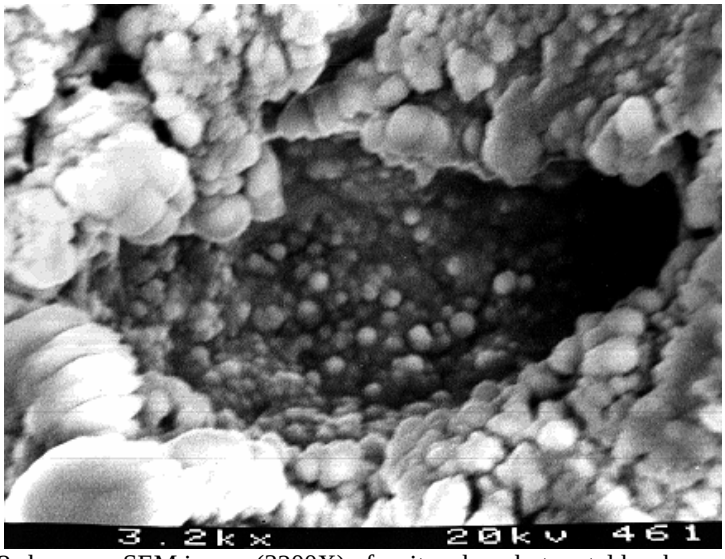

[26] SEM 2 shows an SEM image (3200X) of a site where hot metal has been ejected and solidified with the appearance of “sputtered” beads on bottom of the ejecta crater. beads ~ 1micron in diameter. Photo J. Dash and R. George.

A thorough search of the literature and discussion with experts in cavitation and nuclear damage to metals has resulted in only one possible linkage to a previously observed similar phenomena. This kind of damage to metals is consistent with damage seen in fissionable materials such as californium which undergo spontaneous nuclear fission. (19).

One can calculate the energy involved in such ejecta events. Using the SEM images an accurate measurement of the ejecta vent and crater dimensions are readily obtained. In a simplified treatment, viewing the lattice ions, in electron gas, with heat transfer via electrons we can demonstrate the approximate energies required to cause such an effect. This ejecta volume will, in the general case, be considered as cylindrical and ejecta site having the a $\mathbf{P}(D/2)^2 \times 4D$ geometry. In the simplest terms the associated atomic oscillators and velocity of the electron gas were used to determine the rate of heat loss to the bulk lattice. All the energy in the ^{4}He formation will be passed to the bulk lattice. The rate of heat dissipation to the lattice uses these models.

Assuming a cylinder/mass of Pd ejected from the lattice is at a temperature near its vaporization point. We calculate the nuclear energy densities to accomplish this feat. Indeed in some cases the ejected metal may be in a plasma state.

Figure 27 Table of Eject Event Vent Size and Number

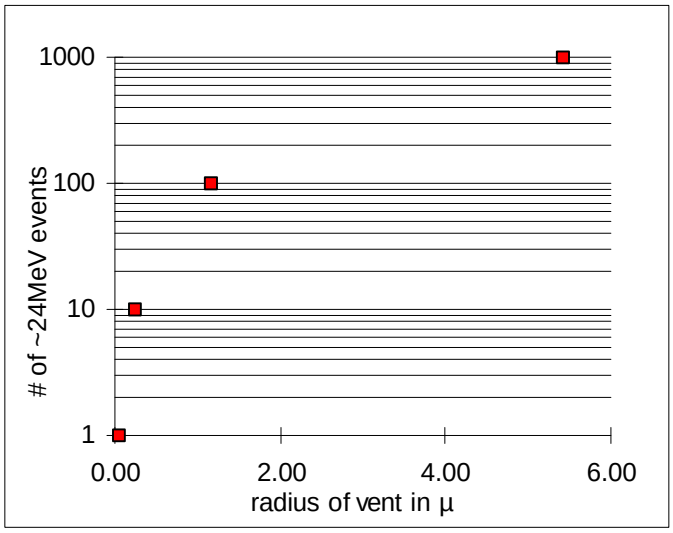

[27] Calculated number of 24MeV events required for cylindrical ejecta at approximately the vaporization point of palladium.

Events of approximately 10 microns in diameter as pictured in the preceding SEM images have required about 24000 MeV of energy. If one assumes, just for the sake of a yardstick, a D+D→^{4}He reaction releases 24 MeV the events pictured in the SEM photos would require some 1000 nearly simultaneous events. The D+D → ^{4}He reaction is not being identified here as a proposed reaction but is one of many candidate reactions possible. Naturally, the absence of a 24Mev gamma suggests this precise reaction as known to science is not likely.

9. Appendix C "Cooling Curve" Calorimetry and Measurement of Total Heat in the System

The calorimetry used to characterize the MKII demonstration experiments is based on three main factors, the heat production, the heat distribution and the heat loss at steady state conditions. The heat production is from the acoustic heating of the D_2O and H_2O and is represented as W. The heat distribution is that heat registering a steady state temperature in all the components and is measured as sum of all the cooling curve, CC, data. The heat loss is defined as the rate of component surface cooling as defined by the cooling curves. The material in this appendix provides a basic description of the E-Quest "cooling curve" calorimetry used in the SRI experiments. The CC calorimetry was complimented with "mass flow", MF, calorimetry which was simpler but are not as reliable in this case as the CC method. These two methods of calorimetry describe the thermal characteristics of the apparatus.

An even simpler and more problem free form of calorimetry is employed at the E-Quest labs in Mountain View on the sister Mark II device where an internal joule heater in the sonication containment provides a calibration standard in the sonicator. The energy of the system is then measured as a function of the heat seen in the large common heat exchanger which is 80% of the heat capacity of the Mark II device. It is important to determine the efficiency E of the acoustic heating which is done by comparison with the heater runs.

Calorimetry in the E-Quest experiments is routinely performed as both a diagnostic and quantitative tool. The apparatus is seen for this purpose as a large complex mass which produces, distributes and loses heat to the air primarily through convection, with a small amount through radiation. The basis for the calorimetry is the cooling curve method which follows Newton's Law of Cooling. In use the determination of excess heat of a particular experiment is made by comparison to calibration runs of a similar configuration. Calibration experiments in the Mark II device using the same flows and pressures were performed with calibrated joule heaters. With this information from the heater runs, inert target (stainless steel) runs, and foilless reactor runs, a typical experiment with Pd or Ti in D_2O, when compared to these calibration runs, reveal a source of excess heat Q(x). See figure - 5.

In operation the prepared apparatus is turned on and begins to heat up. Circulating pumps move D_2O and H_2O between the reactor and sonicator system and a large closed heat exchanger. The water filled closed heat exchanger is kept in motion with a stirring motor. The heating up process takes 6 hours to achieve a steady state temperature where heat input is balanced with heat loss. A very stable laboratory environment is required to achieve a stable steady state.

The data for these demonstration experiments was collected using Keithley data acquisition hardware linked to a Macintosh computer which was in turn linked to the laboratory Apple network. In addition to thermocouples, sensors linked to pressure and power meters also fed data to the computer. Flow rates, pressures, and amplifier input power and output efficiency are also logged. Other data was noted using various auxiliary equipment and logged into the lab notebook.

Figure 28 Calorimetry Block Diagram

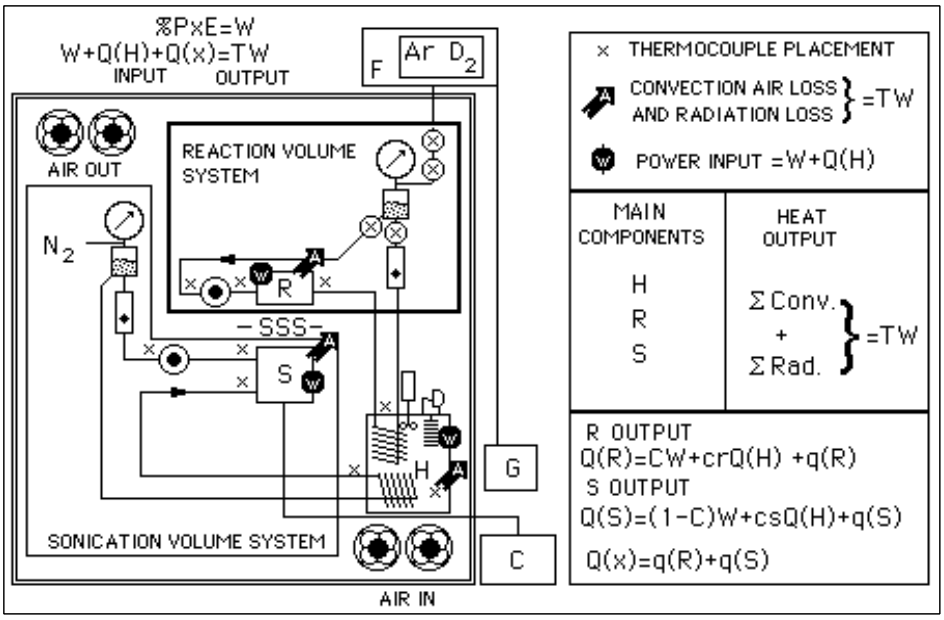

Figure - 28. This figure shows where the heat was produced (w) and lost (A) and the partitioning of the heat in the H, R and S components and the origin of Q(x). Specifically, it takes into account the heat distribution and production for the above components. The diagram also shows the approximate location of some of the thermocouples (indicated by x) that provide temperature data which were recorded every 5 min. throughout the course of each run. In addition, the diagram indicates the total convection and radiation losses TW, which equals W+Q(H)+Q(x), the total input from the sonicator W, the input from the Joule heater Q(H) and excess heat Q(x). These outputs and inputs form the basis for the calorimetric calculations needed to determine the excess heat; Q(x)=TW-(W+Q(H)). The partitioning of Q(x)at its point of origin, R or/and S, represented by q(R) and q(S)should be done but has not been attempted. See equations in the lower right corner of figure. C and (1-C) are the partition factors for W in R and S and cr and cs are the partition factors (using MF data) for Q(H) reaching R and S (most of Q(H) will reside in H). The partition factors for Q(x), K and (1-K) were not calculated and set to 1.00 and 0.

Figure 28 shows the approximate location of all of the thermocouples (indicated by x) that provide temperature data which were read and recorded throughout the course of each run. In addition, the figure indicates the locations of the major heat input and output sources (Conv. and Rad. black arrows with the white "(A)" convection and radiation loss) and the input sources (W and Q(H), black circles with the white "(w)"). These outputs and inputs are the basis of the calorimetric calculations of excess heat Q(x).

The results from the collected data was accomplished using spread sheet calorimetric calculations for each run. The data was put into both graphic and spread sheet forms to study the over all performance of runs at the steady state temperatures. When the entire system is at steady state, that is all of the components are at their steady state temperatures, the **heat in** is equal to the **heat out** [$Q_{in}+Q(x)=Q_{out}$] or [W+Q(H) +Q(x)= TW] and [TW = Q_{out}]. From the TC measurements of the components, the temperature differential between steady state T_{ss} and room temperature T_r are found. Using the Newton Cooling for a given component $hA[T_{ss} -T_r]$ and is the rate of heat loss and is equal to the watts generated by all sources - acoustic, heater and Q(x). Note that the radiation losses Rad. are split out from the $hA[T_{ss} -T_r]$.

During a typical run the sum of the convective and radiative losses is equal to input from the acoustic source, heater and Q(x) with system at steady state temperature. A correction to the convection heat losses is made by determining the constant k. This constant depends on the value of Conv. - the heat lost by convection - using the Joule heater calibration runs at different heat inputs (Conv.=TW-Rad.) is the heat lost by convection. The constant k, as a function of TW, is used to correct all components convective losses and is inserted into the Newton Cooling equation $hA[T_{ss} -T_r]*k$. The value of k changes with the value of TW for all runs in a predictable fashion and is a constant for the M II device. The value for k varies form 0.64 to 0.93 for values of TW from 100 to 300 watts for the heater runs. More on the constant k is found in this appendix in the first part of the (1). THE COOLING CURVE section.

There is a smaller contributor other than Conv. that adds to the cooling curve losses. These are the Stefan-Boltzman radiation losses, Rad.. The heat losses due to radiation from the Mark II are a function of the temperature difference of the surface from its surroundings. The net radiation loss from the reactor is represented by the Stefan-Boltzman equation. The value for e, the emissivity of the surface of the components, is found in reference tables and the value for the Stefan-Boltzman constant, **k**, is $5.672x10^{-8}$ mks. More on the radiative losses is found in this appendix in the (5). RADIATIVE LOSSES section.

The total heat input from the sonicator and the heater is Q_{in} = W+Q(H).

The sonication input watts as heat to R and S is W. There were two power supply types used in the experiments; the Misonix XL 2010 and XL 2020 with a maximum rated outputs of 475 and 550 watts respectively. The later was used in the majority of the runs. The tuned ultrasound power supply acoustically heats the water in the reactor and sonicator using a portion of its output. The value for acoustic heating W is determined by matching acoustic heating to the calibrated Joule heater. The power supply has two operating parameters. The dial setting and the wattmeter percentage with the dial at a values between 1 and 10 and the wattmeter percentage which is a measure of the line power into the power supply. The wattmeter will cutout if the power draw exceeds 100%. The total power input to the converter is the DIAL times the WATTMETER. The efficiency E equals W/[0.1*DIAL*%WATTMETER*RATED MAXIMUM WATTS].

The E value depends on W, the acoustic heating, which is determined from the heater runs. If we look at all the data from calibration and fit the foil runs by vary E (refer to figure - 5) so as to find the best fit for the foil data set with respect to the calibration data, we find that the fit occurs when E equals 0.45. With the value for E in hand the values for acoustic heating, W, are determined. More on the efficiency factor E is found in this appendix in the (4). DETERMINATION OF THE SONICATOR INPUT EFFICIENCY section.

The XL 2010 - W = 0.1*DIAL*%WATTMETER*475*E1 E1= .60
The XL 2020 - W = 0.1*DIAL*%WATTMETER*550*E2 E2= .45

The excess heat is found in the relationships below.

Q_{out} = TW = W+Q(H)+Q(x) and Q_{in} = W+Q(H) ---------- [1]

Q_{out}-Q_{in} = Q(x) ---------- [2]

In the spread sheet of the ratio Q_{out}/Q_{in}, see figure - 31, this ratio is equal to 1.00 if Q(x)=0. If the ratio is larger than 1.00 then Q(x) has a value in watts for the excess heat. This value for the Q(x) is the difference between TW and (W+Q(H)). (TW-(W+Q(H)) = Q(x).

Mark II heat production and distribution.

The accounting of the heat at steady state of all components sampled at 5 min. intervals uses a spread sheet to aid in the accounting for both the heat as it is produced, distributed and lost at steady state running conditions. Two methods used for measuring heat at steady state. The cooling curve method, CC, uses the Newton Cooling relation [$hA(T_{ss}-T_r)*k$], and the mass flow method, MF, uses the relation [MFgm/sec*cal/(gm°C)*DT°C*4.186 J/cal] watts.

The heat is produced at three locations by the joule heater as Q(H) in H, by the sonicator as W in R and S and as Q(x) in R and S (see figure - 29). The production of heat from the components R, S and H in the form of Q(R), Q(S) and Q(H) is transported via the circulation of light and heavy water though the components of the M II device, with each component reaching their specific steady state temperatures. The distributed heat is then measured in R, S and H as Q'(R), Q'(S) and Q'H as determined by the cooling curves, with most of the heat residing in the heat exchanger H.

Figure 29 Calorimetry Block Diagram

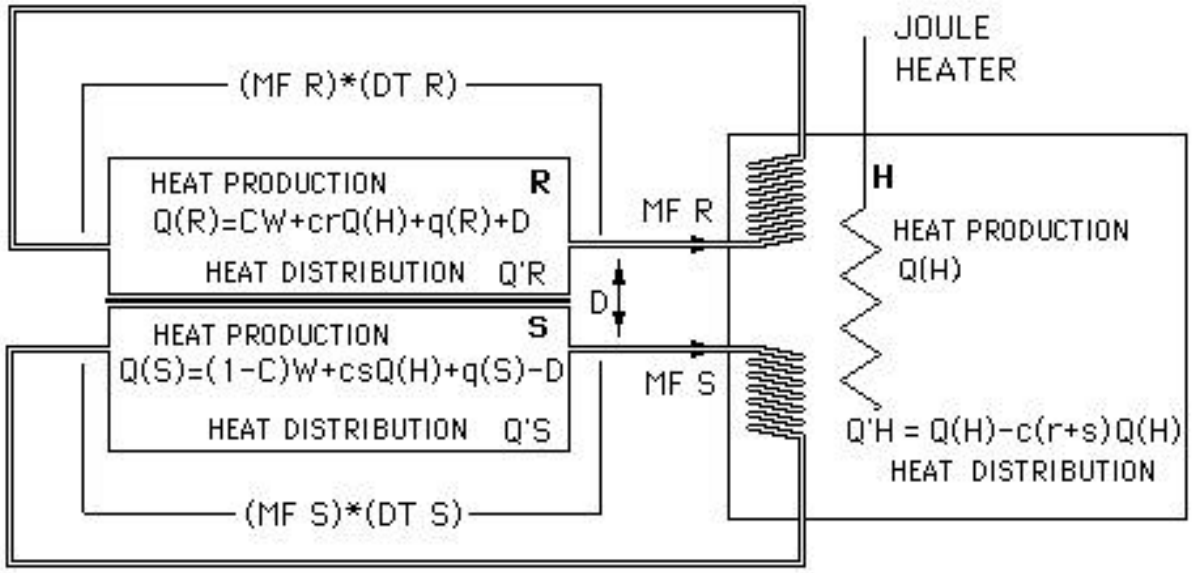

Figure - 29 The block diagram of the Mark II calorimetry system for steady state measurements. The mass flow through for R is (MF R)*(DT R) and the mass flow through for S is (MF S)*(DT S). The heat production for cooling curve CC calorimetry for the components R, S and H are Q(R)=CW+crQ(H)+q(R), Q(S)=(1-C)*W+scQ(H)+q(S)-D and (1-c)Q(H). The heat distribution for the CC calorimetry for the components R, S and H are Q'R, Q'S and Q'H.

The data spread sheets are used to facilitate the reduction of the raw TC data to a usable form and the partitioning of the heat production and its distribution. The production of heat for the components R and S is the equation Q(R)+Q(S) = W + c(r+s)Q(H) + Q(x) is partitioned between R and S. The value from H, c(r+s)Q(H), is actually the heat distributed from H to R and S. The values from R and S, W + Q(x), are the heat production values for R and S. See figure - 29.

The Q(H) from the joule heater is partitioned with the use of the MF flow rates, with the partition constant c = 0.18, so the amount of heat that is distributed to R and S is 0.18* Q(H). The partition constant r divides this heat, 0.18 Q(H), between components R and S. The factors r and s are related to their respective flow rates MF R and MF S. The value for r =[MF R]/[MF R+MF S] where MF R is the flow through rate of D_2O through R and the value for s =[MF S]/[MF R+MF S] through S where MF S is the flow through rate of H_2O through S without any correction for heat transfer through SSS the stainless steel separator, which is in the form of ± D. The heat transferred from R to S through the stainless steel disk separating the two is D and is a function of the temperature differential in °C, DT, between R and S. The rate of heat transfer for D is 2 DT in watts. The partition constant for W between R and S components is C and can be calculated using equation [3].

Q(R)=CW+crQ(H)+q(R) ---------- [3]
Q(S)=(1-C)W+csQ(H)+q(S)

The partition constant K, which distributes Q(x) between the components R and S, has been for this presentation set equal to 1.00 placing the entire Q(x) in R. This was necessary for the information was not there in the data to solve explicitly for K.

q(R) = Q(x)*K
q(S) = Q(x)*(1-K)

Q(x) = q(R)+q(S) ---------- [4]

Some useful ratios and relations at steady state for components R, S and H that use both the CC and MF heat distribution. The CC, cooling curve, heat distribution ratio for R and S must be equal to the MF heat distribution ratio for R and S at steady state; equation [5]. The heat produced by Q(R) and Q(S) can be found using the equations below

(Q'R+D)/(Q'R+Q'S) = [(MF R)*(DT R)+D]/[(MF R)*(DT R)+(MF S)*(DT S)]-----[5]

The steady state heat distribution for R,S and H are taken directly from the CC data.

$Q'R = hiAik(T_i-T_r)$

$Q'S = hiAik(T_i-T_r)$

$Q'H = hiAik(T_i-T_r)$

(1). THE COOLING CURVE AND HEAT DISTRIBUTION AND LOSS

Before Q(x) can be measured, the entire system is calibrated using the Joule heater runs. The calorimetry is based on the measurement of CC of the all components of the Mark II system. The CC are the derived from the natural cooling rate of each component based on a modified form of Newton's Law of Cooling dQ/dt= hA(T(t)-Tr)*k. The modification rests on the fact that the determination of the values of h, A, C and M are not good enough to use without a correction factor k. The value of k changes with temperature and is represented in a quadratic equation. Introducing the constant k forces the ratio of Qout/Qin of the heater run to the value of 1.00 at steady state. The sum of the heat loss of these components is Qout, the total watts lost from the surface, which is also TW.

Figure 30 Cooling Curve Method

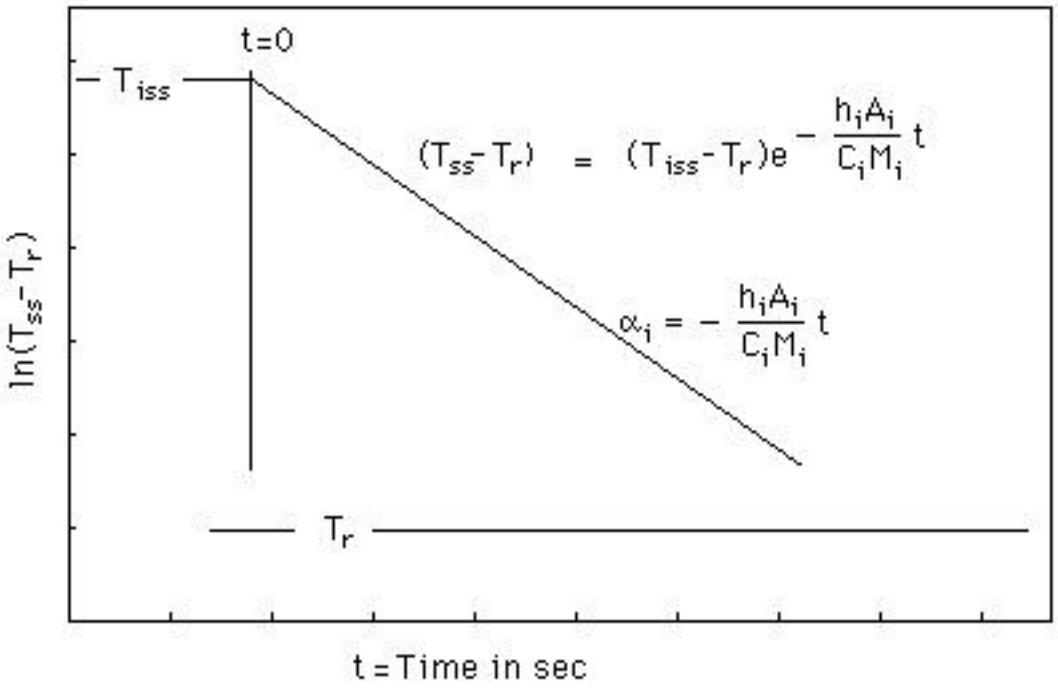

$$(T_{ss}-T_r) = (T_{iss}-T_r)e^{-\frac{h_iA_i}{C_iM_i}t}$$

$$C_iM_i\,(T_{ss}-T_r) = -h_iA_i(T_{iss}-T_r)\,e^{-\frac{h_iA_i}{C_iM_i}t} \quad \text{when } t=0 \text{ then:}$$

$$C_iM_i\,(T_{ss}-T_r) = -h_iA_i(T_{iss}-T_r) \quad \text{when } T_{ss}=T_{iss}$$

FIGURE -30. The steady state cooling curve with each component having its separate curve. The cooling curves follow the Tss the steady state temperature, if there is no input heat during the cooling, for the components H, R, and S and are started at t=0 seconds at temperature of T_{iss}. A given component will cool at a rate that, when plotted as above, has a slope a that contains h, A, C,and M for that component. This straight line with the slope of a is unique to each component. The component cools following the temperature Tss for that component. At the instant, t=0, the sonication and pumps ultrasound power are turned off, at temperature T_{iss}, with continued stirring of the heat exchanger, the cooling curve data from a component's hot surface is collected.

A heated body losses heat by convection and radiation, where the preponderance of the loss is via convection, during the running of the experiments. The heat loss by the radiation process is very nearly linear for the temperature differentials that range up to 60°K. The largest contributor to the minor radiation losses is H with a surface area, A, of 0.5 square meters.

(2). THE COOLING CURVE DETERMINATION OF h_i AND $(\sum A_j)_i$

The quantities of A,C and M can be examined in more detail looking at a sub set j of the parts of each component. These all should be considered when determining the value of these quantities for each component. Where i represents a specific component and j represents a part of the component so $(\sum A_j)_i$ represents the surface area of all the parts of the ith component. The heat that leaves the component by the convection and radiative processes are divided into a major convection losses and a minor radiative losses as the two parts of the CC. To obtain the cooling curves the system was first allowed to reach steady state after which the input power was shut down which included the sonicator, heater and pumps. Temperature data from thermocouples, located at the surface of each component of the apparatus and at several points in the room near it, was collected by the data collection system. Plotting the decrease in temperature at T_{iss}, following Tss as it naturally declines with time, yields the CC for each component of the form:

$$[T_{ss}-Tr]= [T_{iss}-Tr]e^{(-\alpha_i t)}\text{----------} \quad [6]$$

where t is the time, T_{ss} is the temperature at steady state of the surface of ith component at time t, T_{iss} is the temperature at time t=0 when the power was shut down, Tr is the ambient (room) temperature and a_i is a constant and the slope in figure - 30 determined by the rate of exponential decay of the T_{ss}. The subscript, iss, refers to initial steady state conditions, which the system must maintain before the CC can be measured.

The corresponding equation for the rate of convective heat flow from each component at steady state in watts is known to be:

$$\underline{\text{Conv.}} = \sum(h_i(\sum A_j)_i)[T_{ss}-T_r]e^{(-t[h_i(\sum A_j)_i/(\sum M_j C_j)_i])}\text{----------}[7]$$

where h_i is the convection heat transfer coefficient, and $(\sum M_j C_j)_i]$) is the sum of the mass of each material in the component multiplied by its heat capacity.

From a comparison of equations [6] and [7], it can be written:

$$h_i = (\sum M_j C_j)_i/((\sum A_j)_i)\alpha_i$$

From figure - 29 the above equation may take the form:

$$h_i = [(\sum M_j C_j)_i(t_o-t)/(\sum A_j)_i]x[\ln[T_{ss}-T_r]-\ln[T_{iss}-T_r]]\text{----------} \quad [8]$$

The constants, α_i, were obtained from the cooling curves of each component using the method of least squares. h_i was then calculated for each component from equation [8].

To get to the expression that will determine the watts of heat loss from the surfaces of the Mark II device we can refer back to figure - 30, the CC and the rate of heat loss curves. With a run at steady state temperature, at the instant the power is turned off, the CC is started. At this instant the $\exp(-t[h_i \sum A_j)_i /(\sum M_j C_j)_i]) = 1$, at T_{iss} when t=0, and the exponential part of equation is eliminated. This allows for a simpler convection heat loss, equation [9], at any time during any steady state run.

$\underline{\text{Conv.}} = k\sum(h_i(\sum A_j)_i(T_{ss}-T_r)_i)$ ---------- [9]

Equation [9] was used for the calculation of convective heat loss at steady state for each component for all runs described in this paper.

(4). DETERMINATION OF THE SONICATOR INPUT EFFICIENCY, E, AND ITS APPLICATION

The sonicator input efficiency, E, is the fraction of sonicator input W found in components [R] and [S] and is defined as:

$E = [CW + (1-C)W]/Q(P)$

Where CW and (1-C)W are the partitioned inputs to R and S respectively and Q(P) is the power from the sonicator power supply. CW + (1-C)W = W the acoustic heating that goes into the R and S.

At steady state the equation for heat balance is:

$E*Q(P) = W$ ---------- [10]

If all the data is plotted for the more than sixty runs as Qout vs Qin, some of these data points will be on the heater calibration curve if there is no Q(x). If, however, the data points are above the calibration line there is Q(x). The matching of the data without Q(x) to a best fit curve with the calibration data from the Joule heater runs is done by adjusting the value of E. This is easily done with the TW data [TW = total watts out] vs the (W+Q(H)) data [(W+Q(H)) total watts in]. See figure - 5.

$E*Q(P)+Q(H)+Q(x)= TW$

$Q(P) = .1*DIAL*WATTMETER*550$

The DIAL is the a setting on the sonicator power supply that can be varied from 1 to 10. The WATTMETER is the % of power at the dial setting. The number 550 is the maximum watts that can be delivered to the acoustic horn with the Misonix XL 2020.

$E = (TW-Q(H)-Q(x))/[.1*DIAL*WATTMETER*550]$ ---------- [11]

When Q(x) = 0 then E = W/Q(P) and Qout/Qin = 1.00 for both cavitation and heater runs. The best value for E, as determined from the data, was 0.45 and corresponded to a heat output/input ratio of 1.00±.05. This value of E was then used in the calculation of excess heat, Q(x), for all runs.

(5). RADIATIVE LOSSES

The heat losses due to radiation are a function of the temperature of the surface of the ith component T_{iss} and the temperature of the surroundings and walls, T_r. The net loss from the reactor is represented by the Stefan-Boltzman equation $e\,\mathbf{k}[T_{iss}^4-T_r^4]A_i$. This is not important but have some impact for delta temperatures of 60°K in the H. The value for e, the emissivity of surface of the ith component, is found in many chemical handbooks and the value for the Stefan-Boltzman constant, **k**, is $5.672x10^{-8}$ mks. The net radiation loss that was split from CC is added to the convection loss so the total CC loss is equal to the total input Qin plus the excess energy Q(x). This is so the Qout = Qin +Q(x). The radiative heat loss is a small part of the heat loss of the ith component at steady state.

$Rad. = e\,\mathbf{k}[T_{ss}^4-T_r^4]A_i$ ---------- [12]

$TW = k\sum(h_i(\sum A_j)_i(T_{ss}-T_r)_i)+e\mathbf{k}[T_{ss}^4-T_r^4]A_i$ = Watts from CC =Conv.+Rad.

(6). EXCESS HEAT, Q(x)

Having obtained all necessary data reduction, Q(x) may now be determined from the steady-state condition where heat input = heat output. It is convenient to separate Q(x) from the heat production, distribution and losses; that is:

$Q(x) = Qout- Qin = TW-(W+Q(H))$ ---------- [13]

RATIO = Qout/Qin = TW/(W+Q(H)) = 1.00 when Q(x) is zero

Equation [13] was used for the calorimetric calculation of excess heat for all runs considered in this paper. When the RATIO is larger than 1.00 then Q(x) is a measurable amount and a pictorial representation can be found in the figure - 5.

(7). MASS FLOW MF CALORIMETRY

Mass flow, MF, calorimetry was also used in some of the calculations which were simpler but are not as reliable in this case as the CC calorimetry which more completely described the thermal characteristics of the apparatus. The MF depends on the temperature differential between

the input and output flow in both R and S (See figure - 29) . The data from the MF calorimetry can be found in the SPREAD SHEET appendix 10.

The mass flow in R is MF R and in S is MF S in gm/sec, and the delta temperature from input to output for R is DT R and for S is DT S in °C.

The apparent heat production in R and S at steady state using MF calorimetry is:

$Q(R) - crQ(H) = (MF\ R)*(DT\ R)*4.184 + D = CW + q(R)$

$Q(S) - csQ(H) = (MF\ S)*(DT\ S)*4.184 - D = (1-C)W + q(S)$

The expression (MF R)*(DT R)*4.184 is in watts. [MFgm/sec*cal/(gm°C)*DT°C*4.186 J/cal] watts.

$Q(x) = q(R) + q(S)$

$W = CW + (1-C)W$

$Q(R) + Q(S) = W + cQ(H) + Q(x)$

The MF and CC calorimetry give similar results when analyzing the MF data as a grope although some specific run may differ. The simplicity of MF is preferred but the flows and delta temperatures at steady state have more error associated in their measurement. The analysis presented is basically that of CC calorimetry.

List of symbols used in the calorimetric calculations and spread sheet.

α_i =The exponential temperature decay constant= $h_i(\sum A_j)_i/(\sum M_j C_j)_i$
$(\sum A_j)_i$ =The sum of the surface area of the j elements of component i
A_j =Area of the jth element of component i
"(A)" =The air losses
c = The partition factor for split of Q(H) between H and R&S
C = The partition factor for W defining the acoustic heating inputs into R and S.
C_i = Heat capacity of component i
CC = The cooling curve
$(\sum M_j C_j)_i$ = The sum of masses x their heat capacities of the j elements of component i
Conv. = Heat loss due to convection = $k\sum(h_i(\sum A_j)_i)(T_{iss}-T_r)$
E1 = The efficiency of XL 2020 at SRI (.60)
E2 = The efficiency of XL 2010 at EQ (.45)
E = The efficiency factor of the acoustic generator
D = The differential temperature between R and S exit temperatures
DT R = The differential temperature between R input and exit temperatures
DT S = The differential temperature between S input and exit temperatures

DT_i = The delta T at steady state of component i
H = The heat exchange component
h_i = The convection heat transfer coefficient for component i
k = The steady state correlation constant [Qout/Qin = 1.00] (from heater run)
K = The partition factor for Q(x)
k = The Stefan-Boltzman constant
MF = Mass flow calorimetry
MFR = The flow rate through R in ml/sec
MF S = The flow rate through S in ml/sec
Q(i) = The heat input to each component.
Q(x) = The excess heat from run at steady state conditions = TW-(W+Q(H))
Q'H = The disbursed heat at steady state for the component H
Q'R = The disbursed heat at steady state for the component R
Q'S = The distributed heat at steady state for the component S
Q(H) = The heat production at steady state in component H
Q(R) = The heat production at steady state in component R
Q(S) = The heat production at steady state in component S
q(R) = The partitioned Q(x) at steady state in component R
q(S) = The partitioned Q(x) at steady state in component S
Q(P) = The wattmeter % of power from the acoustic power supply
Qin = The acoustic and heater input = [W+Q(H)] = TW-Q(x)
Qout = TW The total watts lost to air at steady state
R = The reactor or reaction volume component
r = The partition factor for c - the split of heat from H going to R
Rad. = The radiative heat loss $e\,\mathbf{k}[T_{iss}^4-T_r^4]A_i$
S = The sonicator containment or sonication volume.
s = The partition factor for c - the split of heat from H going to S
SSS = The 40 mil stainless steel separating disk.
t = Time in seconds
Tr = The ambient temperature
Tss = The steady state temperature of the surface of component i
Tiss = The CC steady state temperature of the surface of component i at t=0 (CC.)
[Tiss-Tr]= The DT temperature at steady state of component i at t=0 (CC.)
TW = Qout The total watts lost to air at steady state
W = E*Q(P) The acoustic heat generated in R and S
"(w)" = The power input

EXPERIMENT MATERIALS

The source, purity, size, durability and type of the active or inactive of metal foils used in R are from Johnson Matthey (JM), Aithica (A) and the Naval Research Laboratory at DC (NRL). The titanium was from (JM) and #316 stainless steel from SRI shop. There were two types of palladium foil from JM used in 34 runs. The four foils were: Puratronic 100µ in thickness, used in runs 2A-F; Puratronic 250µ in thickness(99.9%), lot#HG22E06 used in runs 16A-J, 17A-H, 18A-D and 20A-D. There was a metallic combination of palladium and 2.5% boron in a foil of 127µ thickness, produced by NRL which was used for runs 10A&B. There were two runs using a #316 stainless steel foil, 75µ in thickness, from the SRI model shop. And finally two runs using JM Ti foil, 250µ in thickness (99.5%) with the lot #J12D20. The size of the foils were all 5 centimeters on a side - surface area of 25 sq cm - and varied in thickness from 75 to 250µ. The grain size of the foils varies with the Aithica foils having the largest size and NRL probably having the smallest. The grain size may have some influence on the durability and activity of the foils during cavitation. Higher activity is associated with larger grain size. The durability of the Pd foils appears to be related to both thickness and small grain size. Both the stainless steel and titanium foils have small grain size and do not form much lattice hydride. The formation of hydrides during the cavitation process appears limited in the titanium and stainless steel foils but is very evident in palladium foils and this property may relate to the foil durability.

The reactor R heavy water (R volume of 15 ml) from Aldrich [#7789-20-0] was circulated at flow rates of 2 - 5 ml/sec. The exception was runs 20C and 20D which circulated Aldrich D2O [#7789-20-07], through R with a total liquid volume of heavy water of 140 ml. The external gas pressure in R varied from 30 to 50 PSIA. Argon from Air Products was the primary gas used with 0.02 ppm ^4He. Several runs used D_2 gas for the external pressure at 0.14 ppm ^4He. The containment materials used in the R circulation system are Al_2O_3, cross-linked CF_2 (FEP) and stainless steel.

The sonicator containment S has an active metal in the form of a 2 kg titanium horn with a surface area of 32 sq cm. A volume of 500 ml of light water is circulated through S at a flow rate of 4 to 7 ml/sec. The nitrogen gas from Air Products was used to pressurize S and was usually at 110 PSIA. The containment materials used in the S circulation system are Cu, $Al2O_3$, CF_2 and stainless steel. The temperature in R at steady state was 40 to 80°C and in S about the same. It was good practice to keep the exit temperatures in R and S close to the same value to minimize D the heat transfer through SSS.

10. Appendix D Experiment Summary Spread Sheet

The following pages of spread sheet data show the average results at steady state for all the experiments conducted. The information in the columns is described in the following list.

Column #1, is the sequential number assigned to each run.
Column #2, RUN is the identification of run as found in notebook.
Column #3, DATE is the time and date the run was started.
Column #4, D is the temperature differential across SSS between R and S.
Column #5, TW is the total watts Qout measured by the cooling curves.
Column #6, Q'R is the share of heat distributed to R measured by cooling curves.
Column #7, Q'S is the share of heat distributed to S measured by cooling curves.
Column #8, Q'R+Q'S is the share of heat distributed to R+S measured by cooling curves.
Column #9, W is the total watts Qin from acoustic heating and joule heater,
Column #10, Q(x) is the excess heat produced Qout-Qin or TW-(W+Q(H)).
Column #11, Q(R) is the total heat produced in R.
Column #12, Q(S) is the total heat produced in S.
Column #13, q(R) is the partition of Q(x) with K set equal to 1.00.
Column #14, q(S) is the partition of Q(x) with K set in this case equal to 1.00. [Arbitrarily setting K=1.00 places the Q(x) heat production in R. This partition needs further study.]
Column #15, Q(R)+Q(S) is the heat produced in R+S.
Column #16, EXT. PRESS. is the pressure of argon over D2O in R
Column #17, TIME is the running time in hours of the experimental run.
Column #18, DIAL SET is the power stat dial setting of the ultrasound power supply
Column #19, US% INPUT is percent of the power delivered to the acoustic horn
Column #20, Soni P% is total power input from the power supply based on [DIAL SET]x[Soni P%]x[rated maximum power output] and is equal to W.
Column #21, WATT heater is the heat input from the joule heater that heats the H2O in the heat exchanger H.
Column #22, He4 ppm is the MS measurement of the He4 in ppm sampled from the gas phase of R after the run.
Column #23, He4 atoms in the gas phase of R is the number of gas phase He4 atoms, using the PVT data for the determination. RUN, is the sequential number assigned to each run.
Column #24, FOIL & Source is the foil elemental composition and the supplier.
Column #25, Foil thickness is the thickness in μ of the 5X5 cm foils.
Column #26, PSIG Ext. Pr Ar in R is the pressure of argon over the D2O in R in PSIG.
Column #27, PSIG Ext. Pr N2 in S is the pressure of nitrogen over the H2O in S in PSIG.
Column #28, ml/sec FLOW R is the flow rate in millimeters/sec through R.
Column #29, ml/sec FLOW S is the flow rate in millimeters/sec through S.
Column #30, H DT Delta T is the output minus the input temperatures of H at steady state.
Column #31, R DT Delta T is the output minus the input temperatures of R at steady state.
Column #32, S DT Delta T is the output minus the input temperatures of S at steady state.
Column #33, Comments are the comments and information about a particular run.

EQ/SRI/EPRI EXPERIMENT MATRIX DATA AND PARAMETERS FOR MARK II RUNS - Page #1																								
THREE POWER SUPPLIES WERE USED - 2 EQ AND 1 SRI MISONIX 2020 & 2010 XL ULTRA SOUND																								
E FIELD @20V [P TO P] @ 20KHz																								
1	2	3	4	5	6	7	8	9	10	11	12	13	14	15	16	17	18	19	20	21	22	23	24	25
							Q'R+							Q(R)+	EXT.	TIME	DIAL	US %	Soni	WATT	He4	He4 Atoms	FOIL	FOIL
#	RUN	DATE	D	TW	Q'R	Q'S	Q'S	W	Q(x)	Q(R)	Q(S)	q(R)	q(S)	Q(S)	PRESS.	HR	SET	INPUT	P%	Heater	ppm	of Rx vol	Source	thick
1	1A	2/7/91	-4	195	13	46	60	158	36	43	152	36	0	195	17	21	0.80	70%	56%	0	0.90	0.00E+00	Pd 1 [JM]	100µ
2	2B	5/15/91	-21	322	6	47	53	97	-74	12	74	-74	0	86	25	3	0.60	65%	39%	300	0.90	1.87E+15	Pd 2 [JM]	100µ
3	2C	5/15/91	0	231	20	28	48	147	84	97	134	84	0	231	23	25	0.80	74%	59%	0	0.17	2.07E+14	Pd 2 [JM]	100µ
4	2D	6/21/91	-6	219	16	30	46	158	60	75	144	60	0	219	30	24	0.80	80%	64%	0	0.09	2.29E+14	Pd 2 [JM]	100µ
5	2E	6/19/91	2	50	6	4	10	62	-12	28	22	-12	0	50	18	23	0.50	50%	25%	0	0.70	1.10E+15	Pd 2 [JM]	100µ
6	2F	6/21/91	-14	102	1	18	20	89	-28	5	63	-28	0	68	27	7	0.62	58%	36%	41	0.04	6.30E+13	Pd 2 [JM]	100µ
7	3A	8/12/91	5	101	11	9	20	80	-20	37	30	-20	0	67	16	22	0.50	65%	33%	40	0.08	9.45E+13	Pd 3 [JM]	100µ
8	4A	8/20/91	1	201	16	23	39	175	27	82	119	27	0	201	30	2	0.80	70%	56%	0	0.35	7.09E+14	Pd 4 [Aithica]	100µ
9	5A	8/21/91	2	250	22	31	53	175	76	106	144	76	0	250	20	25	0.86	82%	71%	0			Pd 5 [Aithica]	100µ
10	6A	8/23/91	-2	261	21	34	54	181	81	99	162	81	0	261	25	26	0.86	85%	73%	0	0.43	5.92E+14	Pd 6 [Aithica]	100µ
11	7A	8/23/91	9	222	23	20	43	154	9	93	81	9	0	174	20	1	0.80	78%	62%	60			Pd 7 [Aithica]	100µ
12	8A	9/6/91	-1	135	10	16	26	74	2	33	54	2	0	87	22	31	0.60	50%	30%	60		0.00E+00	Pd 8 [JM]	250µ
13	8B	9/10/91	-1	128	12	13	25	86	-17	40	40	-17	0	80	19	10	0.60	58%	35%	60	0.10		Pd 8 [JM]	250µ
14	8C	9/6/91	-5	385	28	47	75	119	32	71	122	32	0	193	23	26	0.80	60%	48%	240	0.18	7.63E+14	Pd 8 [JM]	250µ
15	8D	9/12/91	-10	306	21	45	66	189	114	96	208	114	0	304	28	21	0.90	85%	77%	0	0.03	1.59E+14	Pd 8 [JM]	250µ
16	8E	9/19/91	4	199	20	21	41	161	38	97	102	38	0	199	26	17	0.87	75%	65%	0			Pd 8 [JM]	250µ
17	9A	9/18/91	-2	298	24	37	62	200	97	118	180	97	0	298	22	1	0.90	90%	81%	0	0.15	5.64E+14	Pd 9 [Aithica]	100µ
18	10A	9/25/91	1	191	16	21	37	97	-5	47	62	-5	0	109	23	17	0.65	60%	39%	100			Pd10 2.5%B	127µ
19	10B	10/1/91	-8	360	25	49	74	167	-7	65	131	-7	0	196	30	24	0.90	75%	68%	200	0.17	7.38E+14	Pd10 2.5%B	127µ
20	11A	10/1/91	-13	360	21	54	75	172	88	78	200	88	0	278	32	18	0.88	79%	70%	100			Pd 11 [Aithica]	100µ
21	12A	10/3/91	10	258	29	26	55	152	6	93	83	6	0	176	28	21	0.75	82%	62%	100	0.20	4.33E+14	Pd 12 [Aithica]	100µ
22	13A	10/8/91	-7	294	20	39	59	156	-12	57	115	-12	0	171	25	46	0.80	89%	71%	150	0.22	5.52E+14	Pd 13 [Aithica]	100µ
23	13B	10/12/91	-8	268	17	37	54	177	-8	59	128	-8	0	186	38	18	0.82	87%	71%	100	0.02	1.22E+14	Pd 13 [Aithica]	100µ
24	13C	10/15/91	5	262	24	27	51	109	-46	46	53	-46	0	99	27	13	0.55	80%	44%	200	0.17	1.00E+15	Pd 13 [Aithica]	100µ
25	14A	10/18/91	3	284	25	31	56	119	16	71	90	16	0	162	24	4	0.60	80%	48%	150	0.12	6.79E+14	Pd 14 [Aithica]	100µ
26	14B	10/18/91	5	347	31	38	69	151	-2	84	101	-2	0	184	20	4	0.70	87%	61%	200	0.27	1.58E+15	Pd 14 [Aithica]	100µ
27	15A	10/23/91	-6	326	31	34	65	156	21	96	108	21	0	204	35	3	0.80	79%	63%	150			Pd 15 [Aithica]	100µ
28	16A	10/24/91	3	317	28	36	63	179	-10	85	110	-10	0	195	73	-83	0.46	85%	39%	150	0.18		Pd 16 [JM]	250µ
29	16B	10/25/91	4	298	27	32	59	113	36	80	96	36	0	176	30	2	0.55	83%	46%	150			Pd 16 [JM]	250µ
30	16C	10/26/91	1	328	27	37	64	168	11	86	121	11	0	206	35	24	0.80	85%	68%	150	0.09	5.71E+14	Pd 16 [JM]	250µ
31	16D	10/30/91	3	370	37	39	76	183	55	126	135	55	0	262	30	28	0.85	87%	74%	150	0.12	6.67E+14	Pd 16 [JM]	250µ
32	16E	12/31/90	7	252	27	27	54	196	56	125	126	56	0	252	32	26	0.85	93%	79%	0	0.09	6.84E+14	Pd 16 [JM]	250µ
33	16F	2/10/91	5	181	19	20	39	163	17	88	92	17	0	181	35	28	0.75	88%	66%	0	0.09	5.53E+14	Pd 16 [JM]	250µ
34	16G	9/10/91	-4	107	6	15	22	121	-14	32	75	-14	0	107	35	25	0.65	75%	49%	0	0.10	6.42E+14	Pd 16 [JM]	250µ
35	16H	14/11/95	6	249	25	25	50	156	-6	83	84	-6	0	168	20	25	0.80	79%	63%	100	4.00	9.68E+15	Pd 16 [JM]	250µ
36	16 I	16/11/95	1	245	22	28	49	158	-13	72	91	-13	0	163	26	25	0.80	80%	64%	100	4.20	1.55E+16	Pd 16 [JM]	250µ
37	16J	16/11/95	2	293	27	34	60	187	8	94	119	8	0	212	24	23	0.85	89%	76%	100	0.18	7.94E+14	Pd 16 [JM]	250µ
38	17A	7/11/91	-3	291	23	36	60	168	23	82	128	23	0	210	24	31	0.82	83%	68%	100	0.25	2.49E+14	Pd 17 [JM]	250µ
39	17B	11/11/91	-4	322	25	41	66	183	40	90	150	40	0	240	35	24	0.83	89%	74%	100	0.10	5.54E+14	Pd 17 [JM]	250µ
40	17C	12/11/91	1	269	24	31	54	173	-4	82	105	-4	0	187	33	8	0.82	85%	70%	100	0.08	4.02E+14	Pd 17 [JM]	250µ

EQ/SRI/EPRI EXPERIMENT MATRIX DATA AND PARAMETERS FOR MARK II RUNS - Page #1																								
THREE POWER SUPPLIES WERE USED - 2 EQ AND 1 SRI MISONIX 2020 & 2010 XL ULTRA SOUND																								
E FIELD @20V [P TO P] @ 20KHz																								
1	2	3	4	5	6	7	8	9	10	11	12	13	14	15	16	17	18	19	20	21	22	23	24	25
							Q'R+							Q(R)+	EXT.	TIME	DIAL	US %	Soni	WATT	He4	He4 Atoms	FOIL	FOIL
#	RUN	DATE	D	TW	Q'R	Q'S	Q'S	W	Q(x)	Q(R)	Q(S)	q(R)	q(S)	Q(S)	PRESS.	HR	SET	INPUT	P%	Heater	ppm	of Rx vol	Source	thick
41	17 H100	13/12/95	-1	98	7	10	17	0	-2	6	10	-2	0	16	6	96							Pd 17 [JM]	250µ
42	17 H200		-1	198	14	21	35	0	-2	13	20	-2	0	34									Pd 17 [JM]	250µ
43	17 H300		-1	298	21	33	54	0	0	21	32	0	0	53									Pd 17 [JM]	250µ
44	17D	19/12/95	-1	319	26	39	65	173	47	96	142	47	0	238	30	22	0.82	85%	70%	100	0.20	1.13E+15	Pd 17 [JM]	250µ
45	17PULSED	20/12/95	0	330	25	36	61	24	8	36	50	8	0	86	24	23	0.82	85%	70%	300			Pd 17 [JM]	250µ
46	17E	21/12/95	-3	335	27	42	69	170	64	98	155	64	0	253	23	23	0.85	81%	69%	100	0.90	4.14E+15	Pd 17 [JM]	250µ
47	17F	22/12/95	-2	322	26	40	66	164	59	96	145	59	0	241	28	7	0.85	78%	66%	100	0.00	0.00E+00	Pd 17 [JM]	250µ
48	17ARGON	2/1/'96	-2	302	44	33	77	0	4						20	23			0%	300	0.13	5.93E+14	Pd 17 [JM]	250µ
49	17G	2/29/92	0	323	27	39	66	170	53	100	142	53	0	241	29	25	0.82	84%	69%	100	0.11	5.24E+14	Pd 17 [JM]	250µ
50	17H	3/31/92	-3	323	25	41	66	178	46	93	149	46	0	242	29	24	0.80	90%	72%	100	0.15	7.61E+14	Pd 17 [JM]	250µ
51	18A	7/31/92	-5	291	23	39	62	223	68	109	182	68	0	291	32	24	0.90	100%	90%	0	0.10	4.60E+14	Pd 18 [JM]	250µ
52	18B	8/31/92	-4	297	23	38	60	179	21	82	135	21	0	217	28	24	0.85	85%	72%	100	0.12	4.64E+14	Pd 18 [JM]	250µ
53	18C	9/30/92	1	310	26	36	63	196	16	97	133	16	0	230	25	24	0.88	90%	79%	100	0.15	9.00E+14	Pd 18 [JM]	250µ
54	18D	10/31/92	-6	282	20	36	56	160	25	73	130	25	0	203	38	17	0.82	85%	70%	100	0.10	5.50E+14	Pd 18 [JM]	250µ
55	SS19A	15/1/96	-11	297	20	40	60	185	14	72	144	14	0	217	31	24	0.87	86%	75%	100	0.20	8.74E+14	SS19 [SRI]	75µ
56	SS19B	16/1/96	-7	282	20	37	57	185	-3	71	129	-3	0	200	29	24	0.85	78%	66%	100	0.14	7.92E+14	SS19 [SRI]	75µ
57	20A	17/1/96	0	286	24	34	58	170	19	86	121	19	0	207	20	100	0.85	81%	69%	100	0.30	2.08E+15	Pd 20 [JM]	250µ
58	Ti 21A	22/1/96	5	224	22	25	48	166	58	105	119	58	0	224	29	24	0.84	80%	67%	0	0.19	1.22E+15	Ti 21 [JM]	250µ
59	Ti 21B	23/1/96	1	311	27	39	66	156	57	93	137	57	0	231	28	24	0.84	75%	63%	100	0.19	1.22E+15	Ti 21 [JM]	250µ
60	20B	26/1/96	6	216	22	23	45	171	45	105	111	45	0	216	29	15	0.83	83%	69%	0	0.33	1.97E+15	Pd 20 [JM]	250µ
61	20C	30/1/96	-2	291	23	38	61	156	37	78	133	37	0	211	37	20	0.82	77%	63%	100	0.12	1.18E+15	Pd 20 [JM]	250µ
62	20D	31/1/96	3	272	24	33	57	160	14	82	110	14	0	192	23	21	0.82	79%	65%	100	0.11	5.55E+14	Pd 20 [JM]	250µ
63	mt22A	2/4/92	-4	103	7	14	22	104	-14	31	61	-14	0	92	24	22	0.70	61%	43%	0	0	0.00E+00	EMPTY	EMPTY
64	mt22B	2/5/92	-5	150	12	21	33	150	0	53	97	0	0	150	20	24	0.82	73%	60%	0	0	0.00E+00	EMPTY	EMPTY
65	mt22C	2/6/92	-6	154	10	20	30	87	-31	24	50	-31	0	73	17	21	0.70	50%	35%	100	0	0.00E+00	EMPTY	EMPTY
66	22 H300	2/7/92	-2	293	20	33	53	0	15	26	42	15	0	68	27	24	0.00	0%	0%	293	0.00	0.00E+00	EMPTY	EMPTY
67	22 H200	2/8/92	-1	195	14	21	35	0	6	16	25	6	0	41	21	28	0.00	0%	0%	195	0.00	0.00E+00	EMPTY	EMPTY
68	22 H100	2/9/92	0	98	5	9	14	0	-1	6	11	-1	0	17	9	46	0.00	0%	0%	98	0.00	0.00E+00	EMPTY	EMPTY
69	mt22A EQ	2/4/92	-5	145	9	23	32	142	3	41	103	3	0	145	17	20	0.70	65%	46%	0	0.00	0.00E+00	EMPTY	EMPTY
70	mt22B EQ	2/5/92	-6	186	12	29	41	192	-7	55	131	-7	0	186	20	21	0.75	90%	68%	0	0.00	0.00E+00	EMPTY	EMPTY
71	mt22C EQ	2/6/92	-14	246	12	42	54	130	17	37	127	17	0	164	20	24	0.70	71%	50%	100	0.00	0.00E+00	EMPTY	EMPTY
72	22 H300 EQ	8/7/92	-30	344	22	66	77	0	-11	48	296	-11	0	344	20	22	0.00	0%	0%	340	0.00	0.00E+00	EMPTY	EMPTY
73	22 H 200 EQ	2/8/92	-18	204	12	38	44	0	-5	28	176	-5	0	204	20	22	0.00	0%	0%	205	0.00	0.00E+00	EMPTY	EMPTY
74	22 H100 EQ	2/9/92	-9	106	6	19	22	0	0	14	92	0	0	106	20	40	0.00	0%	0%	106	0.00	0.00E+00	EMPTY	EMPTY

EQ/SRI/EPRI EXPERIMENT M										
THREE POWER SUPPLIES WI										
E FIELD @20V [P TO P] @ 20										
1	2	3	26	27	28	29	30	31	32	33
			PSIG	PSIG	ml/sec	ml/sec				
			Ext. Pr	P N2	FLOW	FLOW	H DT	R DT	S DT	Comments
#	RUN	DATE	Ar in R	in S	R	S	Delta T	Delta T	Delta T	
1	1A	2/7/91	17	[70]	[3]	[5]	40	5	[3]	Gear pumps
2	2B	5/15/91	25	70	4.1	8.0	52	4	[1]	Pre loaded with D2
3	2C	5/15/91	23	70	4.1	7.0	38	5	6	Data collection blank - new US 2020
4	2D	6/21/91	30	77	3.5	6.0	37	6	7	Displacement pumps FMI
5	2E	6/19/91	18	66	2.5	5.0	13	3	1	very low HX temp.
6	2F	6/21/91	27	65	3.1	6.2	22	3	9	New ring, isolating horn from containment
7	3A	8/12/91	16	70	3.1	7.5	21	5	2	low input - Rx vol. pump failed
8	4A	8/20/91	30	70	3.0	8.0	37	6	7	Very little foil left intact
9	5A	8/21/91	20	87	2.5	5.5	42	10	5	Foil in same condition as 4-A
10	6A	8/23/91	25	80	2.5	5.5	44	5	4	Foil in same condition as 4-A
11	7A	8/23/91	20	77	2.1	5.2	37	8	1	Foil annealed @ 850°C for 3 hr. [rapid foil destruction]
12	8A	9/6/91	22	70	2.5	6.5	27	7	2	Run stopped when US failed
13	8B	9/10/91	19	80	2.5	6.5	24	5	2	Run stopped US problems
14	8C	9/6/91	23	80	2.1	6.0	59	6	2	Started far from SS
15	8D	9/12/91	28	100	2.4	6.3	50	10	8	Increasing SS - Soni V increasing
16	8E	9/19/91	26	90	3.4	5.5	32	8	5	Run stopped - reactor leak - loading check .003mg
17	9A	9/18/91	22	92	2.6	6.5	47	7	2	Short run
18	10A	9/25/91	23	90	3.4	5.5	34	5	2	NRL Pd foil - 2.5% B
19	10B	10/1/91	30	96	2.9	5.0	52	10	9	very slight cav. damage
20	11A	10/1/91	32	88	3.0	5.0	55	4	10	Run stopped when US stuck in HI mode- lost soni water
21	12A	10/3/91	28	88	3.0	5.3	44	4	3	Run stopped - lost soni water
22	13A	10/8/91	25	85	3.4	5.9	46	3	2	Vidio- FEP&Pyrex window
23	13B	10/12/91	38	87	3.0	5.9	43	5	3	Vidio- FEP&Pyrex window- lost soni water
24	13C	10/15/91	27	87	3.8	6.0	44	3	2	Run stopped - US failed - Ar/D2 ; 2/1 Ratio
25	14A	10/18/91	24	88	3.6	5.6	45	3	2	Run stopped US failed
26	14B	10/18/91	20	88	3.5	5.5	53	4	2	Run stopped - US failed - after 4 hours
27	15A	10/23/91	35	87	3.5	5.5	50	7	3	Typical cav. damage for Aithica foil-short run
28	16A	10/24/91	25	85	3.8	5.5	47	7	3	Type 1 cav. damage
29	16B	10/25/91	30	84	3.4	5.5	47	3	2	Run stopped when pump stopped
30	16C	10/26/91	35	78	3.1	6.0	50	7	3	SRI power supply
31	16D	10/30/91	30	86	3.1	6.0	55	10	5	R DT inceased last part of run
32	16E	12/31/90	32	87	3.1	6.5	42	12	5	ok soni water problem
33	16F	2/10/91	35	87	3.2	5.0	32	6	6	20KHz converter Voltage test
34	16G	9/10/91	35	81	3.2	5.0	22	4	3	Run stopped when US overloaded
35	16H	14/11/95	20*	86	3.5	5.0	41	8	3	[D2 from tank 2]* ext pr [He4 background]
36	16 I	16/11/95	26*	86	3.6	5.0	39	6	3	[D2 from tank 2]* ext. pr. [He4 background]
37	16J	16/11/95	24*	87	3.5	4.5	46	7	4	[D2 from tank1]*/Ar is 2/1 ext pr in Rx vol
38	17A	7/11/91	23	96	3.2	5.0	47	7	5	New foil lot# J23F18
39	17B	11/11/91	35	96	3.1	5.5	49	6	6	OK
40	17C	12/11/91	33	96	3.0	5.5	44	7	4	Run stopped - US power supply damage - fixed

EQ/SRI/EPRI EXPERIMENT M										
THREE POWER SUPPLIES WI										
E FIELD @20V [P TO P] @ 20										
1	2	3	26	27	28	29	30	31	32	33
			PSIG	PSIG	ml/sec	ml/sec				
			Ext. Pr	P N2	FLOW	FLOW	H DT	R DT	S DT	Comments
#	RUN	DATE	Ar in R	in S	R	S	Delta T	Delta T	Delta T	
41	17 H100	13/12/95	7	96	3.0	5.5	21	-1	-3	Heater run at 100 watts
42	17 H200		7	96	3.0	5.5	34			Heater run at 200 watts
43	17 H300		7	96	3.0	5.5	48	-1	-3	Heater run at 300 watts
44	17D	19/12/95	31	96	3.2	4.7	50	7	5	OK
45	17PULSED	20/12/95	23	96	3.3	4.8	50	0	0	Pulsed US for .2 sec. on and .8 sec. off
46	17E	21/12/95	23	96	3.2	4.8	51	6	5	Stopped run because D2O was low
47	17F	22/12/95	28	96	3.0	4.8	50	7	5	Run stopped - US quit at 19:00
48	17ARGON	2/1/'96	19	96	3.2	5.1	48	-1	-3	Calibration for He4 BG
49	17G	2/29/92	29	96	3.0	5.0	49	8	5	Measured the Volts input the converter
50	17H	3/31/92	26	96	2.9	5.0	50	7	5	OK
51	18A	7/31/92	32	96	3.0	5.0	47	9	8	Hi US input - RF field pick by pressure gauge
52	18B	8/31/92	28	96	2.9	5.0	47	8	7	OK
53	18C	9/30/92	27	96	2.9	5.0	50	8	6	RF problem again
54	18D	10/31/92	38	96	3.0	5.0	43	6	6	SS separator - Buldge into soni vol
55	SS19A	15/1/96	29	96	3.0	5.0	46	7	8	OK
56	SS19B	16/1/96	29	96	3.0	5.0	45	7	5	OK
57	20A	17/1/96	20	96	3.0	5.0	46	6	4	TC problem- soni out
58	Ti 21A	22/1/96	29	96	3.0	5.0	36	8	4	Try Ti foil-duplication of LANL He4 results
59	Ti 21B	23/1/96	28	96	3.0	5.0	51	10	4	No soni flow for first 2/3 of run
60	20B	26/1/96	29	96	3.0	5.0	36	9	5	US quit - TC soni out problem
61	20C	30/1/96	37	96	2.9	5.0	45	5	6	Stopped run - D2O level low
62	20D	31/1/96	23	96	2.9	5.0	45	6	3	D2O level low -TC S V out ?
63	mt22A	2/4/92	23	96	2.0	3.0	27	9	9	Compare runs SRI & EQ - E= .45 - At SRI
64	mt22B	2/5/92	19	96	2.0	3.0	32	12	12	Compare runs SRI & EQ - E= .45 - At SRI
65	mt22C	2/6/92	16	96	2.0	3.0	40	9	9	Compare runs SRI & EQ - E= .45 - At SRI
66	22 H300	2/7/92	10	96	2.0	3.0	43	-2	-5	Compare runs SRI & EQ - HEATER - At SRI
67	22 H200	2/8/92	10	96	2.0	3.0	31	-2	-3	Compare runs SRI & EQ - HEATER - At SRI
68	22 H100	2/9/92	10	96	2.0	3.0	18	-1	-2	Compare runs SRI & EQ - HEATER - At SRI
69	mt22A EQ	2/4/92	17	95	2.0	3.0	22	5	7	Compare runs SRI & EQ - E=.6 -At EQ
70	mt22B EQ	2/5/92	20	80	2.0	3.0	31	7	8	Compare runs SRI & EQ - E=.6 -At EQ
71	mt22C EQ	2/6/92	20	96	2.0	3.0	33	7	13	Compare runs SRI & EQ - E=.6 -At EQ
72	22 H300 EQ	8/7/92	20	90	2.0	3.0	51			Compare runs SRI & EQ - HEATER -At EQ
73	22 H 200 EQ	2/8/92	20	90	2.0	3.0	35			Compare runs SRI & EQ - HEATER -At EQ
74	22 H100 EQ	2/9/92	20	90	2.0	3.0	20			Compare runs SRI & EQ - HEATER -At EQ

11 Appendix E HEAT RATIO PLOTS Q_{out}/Q_{in}

The plots below are of the ratio TW/(W+Q(H)) = Q_{out}/Q_{in} vs time in hours. When the ratio = 1.00 then there is no production of excess heat Q(x). All the runs are represented here except the calibration runs 22 with the empty reactor.

Plots of the ratio of Q_{out}/Q_{in} vs time in hours of the metal foil runs. The ratios that exceeded 1.00 produced excess heat Q(x) (Q_{out}-Q_{in}=Q(x)). For example run 6A exceeds 1.00 by .54. Q_{in} = 74 watts from the sonicator and 60 watts from the Joule heater for a total 134 watts. The watt value for Q(x) is .54xQ_{in} = 73 watts.

Figure 31 Plots of 61 Experimental Heat Measurements

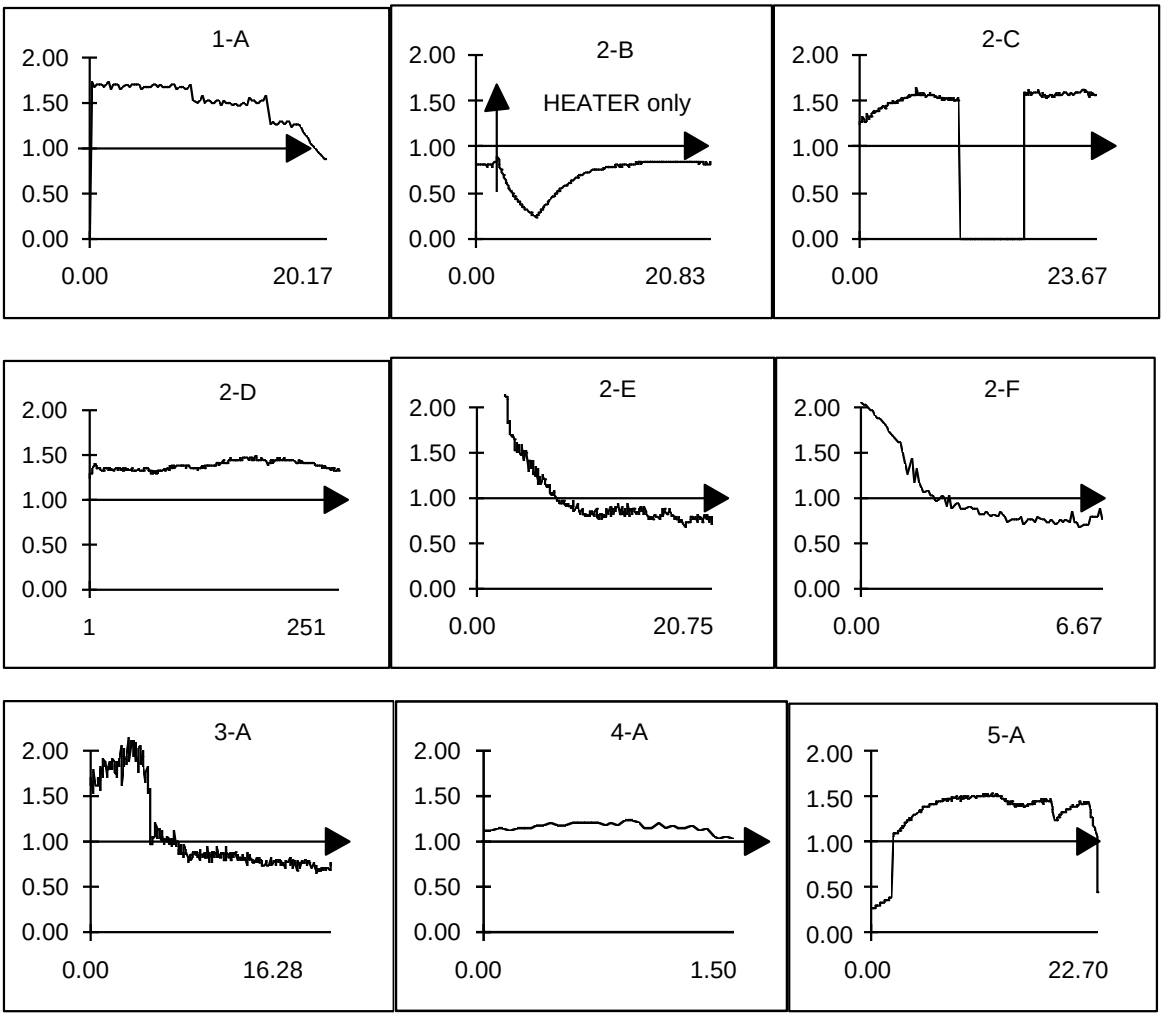

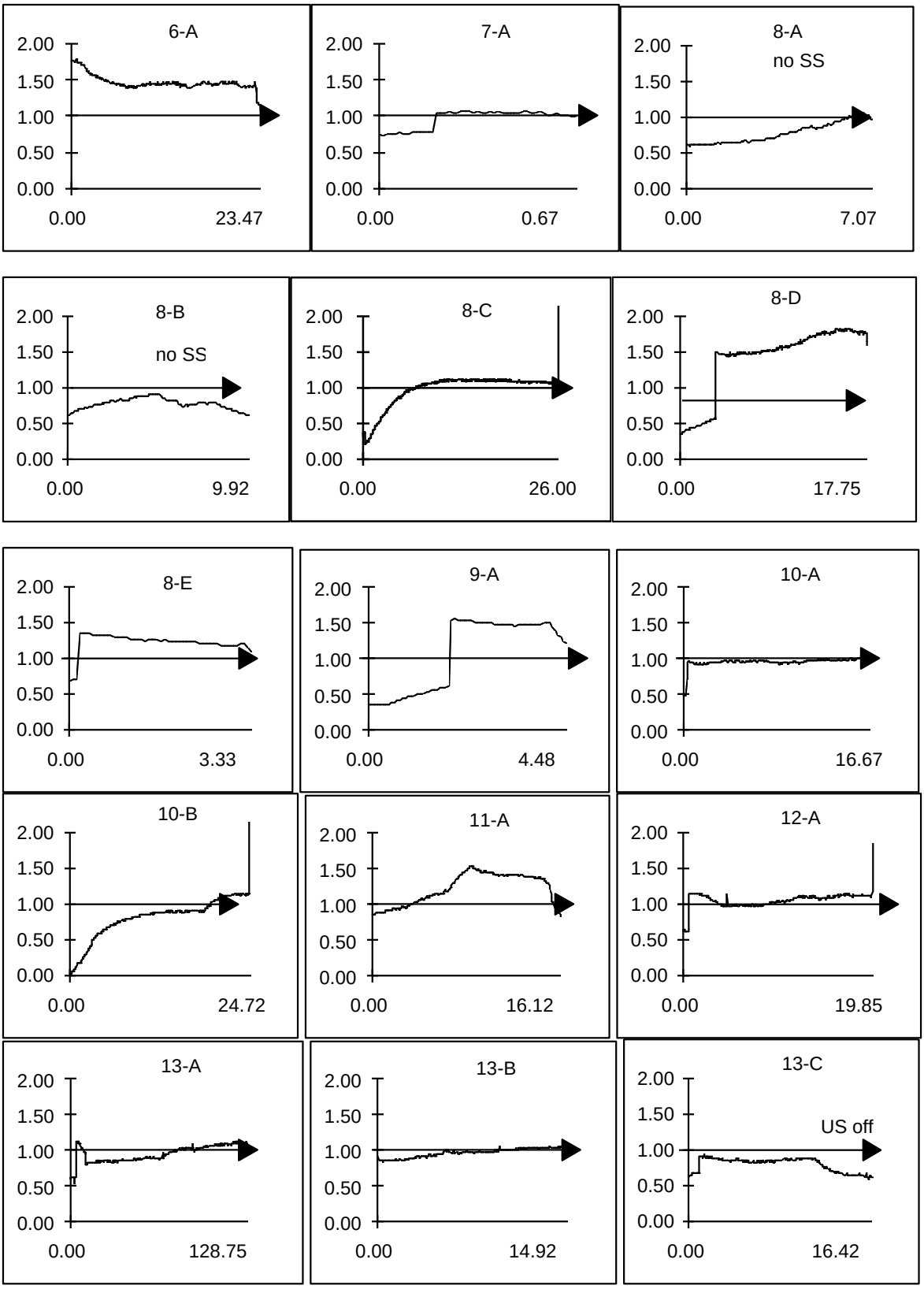
6-A
2.00
1.50
1.00
0.50
0.00
0.00
23.47
7-A
2.00
1.50
1.00
0.50
0.00
0.00
0.67
8-A
no SS
2.00
1.50
1.00
0.50
0.00
0.00
7.07
8-B
no SS
2.00
1.50
1.00
0.50
0.00
0.00
9.92
8-C
2.00
1.50
1.00
0.50
0.00
0.00
26.00
8-D
2.00
1.50
1.00
0.50
0.00
0.00
17.75
8-E
2.00
1.50
1.00
0.50
0.00
0.00
3.33
9-A
2.00
1.50
1.00
0.50
0.00
0.00
4.48
10-A
2.00
1.50
1.00
0.50
0.00
0.00
16.67
10-B
2.00
1.50
1.00
0.50
0.00
0.00
24.72
11-A
2.00
1.50
1.00
0.50
0.00
0.00
16.12
12-A
2.00
1.50
1.00
0.50
0.00
0.00
19.85
13-A
2.00
1.50
1.00
0.50
0.00
0.00
128.75
13-B
2.00
1.50
1.00
0.50
0.00
0.00
14.92
13-C
US off
2.00
1.50
1.00
0.50
0.00
0.00
16.42

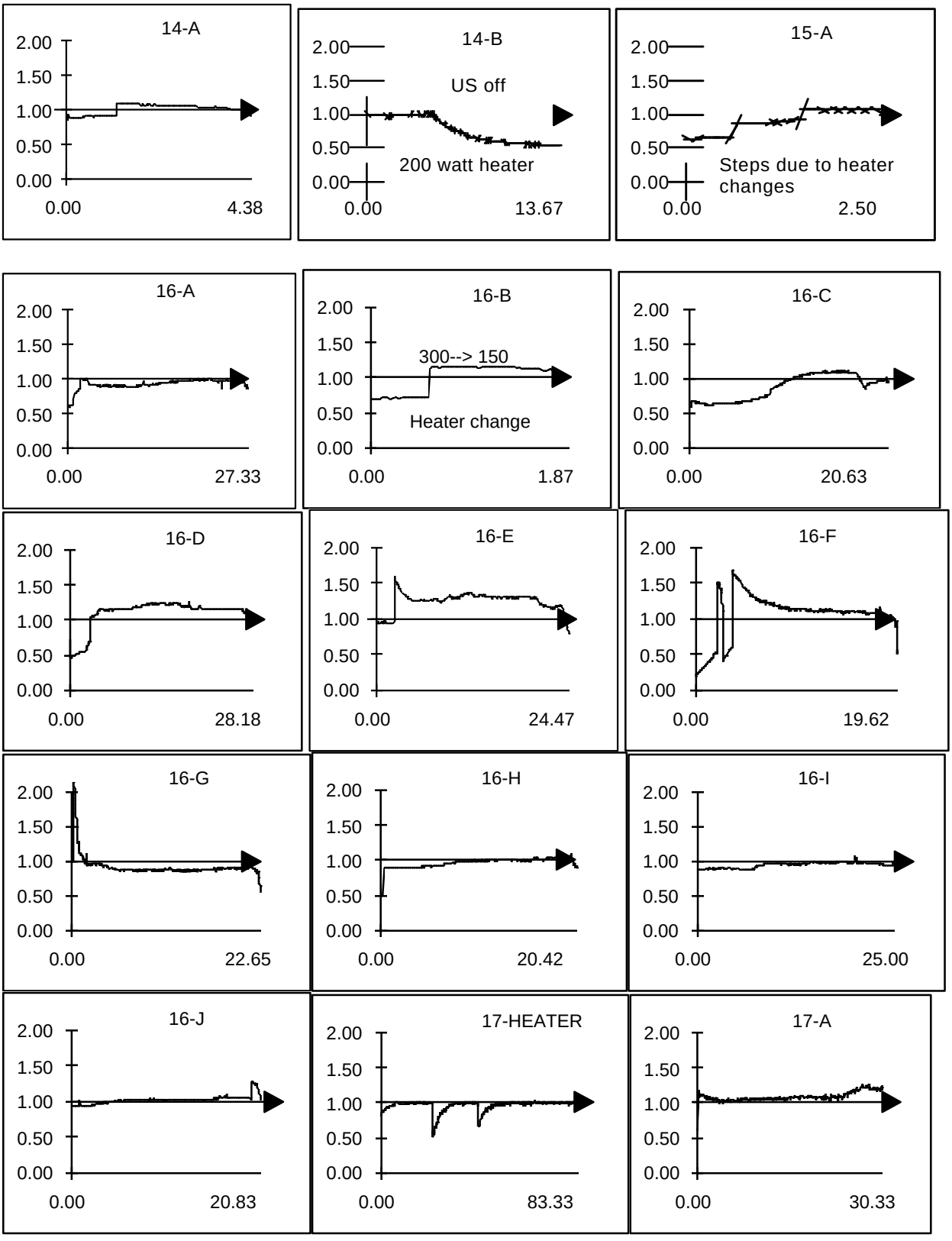
14-A
2.00
1.50
1.00
0.50
0.00
0.00
4.38
14-B
US off
200 watt heater
0.00
13.67
15-A
Steps due to heater changes
0.00
2.50
16-A
0.00
27.33
16-B
300--> 150
Heater change
0.00
1.87
16-C
0.00
20.63
16-D
0.00
28.18
16-E
0.00
24.47
16-F
0.00
19.62
16-G
0.00
22.65
16-H
0.00
20.42
16-I
0.00
25.00
16-J
0.00
20.83
17-HEATER
0.00
83.33
17-A
0.00
30.33

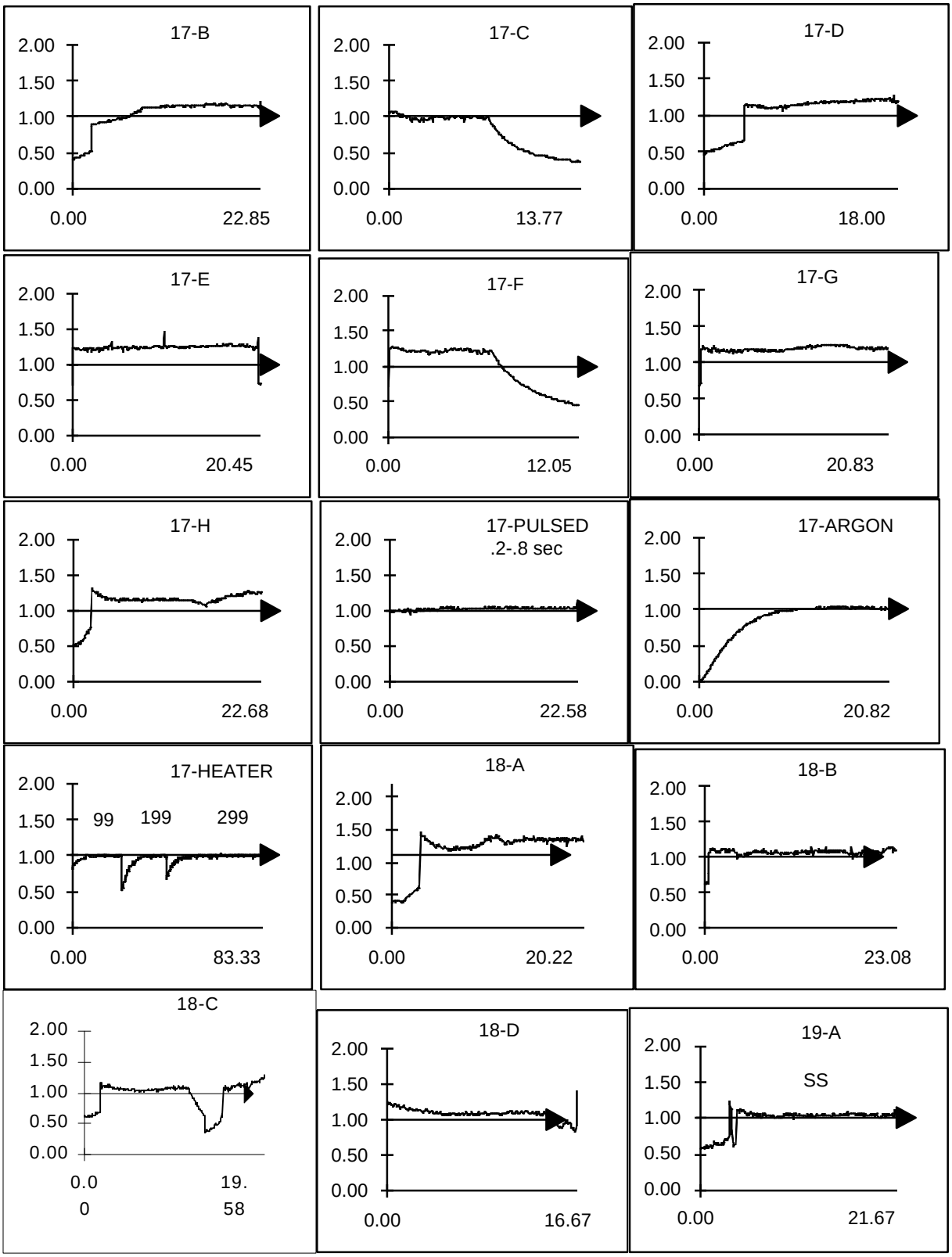
17-B
2.00
1.50
1.00
0.50
0.00
0.00
22.85
17-C
2.00
1.50
1.00
0.50
0.00
0.00
13.77
17-D
2.00
1.50
1.00
0.50
0.00
0.00
18.00
17-E
2.00
1.50
1.00
0.50
0.00
0.00
20.45
17-F
2.00
1.50
1.00
0.50
0.00
0.00
12.05
17-G
2.00
1.50
1.00
0.50
0.00
0.00
20.83
17-H
2.00
1.50
1.00
0.50
0.00
0.00
22.68
17-PULSED
.2-.8 sec
2.00
1.50
1.00
0.50
0.00
0.00
22.58
17-ARGON
2.00
1.50
1.00
0.50
0.00
0.00
20.82
17-HEATER
99
199
299
2.00
1.50
1.00
0.50
0.00
0.00
83.33
18-A
2.00
1.50
1.00
0.50
0.00
0.00
20.22
18-B
2.00
1.50
1.00
0.50
0.00
0.00
23.08
18-C
2.00
1.50
1.00
0.50
0.00
0.0
0
19.
58
18-D
2.00
1.50
1.00
0.50
0.00
0.00
16.67
19-A
SS
2.00
1.50
1.00
0.50
0.00
0.00
21.67

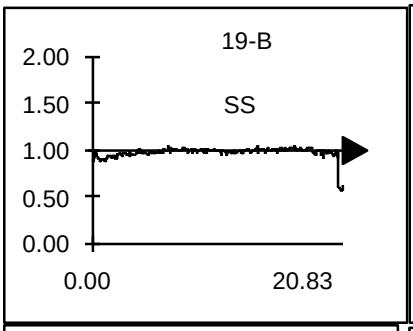
19-B
SS
2.00
1.50
1.00
0.50
0.00
0.00
20.83

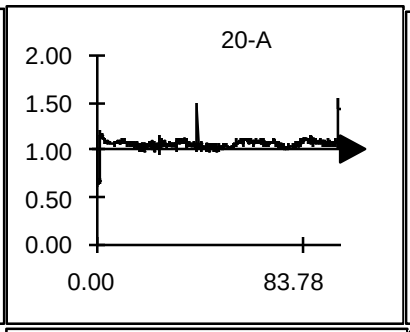
20-A
2.00
1.50
1.00
0.50
0.00
0.00
83.78

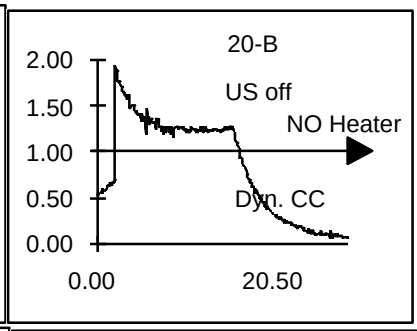
20-B
US off
NO Heater
Dyn. CC
2.00
1.50
1.00
0.50
0.00
0.00
20.50

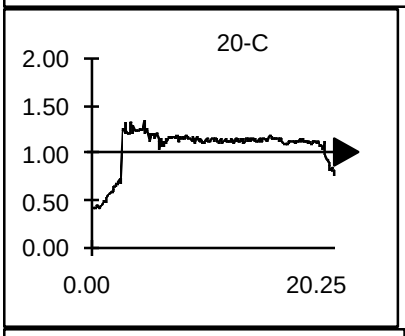
20-C
2.00
1.50
1.00
0.50
0.00
0.00
20.25

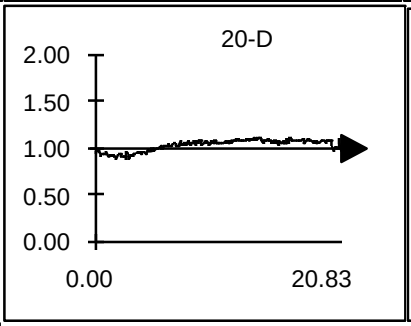
20-D
2.00
1.50
1.00
0.50
0.00
0.00
20.83

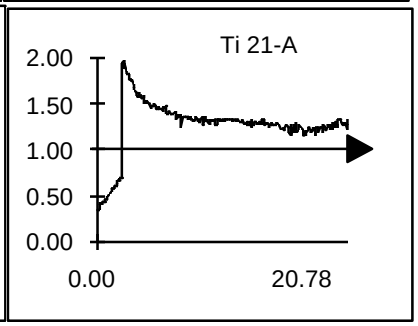
Ti 21-A
2.00
1.50
1.00
0.50
0.00
0.00
20.78

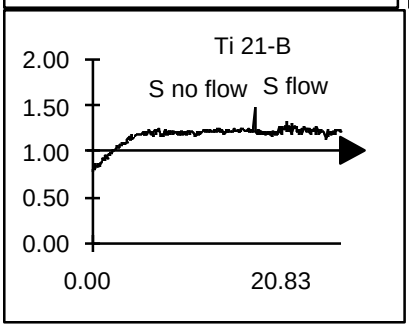
Ti 21-B
S no flow
S flow
2.00
1.50
1.00
0.50
0.00
0.00
20.83

Ultrasonic Cavitation and Micro-Fusion

Abstract: Investigations of extraordinary phenomena in heavy water (D_2O) cavitation experiments have revealed simultaneous evidence of anomalous heating, production of ^{3}He (T), and ^{4}He. Reaction rate is ~10^{12} - 10^{13} Rx/sec. SIMS and bulk MS analysis have produced additional evidence for transmutation of Ti and Pd isotopes. Control experiments are performed in ordinary water (H_2O). The experimental method involves initiating transient bubble collapse on the surface of target foils under the influence of a 20 khz acoustic field and within a prescribed temperature and pressure envelope. The results suggest that nuclear fusion processes are the cause of the observed effects in spite of the absence of expected neutron and gamma radiation.

Bubble Physics - Sonoluminesence & Micro-Fusion

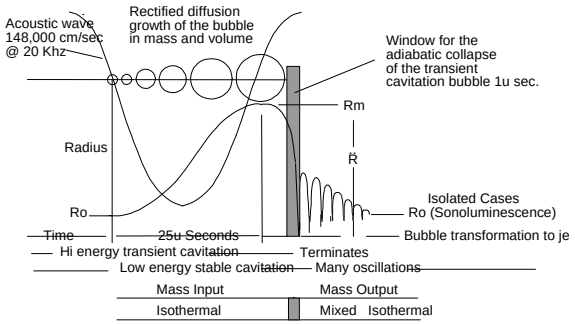

Environment within a cavitating bubble

- Adiabatic collapse and shock wave as bubble wall exceeds Mach 1
- Bubble temperatures reach 6000 + to 1 million degrees Kelvin
- High temperature converts contents to a plasma
- Density in bubble may exceed 12 gm/cm^3

Sonoluminesence

- Free stable cavitating bubble
- 14 picosecond light flashes
- Black body spectra
- No neutrons

Micro-Fusion

- Transient bubble on a target
- Heat at nuclear energy densities
- Nuclear ash ^{3}He and ^{4}He
- No neutron or gamma radiation

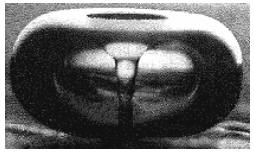

Transient bubble collapse with characteristic "jet".

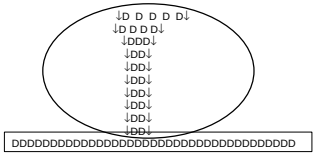

Graphic showing bubble directed plasma

Hypothesis: The cavitating bubble acts as a micro-accelerator for its contents. In the case of micro-fusion experiments those contents are primarily D_2O. Energy concentration occurs in the bubble brought on by rapid collapse. Dissociation and ionization of the species within the bubble produce positively charged deuterons. These deuterons, injected by the bubble, produce locally high D/Pd ratios in the target as well as a high flux of D moving through vacancies in the lattice. Combining with other forces within the lattice the end result is micro-fusion.

Survey of Research To Date

History of the E-Quest Experiments

- 1982, Photo-sonication experiments on novel synthesis
- 1989 April, First micro-fusion experiments
- 1993, E-Quest Sciences formed to pursue discovery
- 1993 Dec., Results first presented in public ICCF-4 Maui
- 1993 Oct., Experiments at Los Alamos and 1994, April
- 1995 Jan., New experiments in collaboration with SRI

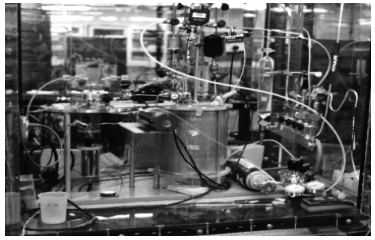

The E-Quest Mark II reactor as set up at Los Alamos National Lab (April-May 1993) - currently pictured at SRI International

Experimental conditions and parameters

- Vacuum tight stainless steel apparatus
- Reactor of charged target 25 c^{m2}, 15 ml D_2O, and high purity Argon
- D_2O and H_2O circulate separately in acoustically coupled vessels
- Calorimetry with multiple TCs, flow, and pressure sensors based on Newton's Law of Cooling and steady state heat flow methods
- Gas sampled in SS vessels for analysis by Mass Spectroscopy
- Target metal analysis by Mass Spectroscopy, SIMS, and SEM,
- Neutron, gamma, and charged particle detection on and off line

Heat Effects

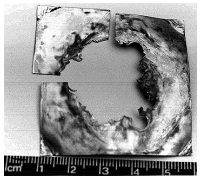

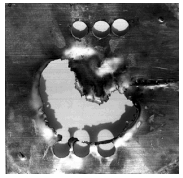

Gross melting of sample targets occurs with anomalous heat as a signatures effect in D_2O experiments

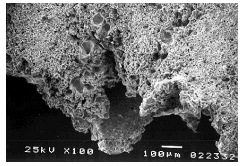

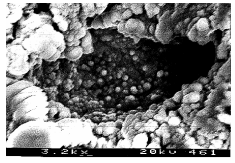

SEM Images of ejecta event sites on melted palladium targets

Two kinds of damage are apparent on the target metals; typical erosional cavitation damage and newly reported ejecta damage characteristic of internal heating. The *volcano* like ejecta sites result from multiple fusion events occurring nearly simultaneously at adjacent sites within the lattice. Calculations of energy required to eject measured volumes of metal suggests reactions with nuclear energy densities.

Results

Nuclear Products

Independent reactor gas analysis has been performed at SRI, U.S. Bureau of Mines Helium Lab, and Rocketdyne. Helium has been found in concentrations of 10 -1000 times the ambient background concentration in many different series of experiments. ^{3}He:^{4}He ratios are anomalously skewed and ^{22}Ne is absent. Time shifted analysis of one sample infers a substantial portion of the ^{3}He results from tritium decay.

Analysis of Helium in Reactor Gas from LANL Experiments Analysis at Rocketdyne

Sample #	^{3}He (10^{14} atoms)	^{4}He (10^{14} atoms)	^{4}He in sample (10^{14} atoms)	^{4}He (ppm)
Reactor gas	<0.0002	0.2506	4.632	0.471
Blank run	NM	0.2436	4.760	0.484
~20 hrs	NM	0.2237	4.621	0.470
Reactor gas	0.0042	0.7696	31.31	2.548
Short run	0.0042	0.7521	31.37	2.552
<20 hrs	0.0039	0.7357	31.46	2.560
Reactor gas	<0.0002	188.2	7483	553.5
Long run	NM	182.6	7447	550.9
~20 hrs	NM	178.3	7460	551.8
Argon	NM			<0.475
Air	NM			5.22

Helium in Target Metals - Analysis at Rocketdyne

Sample	Sample	^{4}He atoms	Max. ^{4}He atoms
Pd ~8-10mg	10.92 mg	0.2 - 8.3 x 10^9	
Total Pd ~ 3gms			2.2 x 10^{12}
Ti ~7-8mg	8.0 mg	0.6 - 83.8 x 10^9	
Total Ti ~ 1 gm			1.1 x 10^{13}

SIMS analysis of target materials

Studies of target metals by SIMS using equipment at LBL-NCEM reveal the presence of mass 3 and 4 in fresh samples and unexpected isotope ratios in titanium and palladium. Additional studies of isotopic ratios in target metals is planned using prompt neutron activation analysis.

Typical Excess Power Plots

Excess heat in Pd/D2O

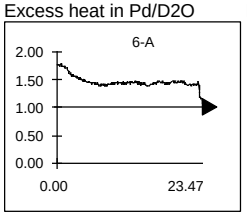

No excess heat in Stainless steel/ D2O

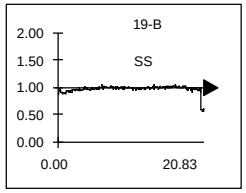

E-Quest Sciences wishes to thank the many scientists in the following organizations for their valued support and participation in this work:
Los Alamos National Lab, Electric Power Research Institute, Rockwell/Rocketdyne Lab, Naval Research Lab, Portland State Dept. of Physics, US Bureau of Mines Helium Lab, Battelle Pacific National Lab, SRI International, Balez Lab, Lockheed, and Lawrence Berkeley National Center for Electron Microscopy.

13 Sample plot of data from one experiment

The following plots are presented to show the appearance of data collected by SRI and used in analyzing these experiments. The calorimetry methods used to analyze the experiments are complex and a simple view of the raw data may be insufficient to dramatically illustrate the excess heat effect. However an indication of excess heat can be seen as the experiments are in process and is revealed by comparison of the following plots of abbreviated data. The small figure shows a full data set.

In this plot (below) four data traces (thermocouples) are presented. The bottom trace tracks room temperature. The thick data trace illustrates the large heat exchanger note this data trace being below those from the reactor and sonicator volume shows that heat source is the reactor /sonicator. The remaining two plots reveal separation which when compared with runs which produced no excess heat reveal the real time clue that an excess heat reaction is underway. The cooling curve shows that in this case the system was powered down but the circulating pumps were left running.

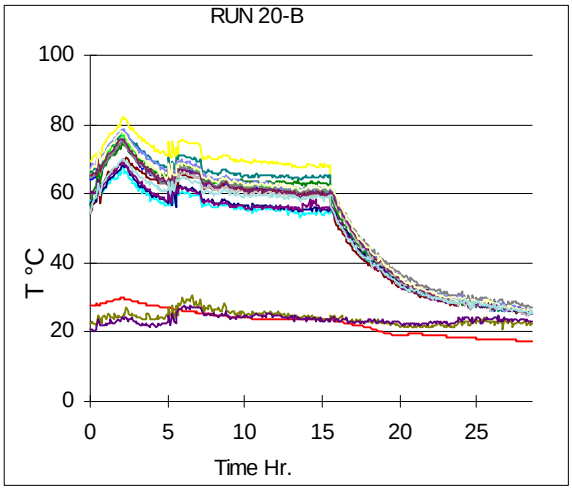

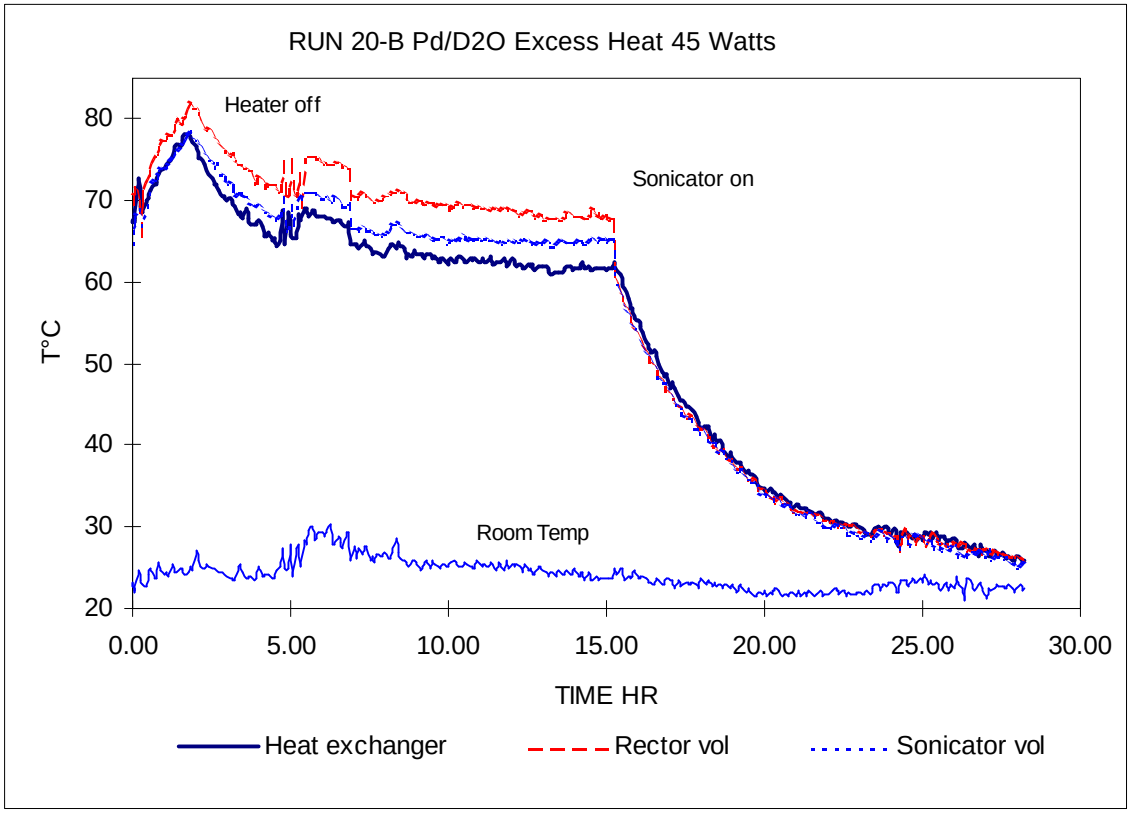

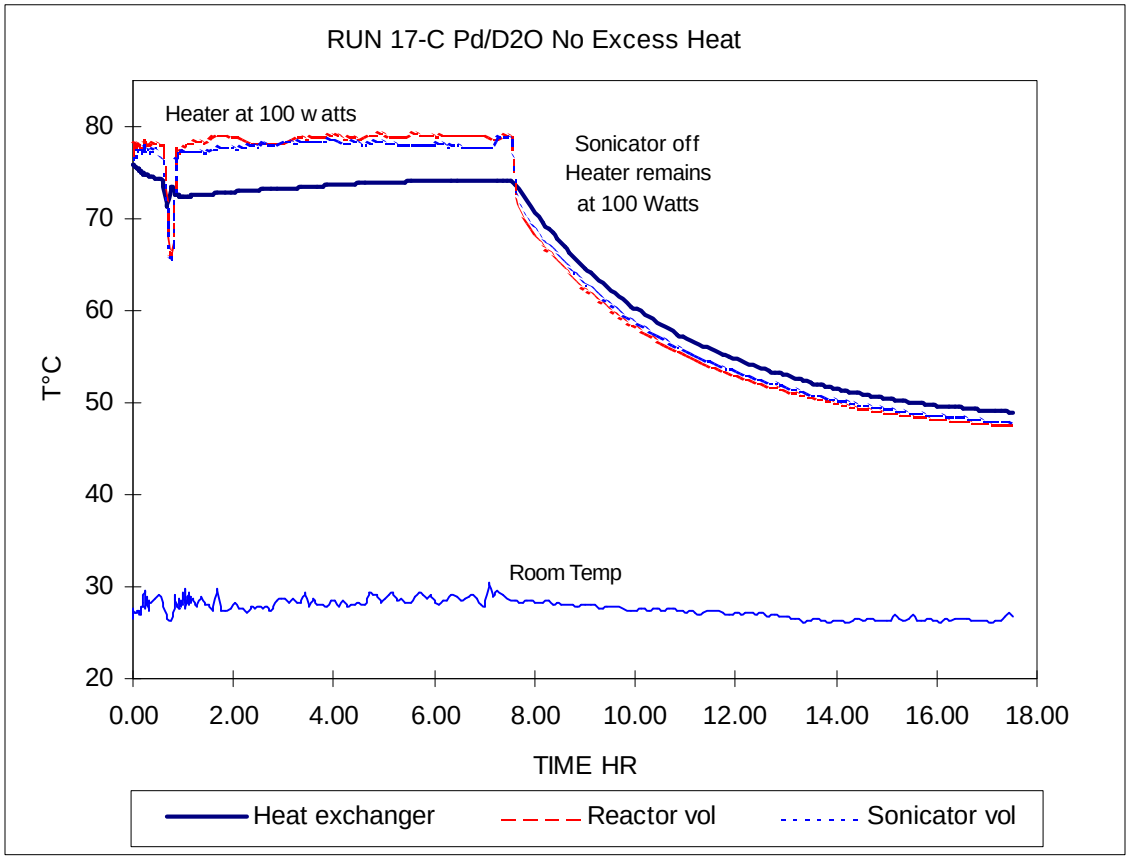

In this experiment which produced no apparent excess heat the two top most traces reactor and sonicator show little separation which is interpreted as indication of no excess heat reactions in progress. Again the position of the thick data trace from the large heat exchanger reveals a source of sonication heat (although no large excess heat) is in the reactor/sonicator side of the system. The cooling curve shows in this case that the 100 watts of Joule heat being added to the heat exchanger results in separation of the data traces.

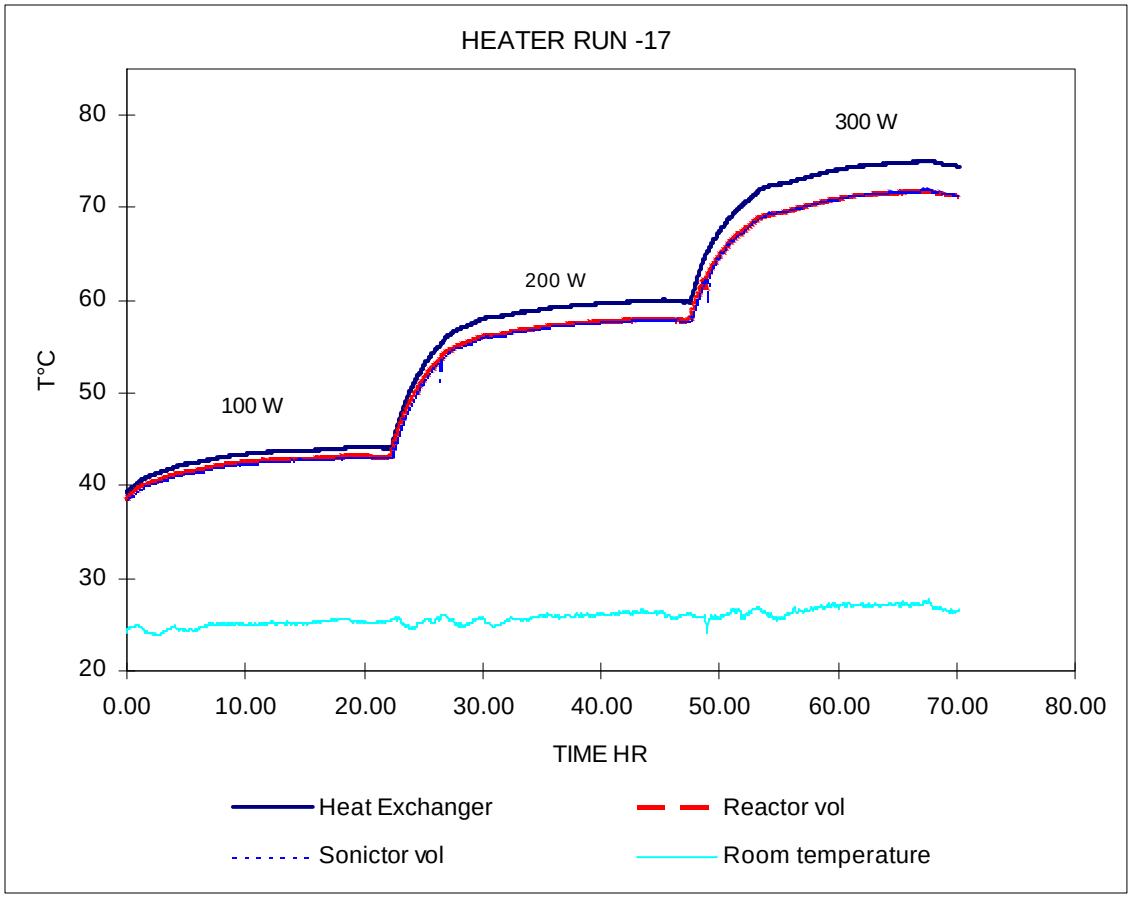

Finally in this experiment only an electrical resistance heater or Joule heater was providing heat into the apparatus via the heat exchanger. The thick data trace which is now top most reveals that the source of the heat is in the large heat exchanger as seen in the cooling curve from the preceding graph. No separation of the data traces from the reactor and sonicator is observed.

The total heat in the system is seen in this abbreviated data as the delta T between the room temperature and the temperatures taken from the rest of the apparatus at steady state.

14 Appendix H References

[1] Lord Raleigh, Phil. Mag. 34, 94 (1917)

[2] A. J. Walton and G. T. Reynolds, "Sonoluminescence," Advances in Physics, 33, 6 595-660 [1984]

[3] B. P. Barber, C. C. Wu, R. Lofstedt, P. H. Roberts and S. J. Putterman, " Sensitivity of Sonoluminescence to Experimental Parameters," Phys Rev. Let., 72, 9, 1380 [1994]

[4] C. C. Wu and P. H. Roberts, "Shock Wave Propagation in a Sonoluminescing Gas", Phys. Rev. Let. , 70, 22, 3424 [1993]

[5] H. G. Flynn, " Cavitation Dynamics 2. Free Pulsations and Models for Cavitation Bubbles", J. Acoustic Soc. Am., 58 1160 (1975)

[6] R. Heller, S. J. Putterman and B. P. Barber, "Spectrum of Synchronous Picosecond Sonoluminescence," Phys. Rev. Let., 69, 8, 1182 [1992]

[7] R. Stringham and R. George, "Cavitation Induced Micro-Fusion", ICCF-4 Conf. on Cold Fusion, Maui, Oct. 1993

[8] R. George and R. Stringham, "Production of heat, 3He, and 4He", American Chemical Society Conf., Nuclear Chemistry Division, Anaheim, April 1995

[9] R. George and R. Stringham, "Cavitation Micro-Fusion", ICCF-5 Conf. on Cold Fusion, Monaco, April 1995

[10] W.C. Moss, D.B. clark, J.W. White & D.A. Young, “Sonoluminesence and Prospects for Table-Top Micro-Thermonuclear Fusion”, Lawrence Livermore National Labs, (1995)

[11] L. A. Crum, " Rectified Diffusion" Ultrasonics 22 215 (1984)

[12] A. I. Eller "Bubble Growth by Diffusion in an 11kHz Sound Field," J. Acoust. Soc. of Am. 52 1447 [1972]

[13] M, Strasberg "Rectified Diffusion: Comments on a Paper by Hsieh and Plesset", J. Acoustic Soc. Am., 33 359 (1961)

[14] A. I. Eller and H. G. Flynn "Rectified Diffusion During Nonlinear Pulsations of Cavitation Bubbles" J. Acoustic Soc. Am., 43 1188 (1968)

[15] L. Crum and R. Roy, "Sonoluminesence", Science Vol. 266 Oct. 1994

[16] W. Moss, Personal Communication, LLNL April 95

[17] S. J. Putterman, "Sonoluminesence", Science, Dec. 14, 1994

[18] S. Putterman, "Sonoluminesence", Scientific American, Feb. 95

[19] T. Talley, Personal Communication, LANL May 94

[20] P.N.T. Wells, M.A. Bullen, and H. F. Freeundlich, “Ultrasound 2, 214, 1969

[21] M.E. Haran, B.D. Cook and H.F. Stewart, J. Acoust. Soc. Am. 57, 1436, 1975

[22] R.T. Beyer and S. V. Letcher, Physical Ultrasonics, Academic Press, (1969)

[23] T.F. Hueter and R.H. Bolt, Sonics, John Wiley and Sons, (1955)

[24] "Cold Fusion and Sonoluminesence", NY Times Dec. 15, 94

[25] C. Eberline, Physics Letters A, May,1996

Additional reading

H. Farrar and B. Oliver, "A Mass Spectrometer to Determine Very Low Levels of Helium in Small Solid and Liquid Samples", J. Vac. Science Technology, A4, 1740 (1968)

P.W. Holland and D.E. Emerson, " determination of Helium content of the Near Surface Atmospheric Air Within the Continental United States", J. Geophysi. Res. 92, No. B12, 12557

G. H. Miley, "Comments about Nuclear Reaction Products", Proc. ICCF-4 Conf on Cold Fusion, Vol. 2, EPRI TR-104188-V2 (July 1994)

SRI, EPRI, Lockheed, "Development of Advanced Concepts for Nuclear Processes in Deuterated Metals", EPRI TR-104195 Final Report, (1994)

R. E. Apfel, "Acoustic Cavitation" Chap. #7, Methods of Experimental Physics, Vol. #19, Ed. by P. Edmonds, Published the Academic Press, 335, [1981]

A. A. Atchley and L. A. Crum, "Acoustic Cavitation and Bubble Dynamics", Chapt. #1, "Ultrasound" Ed. by K. S. Suslick, Published by VCH, 1, [1988]

M. S. Plesset and R. B. Chapman, "Collapse of an Initially Spherical Vapor Cavity in the Neighborhood of a Solid Boundary," J. Fluid Mech. 47, 283 (1971)

M. P. Felix and A. T, Ellis, "Lazer-Induced Liquid Breakdown-a Step-By-Step Account," Appl. Phys. Let. 19, 484 (1971)

W. Lauterborn and H. Bolle, "Experimental Investigations of Cavitation-bubble collapse in the Neighborhood of a Solid Boundary,"J. Fluid Mech. 72, 391 (1975)

Y. Tomita, A. Shima, " High-Speed Photographic Observations of Laser- Induced Cavitation Bubbles in Water," Phys. Rev. Let., 70, 22 3424 [1993]

T. B. Benjamin and A. T. Ellis, "The Collapse of Cavitation Bubbles and the Pressures thereby Produced Against Solid Boundaries," Philos. Trans. R. Soc. London Sect. A. 260, 221 (1966)

L. A. Crum, "Sonoluminesence," Physics Today, 22 [Sept. 1994]

A. Prosperetti, Ultrasonics, 22, 77 [1984]

B. P. Barber and S. J. Putterman, " Light Scattering Measurements of the Repetitive Supersonic Implosion of a Sonoluminescing Bubble," Am. Phys. Soc., 69, 26, 3839 [1992]

D. F. Gaitan, L. A. Crum, C. C. Church and R. A. Roy, " Sonoluminescence and Bubble Dynamics for a Single, Stable, Cavitation Bubble" J. Accoust. Soc. Am. 91, 6 (1992)

T. B. Flanagan, W. A. Oates, "The Palladium-Hydrogen System" Annu. Rev. Mater. Sci. 21 269 (1991)

Ivars Peterson, "Beating a Fractal Drum", Science News, vol.146, 184, [Sept. 17 '94]

L. Motz, "Astrophysics and Stellar Structure," Pub. by Ginn, Chap. 10, (1970)

Ch. H. Fischer, F. J. Hart and A. Henglein, "J. Phys Chem" 90 222 (Jan. 1986)

J. Schwinger, "Cold Fusion Theory: A Brief History of Mine",
The Third International Cold Fusion Conference, Maui 6-9 Dec. (1993)

G. Preparata, "Cold fusion '93: Some Theoretical Ideas"
The Third International Cold Fusion Conference, Maui 6-9 Dec. (1993)

WARNING: This Document contains information classified under U.S. Export Control regulations as restricted from export outside the United States. You are under an obligation to ensure that you have a legal right to obtain access to this information and to ensure that you obtain an export license prior to any re-export of this information. Special restrictions apply to access by anyone that is not a United States citizen or a Permanent United States resident. For further information regarding your obligations, please see the information contained below in the section titled "Export Control Restrictions."

Export Control Restrictions

Access to and use of EPRI Intellectual Property is granted with the specific understanding and requirement that responsibility for ensuring full compliance with all applicable U.S. and foreign export laws and regulations is being undertaken by you and your company. This includes an obligation to ensure that any individual receiving access hereunder who is not a U.S. citizen or permanent U.S. resident is permitted access under applicable U.S. and foreign export laws and regulations. In the event you are uncertain whether you or your company may lawfully obtain access to this EPRI Intellectual Property, you acknowledge that it is your obligation to consult with your company's legal counsel to determine whether this access is lawful. Although EPRI may make available on a case by case basis an informal assessment of the applicable U.S. export classification for specific EPRI Intellectual Property, you and your company acknowledge that this assessment is solely for informational purposes and not for reliance purposes. You and your company acknowledge that it is still the obligation of you and your company to make your own assessment of the applicable U.S. export classification and ensure compliance accordingly. You and your company understand and acknowledge your obligations to make a prompt report to EPRI and the appropriate authorities regarding any access to or use of EPRI Intellectual Property hereunder that may be in violation of applicable U.S. or foreign export laws or regulations.

About EPRI

EPRI creates science and technology solutions for the global energy and energy services industry. U.S. electric utilities established the Electric Power Research Institute in 1973 as a nonprofit research consortium for the benefit of utility members, their customers, and society. Now known simply as EPRI, the company provides a wide range of innovative products and services to more than 1000 energy-related organizations in 40 countries. EPRI's multidisciplinary team of scientists and engineers draws on a worldwide network of technical and business expertise to help solve today's toughest energy and environmental problems.

EPRI. Electrify the World

Program:

Nuclear Power

TR-108474

EPRI • 3412 Hillview Avenue, Palo Alto, California 94304 • PO Box 10412, Palo Alto, California 94303 • USA
800.313.3774 • 650.855.2121 • askepri@epri.com • www.epri.com